EMBRY-RIDDLE
Aeronautical University™
SCHOLARLY COMMONS

4-2021

Investigation of Trajectory and Control Designs for a Solar Sail to the Moon

Michelle Nadeau
nadeaum1@my.erau.edu

Follow this and additional works at: https://commons.erau.edu/edt

Part of the Engineering Physics Commons

INVESTIGATION OF TRAJECTORY AND CONTROL DESIGNS
FOR A SOLAR SAIL TO THE MOON

by

Michelle Lara Nadeau

A Thesis Submitted to the College of Arts and Sciences Department of Physical Sciences in
Partial Fulfillment of the Requirements for the Degree of
Master of Science in Engineering Physics

Embry-Riddle Aeronautical University
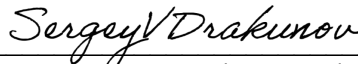Daytona Beach, Florida
April 2021

INVESTIGATION OF TRAJECTORY AND CONTROL DESIGNS FOR A SOLAR SAIL TO THE MOON

by

Michelle Lara Nadeau

This thesis was prepared under the direction of the candidate's Thesis Committee Chair, Dr. Sergey V. Drakunov, Professor, Daytona Beach Campus, and Thesis Committee Members, Dr. William MacKunis, Professor, Daytona Beach Campus, and Dr. Edwin J. Mierkiewicz, Professor, Daytona Beach Campus, and has been approved by the Thesis Committee. It was submitted to the Department of Physical Sciences in partial fulfillment of the requirements for the degree of Master of Science in Engineering Physics

Thesis Review Committee:

Sergey V. Drakunov, Ph.D.
Committee Chair

William MacKunis, Ph.D.
Committee Member

Edwin Mierkiewicz
Digitally signed by Edwin Mierkiewicz
DN: cn=Edwin Mierkiewicz, o, ou,
email=mierkiee@erau.edu, c=US
Date: 2021.04.26 19:15:10 -05'00'

Edwin J. Mierkiewicz, Ph.D.
Committee Member
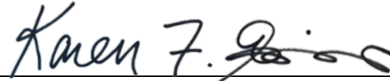
John M. Hughes, Ph.D.
Interim Chair,
Department of Physical Sciences

Karen F. Gaines, Ph.D.
Dean, College of Arts and Sciences

Christopher D. Grant, Ph.D.
Associate Provost of Academic Support

Date

i

Acknowledgements

First, I would like to thank my thesis committee chair and research advisor, Dr. Drakunov, for his spectacular guidance this past year. Hearing about my internship on the Artemis program, it was he who came up with the project idea of designing the controls for a solar sail to deliver supplies the moon. I greatly appreciate his eager support to tie this project into my interests and all the time, energy, and expertise he dedicated to answering my questions and pointing me in the right direction.

I would also like to thank my committee members, Dr. Mierkiewicz and Dr. MacKunis, for their valuable time and critique.

An additional thanks goes to the folks in the Engineering Physics Propulsion Lab for letting me reference their related work herein and in my defense presentation. I look forward to our possible collaboration on a paper in the near future.

Last but certainly not least – Many, many thanks to my partner, family, and friends who supported and encouraged me to be able to reach this point today. They probably did not expect such barbaric math to be on the slides, but they watched my thesis defense presentation anyway. I appreciate you all and cannot wait until the next time I see you in person again.

Abstract

Researcher: Michelle Lara Nadeau

Title: Investigation of Trajectory and Control Designs for a Solar Sail to the Moon

Institution: Embry-Riddle Aeronautical University

Degree: Master of Science in Engineering Physics

Year: 2021

     NASA's Artemis program and other government and commercial projects are working toward establishing a sustainable human presence on the moon. This thesis investigates the technical feasibility of a solar sail-based spacecraft (sailcraft) as a low-cost method of delivering cargo or science instruments to the moon and demonstrates how this sailcraft could be controlled to change its orbit. The concept is a low-cost, commercial launch vehicle-deployable, CubeSat-based sailcraft with a square sail, assumed attitude control, and a small payload traversing from low-Earth orbit toward the moon with zero propellant use. In this thesis, methods for sailcraft to increase altitude, the trajectory design process, and zero-propellant attitude control actuator options are explored. Three increasingly complex mathematical models were built in MATLAB around thrust vector control designs to get the concept sailcraft from Earth orbit toward the moon and transit simulations conducted. The third and most promising model developed a linear quadratic regulator controller to follow a logarithmic spiral reference trajectory and ensure the stability of the solution. As a result, a robust thrust vector control solution to minimize error from the reference trajectory was found and a solution method to assign the control gain matrix was developed.

Table of Contents

vi

ix

List of Tables

List of Figures

Nomenclature

A	Sail area, [km^2]
$A_\perp$	Sail area normal to the incident radiation, [km^2]
$\boldsymbol{A}$	State matrix
$\boldsymbol{A_{IB}}$	State matrix of Earth relative to Earth-moon system barycenter
$\boldsymbol{A_{IE}}$	State matrix of Earth relative to sun
a	Semimajor axis of orbit, [km]
a_r	Radial component of SRP acceleration, [km / min^2]
a_t	Transverse component of SRP acceleration, [km / min^2]
$\vec{a}$	Acceleration of ideal sailcraft due to SRP, [km / min^2]
B	Earth-moon system-centered rotating reference frame
$\vec{B}$	Earth's magnetic field, [kg km^2 / A min^2]
$\boldsymbol{B}$	Input matrix
$(\hat{b}_1, \hat{b}_2, \hat{b}_3)$	Basis vectors of Earth-moon system-centered rotating reference frame B
$\boldsymbol{C}$	Output matrix
c_0	Speed of light, [km / min]
D	Constant distance between two primary bodies in CR3BP, [km]
D_1	Distance from M_1 to barycenter, [km]
D_2	Distance from M_2 to barycenter, [km]
dt	Time interval between t_k and t_{k+1}, [min]
E	Earth-centered inertial (ECI) reference frame
e	Eccentricity of orbit, [unitless]

$\boldsymbol{e}$	Sailcraft error state vector
$\boldsymbol{e_{out}}$	Sailcraft position error state vector, [km]
$\vec{e}_{out}$	Sailcraft position error, [km]
$\vec{e}_1$	Difference in sailcraft's actual and desired position vectors from the Earth, [km]
$\vec{e}_2$	Difference in sailcraft's actual and desired position vectors from the moon, [km]
$(\hat{e}_1, \hat{e}_2, \hat{e}_3)$	Basis vectors of Earth-centered inertial reference frame E
$\vec{F}$	Force on ideal sailcraft due to SRP, [kg km / min^2]
$\boldsymbol{f}$	Vector field
G	Gravitational constant, [km^3 / min^2]
I	Heliocentric ecliptic inertial reference frame
$\boldsymbol{I}$	Identity matrix
i	Inclination of orbit, [deg]
$(\hat{\imath}_1, \hat{\imath}_2, \hat{\imath}_3)$	Basis vectors of heliocentric ecliptic inertial reference frame I
J	Linear quadratic performance index, [kg km^2 / min^2]
$\boldsymbol{K}$	Control gain matrix
L	Solar luminosity, [kg km^2 / min^3]
$\vec{M}$	Magnetic dipole moment, [A km^2]
M_1	Mass of one primary body in R3BP, [kg]
M_2	Mass of other primary body in R3BP, [kg]
m	Mass of sailcraft, [kg]
m_1	Mass of inertially fixed primary body in R2BP, [kg]
m_2	Mass of orbiting body in R2BP, [kg]
$\vec{N}$	Control torque vector, [kg km^2 / min^2]

N_1	Reference trajectory scalar coefficient, [unitless]
N_2	Reference trajectory scalar coefficient, [unitless]
$\boldsymbol{N_3}$	Reference trajectory matrix
$\hat{n}$	Unit vector normal to the sail plane
O	Origin of the given reference frame
P	Solar radiation pressure, [kg / km min^2]
P^*	Solar radiation pressure at 1 AU, [kg / km min^2]
$\boldsymbol{P}$	Solution matrix
$\hat{p}$	Unit vector normal to orbital plane
$\boldsymbol{Q}$	State weighting matrix
$\hat{q}$	Arbitrary unit vector
$\boldsymbol{R}$	Control input weighting matrix
$\vec{R}$	Sailcraft reference position vector, [km]
$\vec{R}_{IB}$	Earth-moon barycenter's position vector from the center of the sun, [km]
$\vec{R}_{IE}$	Earth position vector from the center of the sun, [km]
$\vec{R}_1$	Reference trajectory position vector from Earth, [km]
$\vec{R}_2$	Reference trajectory position vector from the moon, [km]
r	Distance from sun to sailcraft, [km]
r_{crit}	Point at which the orbiting sailcraft enters or exits Earth's umbra, [km]
r^*	One astronomical unit, [AU]
$r_{\oplus}$	Radius of the Earth, [km]
r_O	Radius of the sun, [km]
$\vec{r}$	Sailcraft inertial position vector from the center of the sun, [km]

$\hat{r}$	Unit vector along the sun-line
$\vec{r}_b$	Sailcraft position vector from the Earth-moon barycenter, [km]
$\vec{r}_E$	Sailcraft position vector from the center of the Earth, [km]
$\vec{r}_1$	Sailcraft position vector from M_1, [km]
$\vec{r}_2$	Sailcraft position vector from M_2, [km]
s	Distance from center of primary to spacecraft, [km]
$\vec{s}$	Position of particle from an arbitrary point O of frame B, [km]
$\left\{\dfrac{d\vec{s}}{dt}\right\}_A$	Rate of change of position vector $\vec{s}$ as seen from reference frame A, [km/min]
$\left\{\dfrac{d\vec{s}}{dt}\right\}_B$	Rate of change of position vector $\vec{s}$ as seen from reference frame B, [km/min]
$\boldsymbol{T}$	Error thrust control input vector
$\widetilde{\boldsymbol{T}}$	Actual thrust control input vector
$\boldsymbol{T}^*$	Reference thrust control input vector
$\vec{T}$	Error thrust vector due to SRP and controls, [km kg /min^2]
$\vec{\widetilde{T}}$	Actual thrust vector due to SRP and controls, [km kg /min^2]
$\vec{T}^*$	Thrust vector to follow the reference trajectory, [km kg /min^2]
$\widetilde{T}_t$	Transverse thrust due to SRP and controls, [km kg /min^2]
t	Time, [min]
t_k	Initial time step, [min]
t_{k+1}	Subsequent time step, [min]
$U(\vec{r}_b)$	Three-body gravitational potential, [km^2 / min^2]
$\boldsymbol{u}$	Acceleration control input vector
$\vec{u}$	Acceleration control input vector, [km / min^2]

(u_x, u_y, u_z)	Error control acceleration components, [km / min^2]
$(\tilde{u}_x, \tilde{u}_y, \tilde{u}_z)$	Actual control acceleration components, [km / min^2]
(u_x^*, u_y^*, u_z^*)	Reference control acceleration components, [km / min^2]
V	Tangential velocity of a spacecraft in a circular orbit, [km/min]
V_1	Velocity before a ΔV burn, [km/min]
V_2	Velocity after a ΔV burn, [km/min]
$\vec{v}$	Sailcraft velocity vector relative to the Earth, [km/min]
W	Desired eigenvalues
X	Desired state vector
x	Actual state vector
Y	Desired output, [km]
y	Output vector
y	System output, [km]
Z	State vector for Earth position and velocity
α	Sail cone angle, [deg]
β	Solar sail lightness number, [unitless]
Γ	Instantaneous radius of trajectory, [km]
Γ_0	Initial radius of trajectory, [km]
γ	Spiral angle, [deg]
Δi	Inclination angle change required, [deg]
Δi_p	Inclination change per orbit, [deg]
Δo	Disturbing term from circular orbit to cause a logarithmic spiral out
$\Delta \vec{o}$	Disturbing term from circular orbit to cause a logarithmic spiral out, [km / min^2]

Δp	Momentum transferred by incident photons, [kg km / min]
Δt	Time interval, [min]
ΔV	Change in spacecraft velocity, [km/min]
δ	Sail clock angle, [deg]
ε	Eclipse factor, [unitless]
η	Sail efficiency, [unitless]
θ	True anomaly of spacecraft orbit, [deg]
θ_E	Angle between sun-Earth vector $\vec{R}_{IE}$ and Earth-sailcraft vector $\vec{r}_E$, [deg]
κ	Solar sail characteristic acceleration, [km/min^2]
λ	Eigenvalue
μ	Gravitational parameter of the primary body, [km^3/min^2]
μ_1	Gravitational parameter of M_1, [km^3/min^2]
μ_2	Gravitational parameter of M_2, [km^3/min^2]
$\mu_\oplus$	Gravitational parameter of the Earth, [km^3/min^2]
μ_O	Gravitational parameter of the sun, [km^3/min^2]
ρ	Mass ratio of Earth-moon system, [unitless]
σ	Sail loading parameter, [kg/km^2]
Φ	Angle subtended by the arc between instantaneous and initial radii, [deg]
Ω	Right ascension longitude of the ascending node of orbit, [deg]
ω	Argument of perigee of orbit, [deg]
$\vec{\omega}_b$	Angular velocity of Earth-moon system, [min^{-1}]
$\vec{\omega}^{B/A}$	Angular velocity of reference frame B with respect to reference frame A, [min^{-1}]

$\vec{\omega}^{B/I}$ Angular velocity of the Earth-moon system in motion around the sun, [min^{-1}]

∇U Gradient of the pseudo-potential, [km / min^2]

Chapter I
Introduction

Solar sail-based spacecraft (henceforth "sailcraft") use solar radiation pressure (SRP) as their means of propulsion. The impulse of photons on the highly reflective solar sail material can accelerate a lightweight sailcraft. Every second, the sun emits 10^{26} Joules in the form of 10^{45} photons, which can be used to power a sailcraft for free [1]. In this regard, solar sail propulsion has a massive advantage over other propulsion methods: sailcraft do not require propellants or propellant storage, whereas chemical propellant is heavy, expensive to launch, and limited to what the spacecraft can carry.

Chemical propulsion is by far the leading spacecraft propulsion method to transit from the vicinity of the Earth to the vicinity of the moon, usually in as little as 3 days [2]. However, solar sail propulsion offers a desirable alternative to chemical propulsion. Solar sail propulsion is well-suited for uncrewed missions with low mass payloads that can survive a longer transit time, e.g., cargo or science instruments resistant to solar, galactic cosmic, and Van Allen belt radiation.

Problem Statement and Significance

U.S. agencies' interests in solar sail propulsion appear focused on deep-space applications unsuitable for conventional propulsion spacecraft or on polar orbits around planets, including Earth. The National Academy of Sciences is particularly interested in solar sails for the Solar Polar Imager mission concept, an interstellar probe with more sophisticated instruments than Voyager I and II, and a solar wind monitor closer to the sun than L1 [3]. NASA's solar sail missions under development or consideration include NEA Scout, a near-Earth asteroid rendezvous mission launching November 2021 [4]; the New Moon Explorer mission concept, a proposed asteroid rendezvous mission [5]; and an in-orbit demonstration of the Advanced Composite Solar Sail System built in partnership with NanoAvionics [6]. While it is completely

sensible for these agencies to consider solar sail propulsion for missions that are unsuitable for conventional propulsion spacecraft, it is unclear what consideration has been given to replacing conventional spacecraft with sailcraft anyway for the suitable missions. This lack of clear consideration is the first problem. A mission that is suitable for a conventional propulsion spacecraft does not necessarily need to be completed by one.

In addition, in the next 10-15 years alone, many government and commercial projects expect to drastically ramp up their crewed missions to the vicinity of the moon. Of note, the "vicinity of the moon" encompasses both the lunar surface itself and lunar orbits. NASA's Artemis program intends to send the first woman and second man to the moon by 2024 and then establish a sustainable human presence on the moon as a training ground for Mars [7]. Commercial companies Dynetics, Blue Origin, and SpaceX have competed for the past year to provide the human landing system for this program; in April 2021, NASA awarded the contract to SpaceX [8], [9]. Also part of the Artemis program is Gateway, a crewed habitat that will orbit the moon in a near-rectilinear halo orbit (NRHO) and built in partnership between NASA and the Canadian, Japanese, and European space agencies (CSA, JAXA, and ESA, respectively) [7]. China's space agency (CNSA) recently completed an uncrewed sample return mission (Chang'e-5) from the moon in December 2020, an important step in their plan to build a robotic international scientific research station at the moon's South Pole for follow-on crewed exploration missions in the near future [10], [11]. CNSA and the space agency for Russia (ROSCOSMOS) have announced their plans to collaborate on crewed space missions, including the research station, signing a memorandum of understanding to this effect in March 2021 [12], [13].

All such crewed missions to the vicinity of the moon will require – in addition to the astronauts themselves – a significant amount of supplies and equipment: what the astronauts will breathe, drink, eat, wear, live in, return home in, communicate with, do experiments with, use to explore the lunar surface, use to get power, plus spares and back-up systems. NASA's Apollo missions could only stay for a few hours on the moon because they were limited to what they could carry in one lunar module. Apollo 17 spent the most time on the moon and that was only 75 hours on the surface, including a mere 22 hours in extravehicular activity [14]. A sustainable human presence on the moon will require both pre-emplaced supplies and periodic resupply, as well as reliable communications [15]. Due to this large quantity of logistical support required and the small amount of available mass and volume for payloads on current launch vehicles, only a limited amount of the necessary supplies may be sent with the astronauts - and at great expense; the remainder of the supplies must be sent separately.

We typically think of uncrewed missions as science data collection missions, such as robotic orbiters and rovers. However, uncrewed spacecraft can also be used to deliver this significant amount of supplies needed for crewed missions. For example, uncrewed spacecraft currently deliver cargo to astronauts at the International Space Station. In fact, they are a much cheaper cargo delivery vehicle than a crewed spacecraft is. For example, a crewed SpaceX Dragon 2 costs about $385 million compared to $209 million for a cargo Dragon 1 in 2019-2020 dollars [16], [17]. Thus, to support the drastic increase in crewed missions to the vicinity of the moon in the next ten years, governments and commercial companies in the space industry are expected to also drastically increase uncrewed missions – yet they lack low-cost methods to do so. This is the second problem. That is, the demand is going up, but these missions are going to

be very expensive. My concern is that the mission costs could be prohibitive and humanity misses out on opportunities to collect important data.

To address the two problems described above, this thesis considers solar sail propulsion as a low-cost alternative in missions that are suitable for conventional propulsion spacecraft, specifically uncrewed missions to the vicinity of the moon.

Purpose Statement

The purpose of this thesis is to explore orbit raising methods for sailcraft and the trajectory design process. This thesis uses the same "concept sailcraft" throughout for like comparison across each orbit raising method: a commercial launch vehicle-deployable, CubeSat-based sailcraft with a square sail, assumed attitude control, and a small payload, traversing from low-Earth orbit (LEO) toward the moon with zero propellant use. This thesis investigates the technical feasibility of the uncrewed concept sailcraft as a low-cost method of delivering cargo to the vicinity of the moon: it discusses zero-propellant attitude control actuator options; explores multiple thrust vector control designs for a sailcraft to transit from Earth to the moon; and describes the results from such transit simulations.

Research Questions

1. What are simple control methods to increase altitude via solar sail propulsion?

2. What is the relationship between thrust vector control design, attitude control design, and trajectory planning and design for a sailcraft? For any spacecraft?

3. Does control theory offer a reasonable linearized solution method for a sailcraft to traverse from LEO to the vicinity of the moon?

Applications

      Sailcraft missions that could use the thrust vector control designs within include the transit of small cargo payloads from Earth orbit to the vicinity of the moon. The cargo payloads may be supplies to support a crewed mission on the moon or at Gateway; science equipment to collect data from cislunar space (e.g., observing the Earth or moon from orbit); or communication satellites to relay communications between landing modules on the lunar surface, lunar terrain vehicles that may be in a crater, Gateway in NRHO, and Earth-based controllers. Based on NASA's published Artemis program timeline, I expect demand for lunar communications relay capability within the next 5-10 years. Artemis plans to go to the moon's South Pole. But if humans also want to go to the far side of the moon, Simo and McInnes proposed a sailcraft-based satellite at L2 for communication [18].

      Although a supply mission more or less ends when the supplies are delivered, the missions transporting space science equipment and communications satellites also require thrust vector control designs for stable orbit station-keeping at their destination. The intended orbit drives the control solution: controls to orbit L2, which is an unstable Lagrange point, is different than station-keeping controls for a halo orbit. Alternatively, science missions may require thrust vector control designs for special fly-by maneuvers at their destination, e.g., to rendezvous with near-Earth asteroids for data collection.

      Lastly, the thrust vector control designs can offer stable orbit station-keeping to spacecraft that start in Earth orbit and then remain there. Such applications include spacecraft that need to maintain their orbit, e.g., geostationary satellite station-keeping, or to raise their orbit a limited amount, e.g., orbital debris removal.

Delimitations

Overall, this thesis considers a sailcraft's thrust vector control, attitude control, and trajectory designs and their large-scale mission application to increase altitude and to station-keep. I study five different thrust vector control designs to achieve one theoretical mission: get a sailcraft from Earth orbit toward the moon. Of the five, I select three control designs to model and simulate in MATLAB with the concept sailcraft. I start with the most basic of the three and increase complexity from there.

I build and explore three mathematical models around these control designs for increasing altitude and station-keeping. These are relatively low-fidelity models to determine an initial, rough sense of the mission's technical feasibility to inform future work. The first model is the simplest of the three, just orbiting Earth. It does not try to increase altitude and it ignores SRP effects and controls. The second model is a step up in complexity from the first model, introducing SRP effects on the sailcraft. It models the sailcraft increasing its altitude using on-off switching, an exact, "pre-made" thrust vector solution to increase altitude. The model simulations study the sailcraft kinematics, and the stability of the solution is largely ignored. The third model keeps the SRP effects from the second model and adds a more complex method to increase altitude. A linear quadratic regulator (LQR) controller is developed to limit the sailcraft's trajectory error from a reference logarithmic spiral trajectory toward the moon. The simulations of this model study the stability of the thrust vector solution, and the sailcraft kinematics are largely ignored.

The overall scope of this thesis is limited to cislunar space, the region between Earth and the moon. For the first two models, the scope is further limited to the vicinity of Earth, defined here as less than 240,000 km from the center of the Earth, and the orbit raising simulations in

those two models do not exceed that distance. This distance upper boundary was selected in

order to use a simplified physical model involving only the Earth and sailcraft, the gravitational

force between them, and SRP as applicable. At distances greater than 240,000 km from Earth,

the gravitational forces of the sun and moon are non-negligible (i.e., within an order of

magnitude) as shown in Figure 1.1. The third model – being more complex – accounted for the

influence of the moon's gravity.
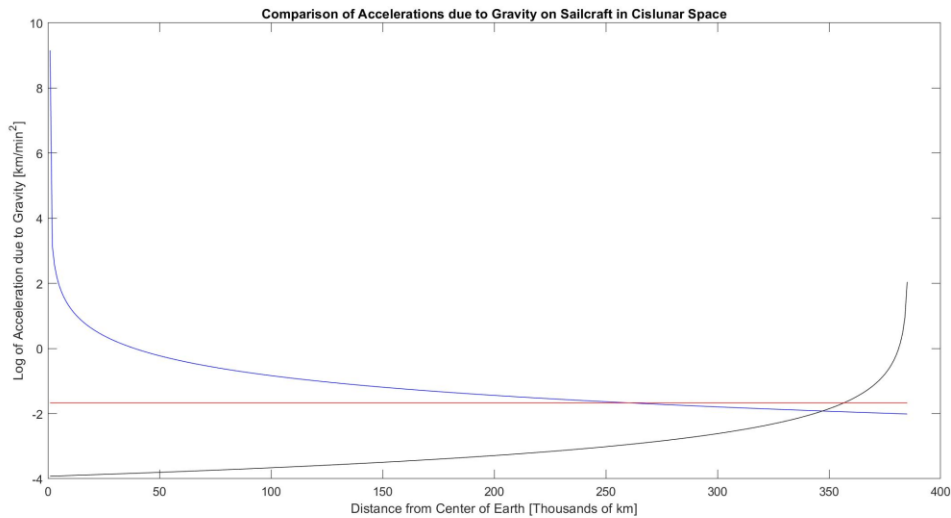
Figure 1.1 Comparison of Accelerations Due to Gravity on Sailcraft in Cislunar Space. Near
Earth (i.e., <240,000 km from center of Earth), the acceleration due to Earth's gravity (blue)
dominates. Near the moon (i.e., >360,000 km from center of Earth), the acceleration due to the
moon's gravity (black) dominates. In between the two regions, the gravities of the sun (red),
Earth, and moon must be considered.

Limitations and Assumptions

Unless otherwise specified, all orbits discussed within this thesis are assumed to be

approximately Keplerian orbits. That is, orbits that adhere to Kepler's three laws, and the

primary body is within – not adjacent to – the spacecraft's orbital plane [19]. The sun's center is

centered at the origin of an inertial reference frame *I*. The Earth's center orbits around the sun at the origin of a rotating and translating reference frame *E* at $\vec{\omega}^{E/I}$. The sun, Earth, and moon are assumed to be spheres of uniform density so they can be approximated as point masses with no gravitational force disturbances, therefore the Earth's oblateness is ignored. In this simplified analysis the Earth does not rotate. The sailcraft is assumed to be an infinitesimal mass compared to the sun, Earth, and moon. Based on the sailcraft's initial altitude, atmospheric drag is assumed negligible.

For the first two models, the Earth's orbital plane defines the z = 0 plane of the inertial reference frame *I*. The Earth's orbit's eccentricity value is close to 1 so Earth's orbit around the sun is approximated as a circle with constant radius R_{IE} = 1 AU. Earth is assumed to have a negligible axial tilt (zero obliquity) and the sailcraft has an initial circular orbit around Earth's equator. Thus, the ecliptic planes of the Earth around the sun and the sailcraft around the Earth are treated as coplanar. In truth, the geocentric-equatorial reference frame has an inclination of 23.45° with respect to the heliocentric ecliptic inertial (HEI) reference frame [20].

For the third model, the Earth-moon (E-M) system's orbital plane defines the z = 0 plane of the inertial reference frame *I.* The E-M system's orbit's eccentricity value is close to 1 so system's orbit around the sun is approximated as a circle with constant radius R_{IB} = 1 AU. The E-M system is assumed to have a negligible inclination to the sun and the sailcraft has an initial circular orbit around the E-M barycenter. Thus, the ecliptic planes of the E-M system around the sun and the sailcraft around the E-M system are treated as coplanar.

The concept sailcraft is assumed to be self-sufficient in terms of sensing and navigating/correcting course. To limit complexity, the sailcraft's attitude controls are assumed to

be capable of changing attitude immediately and without momentum issues, including providing

instantaneous switching between desired positions.

The concept sailcraft model assumes a rigid, ideal square sail. The solar sail is assumed

to be rigid because "attitude control and thrust vector steering are to be performed very slowly

not to excite structural mode vibrations." [20]. That said, two of the control designs investigated,

on-off switching and orbit rate steering, do require quick 90- or 180-degree turns, respectively.

An ideal sail is here defined as a perfectly reflecting and flat Lambertian surface, devoid of

wrinkles or billowing. A Lambertian surface is "one which appears equally bright when viewed

from any aspect angle" [19]. If the solar sail billowed or had micrometeoroid and orbital debris

(MMOD) damage, it would degrade the sail efficiency.

The following topics are beyond the scope of this thesis. Solar sail design (e.g., sail

material, spar material, or exact layout) is not considered. The concept sailcraft is not confirmed

to be statically stable, i.e., whether the center of mass lies between sun and center of pressure,

which has carryover effects on other aspects of stability [20]. Controls for precession and

nutation or to improve sail attitude stability and thrust vector pointing performance are not

considered. Attitude Determination and Control System (ADCS) sensor options and attitude

control design for conventional spacecraft are not covered.

Thermal and radiation environments are also not considered, including variations in solar

activity and sail operating temperatures. However, it should be noted that the Van Allen radiation

belts would likely negatively affect the solar sail until it reached 45,000 km in altitude. Above

approximately 1,000 km, the Van Allen belts' high level of trapped radiation can greatly reduce

the lifetime of spacecraft components [21]. Depending on geomagnetic conditions, the inner belt

typically spans 6,000 to 12,000 km above Earth's surface and the outer belt spans 25,000 to

45,000 km [22]. A temporary third belt between the inner and outer belt was detected in 2013 [22]. A sailcraft would likely need additional shielding or higher quality materials that can perform the mission at a reduced lifetime in order to counteract the effect of the radiation belts [21]. This thesis focuses on the mission's physical feasibility, not costing feasibility, and therefore does not further explore the Van Allen radiation belts' effects.

Definition of Terms

CubeSat Cube nanosatellite

Sailcraft Solar sail-based spacecraft

List of Acronyms

ADCS Attitude determination and control system

BCR Earth-moon system-centered rotating

CMG Control moment gyros

CNSA China National Space Administration

CR3BP Circular restricted three-body problem

CSA Canadian Space Agency

ECI Earth-centered inertial

ESA European Space Agency

E-M Earth-moon

FDM Finite difference methods

GMAT General Mission Analysis Tool

HEI Heliocentric ecliptic inertial

JAXA Japan Aerospace Exploration Agency

LEO Low-Earth orbit

LQR   Linear quadratic regulator

MALTO   Mission Analysis Low-Thrust Optimization

MMOD   Micrometeoroid and orbital debris

NASA   National Aeronautics and Space Administration

NRHO   Near-rectilinear halo orbit

RCD   Reflectivity control devices

ROSCOSMOS Russian Space Agency

RTN   Radial-tangential-normal

R2BP   Restricted two-body problem

R3BP   Restricted three-body problem

SPICE   Spacecraft Planet Instrument Camera-matrix Events

SRP   Solar radiation pressure

STK   Systems Tool Kit

The thesis is organized as follows: Section 2 reviews the relevant literature on previous solar sail missions, how solar sails work, orbital mechanics, the trajectory design process, actuators, and state space math. Section 3 presents the equations of motions and control algorithms for an ideal solar sail in Earth orbit, using on-off switching to increase altitude, and following a reference logarithmic spiral trajectory to increase altitude. Section 4 reports the simulation results, and the thesis ends with some discussion, conclusions, and recommendations.

Chapter II
Review of the Relevant Literature

Previous Work

This section reviews completed solar sail missions, and relevant solar sail concept papers. Solar sail missions that were halted in development or failed to reach orbit were not included.

Completed solar sail missions. While there are multiple, successfully launched projects with solar sails as their primary means of propulsion [23]–[25], only one has left the vicinity of Earth: IKAROS [24].

IKAROS. JAXA's IKAROS (Interplanetary Kite-craft Accelerated by Radiation Of the Sun) was the first successful solar sail vehicle. It was launched in 2010 and completed an interplanetary mission to Venus. Using only solar sail propulsion, IKAROS spiraled inward from Earth to Venus in six months, completing its initial mission. Over the six months of the nominal cruising phase, the accumulated acceleration was over 100 m/s [24]. Its extended operational phase lasted another 5 years [26]. Its primary objective was to demonstrate key solar sail technologies. It also carried two pieces of equipment for its secondary science missions to perform precise ranging and observe gamma-ray bursts. IKAROS had a total mass of 323 kg and a square solar sail with an area of 196 m^2 [24].
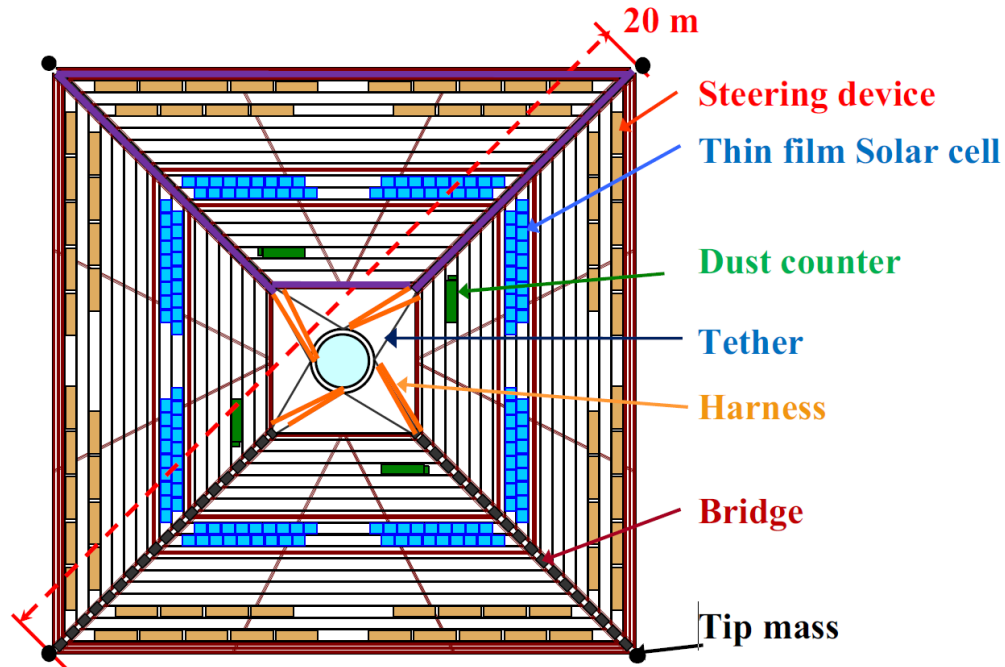
Figure 2.1 IKAROS Solar Sail Layout. The reflectivity control devices are located along the four outer edges of the solar sail (shown in gold) and applied currents change the optical reflectance of their surfaces between diffuse and specular to steer the sail [24].

Reflectivity control devices (RCD) acted as both attitude and thrust vector controls, with a reaction control system for back-up. Once the sail and RCD were unfurled, it stopped using the propellant-dependent conventional thrusters entirely, to prove the sailcraft's viability without propellant. As shown in Figure 2.1, the RCD were located along the four outer edges of the sail and applied currents changed the optical reflectance of their surfaces between diffuse and specular. For example, when one side of the sail had RCD with diffuse reflection and the other side had specular reflection, the SRP on the two sides was inequal and torque was induced to rotate the spacecraft. To complicate matters, IKAROS had to spin constantly to keep its solar sail extended [24]. Therefore, the applied currents' timing had to be designed both to constantly adjust the RCD reflectance to ensure the spacecraft rotated normally and to account for the

baseline rotation when making any course corrections. I thought that was quite an impressive control design.

   NanoSail-D2. NASA's NanoSail-D2 was the first sailcraft to orbit the Earth; it was also the first CubeSat-based sailcraft to do so. It was launched in 2011 to orbit the Earth and re-entered the atmosphere several months later due to atmospheric drag [23]. It also had a secondary objective to investigate the use of a solar sail as a drag sail [27]. Its solar sail was 10 m^2 and the spacecraft mass was 4 kg. NanoSail-D2 lacked active controls; instead, its orbit was determined by SRP, gravity, and atmospheric drag. Katan found that, as a result, the 3U CubeSat presented "varying drag areas throughout its orbit," ranging from 7% to 69% of the total sail area [23]. Unfortunately, limited orbital data was available because it only delivered data for three days. An important finding was that the solar center of pressure was not at the geometric center of the sail, but offset, as a result of manufacturing defects and exposure to the environment [23].

   LightSail 1. The Planetary Society's LightSail 1 was a proof-of-concept demonstration in preparation for LightSail 2. Launched in May 2015, LightSail 1 was a 3U CubeSat with a 32 m^2 solar sail and a mass of 4.93 kg. Notably, it had a solar sail but did not attempt solar sailing due to its low insertion orbit (perigee at 356 km). Instead, its solar sail acted more like a drag sail: just seven days after the solar sail was deployed, the spacecraft burned up on reentry in June. LightSail 1 used torque rods for attitude control to detumble the spacecraft and orient for ground communication, but it did not include a method to change the solar sail's orientation on orbit. A major lesson learned from the mission was to automate sail slewing in LightSail 2 [28].

   LightSail 2. The Planetary Society's LightSail 2 was the first successful demonstration of controlled solar sail propulsion using a CubeSat platform. It was launched in June 2019 to demonstrate the on-off switching method to increase altitude [25]. The sailcraft is expected to

last until late 2021 [29]. Similar to LightSail 1, it was a 3U CubeSat with a total mass of 5 kg and

a square solar sail with an area of 32 m^2 [25]. The sailcraft is shown in Figure 2.2.
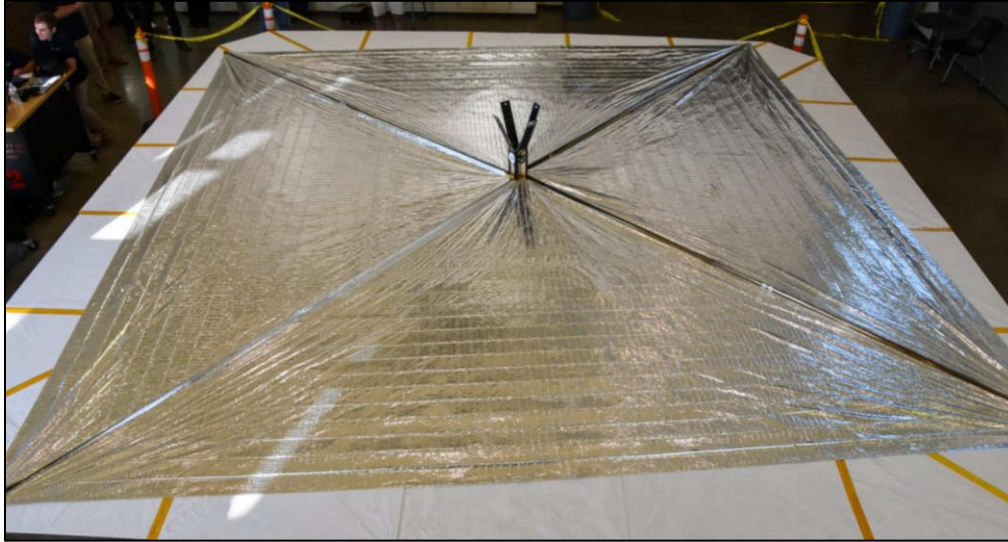
Figure 2.2 LightSail 2 Solar Sail Layout. The attitude control devices (primary gyros and a momentum wheel) are in the 3U CubeSat in the center of the square solar sail [30].

LightSail 2 used primary gyros and a momentum wheel as its active controls and

successfully changed its orbital altitude, the eccentricity of its orbit, and its rate of orbital decay.

Its ADCS software included six operation modes, including Detumble, Magnetic Alignment, and

Solar Sailing. Its Solar Sailing mode is on-off switching, the simplest method to raise the

spacecraft's orbit, helping it compensate for its atmospheric drag. The on and off commands in

the on-off profile sequence were about 50 minutes each, which matches the timing of the pre-

deployment model. However, the spacecraft had difficulty with precision attitude control during

the Solar Sailing mode "due to the large moment of inertia of the deployed sail and the limited

actuators of the CubeSat bus" [25]. The authors were unable to replicate in flight the control gain

solutions found in simulation, potentially due to the sail's non-rigid dynamics, which were not

accounted for in the simulations. Instead, trial-and-error control gains eventually produced successful attitude control [25]. Due to the momentum dumping and imprecise slewing limitations, the apogee altitude increased more slowly than pre-deployment models expected [25], [28].

Since the spacecraft experienced considerable atmospheric drag at 720 km altitude, the authors reported that "solar sails are better-suited to higher orbits … where atmospheric drag is negligible" [25]. This informed my decision to start my sailcraft models higher up at 1,000 km altitude.

Concept papers. Relevant concept papers modeled sailcraft trajectory and thrust vector control designs for possible periodic orbits around a planet [31]; periodic orbits in the Earth-moon three-body problem [18], [32], [33]; and transfer orbits in the Earth-moon system [34]–[36]. Additional concept papers investigated heliocentric logarithmic spiral trajectories [37] and interplanetary transfers to Venus or Mars [38]. Other work involving sailcraft included minimum time trajectories for rendezvous with a near Earth asteroid [39]; active controls in formation flying [40]; and next generation RCDs [41].

The Physics of Solar Sails

This section describes what solar sails look like and how they work.

Solar sail structures. The shape of a solar sail may be a square, a heliogyro, or a disc with a central payload, as shown in Figure 2.3. A square sail has diagonal spars to stretch the sail material taut. It is one of the easiest to model and does not need to spin but the spars can comprise a significant fraction of the sailcraft mass. The heliogyro sail rotates to maintain tension in long, narrow sail "blades" that radiate from the central payload. It does not require spars, but it may need stiffeners along the length of the blades. The disc sail is also kept flat by

spin-induced tension. The disc sail needs no or fewer radial spars than the square sail, but it may require a structural stiffener around its circumference. Since the heliogyro and disc sail configurations must spin, they must be controlled for precession [19].
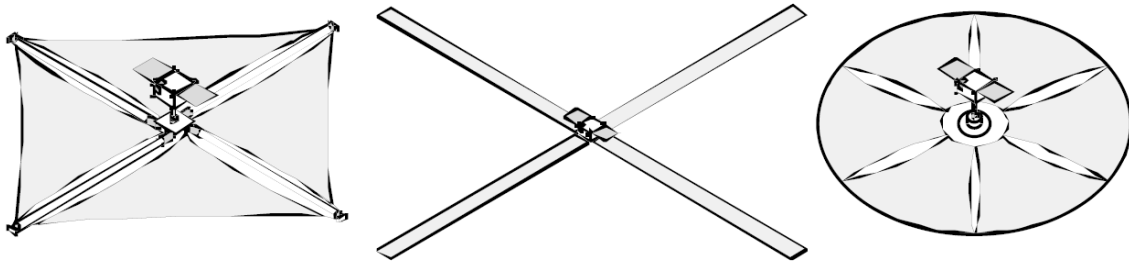
Figure 2.3 Common Solar Sail Structures. The shape of a solar sail may be a square, a heliogyro, or a disc with a central payload. Adapted from [42].

The material of a solar sail should be a suitable substrate and a reflective coating. The substrate ensures the sail can withstand folding, packing, deploying, and performing in the solar wind environment with minimal wrinkles, tears, or degradation. One commonly used substrate is Kapton[1]. The coating ensures maximum photon reflection. The reflective coating may be on one side or on both sides of the solar sail, depending on the sailcraft's trajectory design and weight limit. Both the substrate and coating must be selected with thermal control in mind [19].

Solar radiation pressure. When incident photons strike a solar sail, they transfer momentum from the photons to the sail. The momentum of a single photon is extremely small; therefore, solar sail areas must be extensive to intercept large numbers of photons, so the total momentum transfer is large. The solar radiation pressure (SRP) P exerted on the surface of a flat

---

[1] Registered trademark.

solar sail is the momentum transported <u>by incident photons</u> per unit time per unit area normal to the incident radiation and may be written as

$$P = \frac{1}{A_\perp} \frac{\Delta p}{\Delta t} \qquad (2.1)$$

Where:

P = Solar radiation pressure.

$A_\perp$ = Sail area normal to the incident radiation.

Δp = Momentum transferred by incident photons.

Δt = Time interval.

It is important to note that this relationship remains the same regardless of whether the photons are treated as particles or waves. Also, additional momentum is transferred if the incident photons then reflect off the surface, as is the case for a highly reflective solar sail coating. The pressure exerted on the surface of an ideal (i.e., perfectly reflecting and flat) solar sail due to the total momentum transfer by <u>both</u> incident and reflecting photons is twice that given in Equation 2.1 [19].

As shown in Figure 2.4, incoming photons travel in the direction of $\vec{r}$, the sailcraft inertial position vector that points from the sun to the sailcraft; $\hat{r}$ is the unit vector along that sun-line. The unit vector $\hat{n}$ is normal to the sail plane and $\hat{t}$ is transverse. For an ideal sail, the sail cone angle α is the angle between $\hat{n}$ and $\hat{r}$, and the net force $\vec{F}$ of the photons acting on the sail is in a direction normal to the sail surface [19].

Sail

$\vec{F}$ $\vec{n}$

Incoming
Photons

α

α

$\vec{r}$

α

$\vec{t}$

Specularly
Reflected
Photons
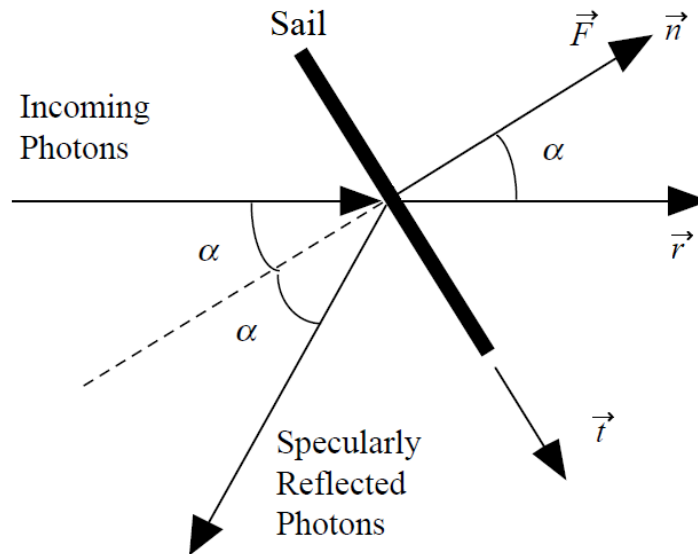
Figure 2.4 Photons Transferring Momentum to an Ideal Solar Sail. The sail cone angle α is the angle between $\hat{n}$, the unit vector normal to the sail plane and $\hat{r}$, the unit vector along the sun-line. Adapted from [20].

The SRP depends on the number of incident photons per time interval, which is in turn dependent on the energy flux from the sun. By extension, P can be rewritten in terms of the sail's distance from the sun and the sun's luminosity:

$$P(r) = \frac{1}{c_0} \frac{L}{4 \pi r^2}$$ (2.2)

Where:

r = Distance from sun to sailcraft.

c_0 = Speed of light.

L = Solar luminosity.

The SRP is assumed to have an inverse square variation with heliocentric distance. This assumption is a decent approximation in this thesis because the sailcraft is not very close to the

sun (greater than 0.047 AU) and the sail area is relatively small and therefore solar radiation incident on opposite ends of the sail is incident along parallel rays [19].

    Force due to SRP. Now armed with an understanding of SRP, the force on – and, by extension, the acceleration of – a solar sail can be found. Using the idealized force model, the total force $\vec{F}$ exerted by SRP on an ideal solar sail is given by [19]

$$\vec{F} = 2\, P\, A\, (\hat{r} \cdot \hat{n})^2\, \hat{n} \tag{2.3}$$

Where:

    $\vec{F}$ = Force on ideal sailcraft due to SRP.

    A = Sail area.

    $\hat{r}$ = Unit vector along the sun-line.

    $\hat{n}$ = Unit vector normal to the sail plane.

Note the factor of two accounts for the pressure from both incident and reflecting photons. Recall the total force on an ideal sail is entirely in the $\hat{n}$ direction.

    Acceleration due to SRP. Dividing Equation 2.3 by the mass of the sailcraft and substituting Equation 2.2 for P, the acceleration $\vec{a}$ of an ideal solar sail due to SRP can be written as [19], [43]

$$\vec{a} = \frac{2\, \eta\, A}{m\, c_0}\, \frac{L}{4\, \pi\, r^2}\, (\hat{r} \cdot \hat{n})^2\, \hat{n} \tag{2.4}$$

Where:

    $\vec{a}$ = Acceleration of ideal sailcraft due to SRP.

η = Sail efficiency.

m = Mass of sailcraft.

Again, a factor of two is included to account for the pressure from both incident and reflecting photons on an ideal sail. The sail efficiency accounts for optical imperfections in the sail's reflective coating and billowing shape. For an ideal sail, $\eta = 1$ [19].

The solar sail characteristic acceleration κ is the magnitude of the acceleration due to SRP at Earth's distance from the sun: one astronomical unit. For an ideal solar sail, the characteristic acceleration κ is given as

$$\kappa = \frac{2\,\eta\,P^*A}{m} = \frac{2\,\eta\,A}{m\,c_0}\frac{L}{4\,\pi\,r^{*2}} \tag{2.5}$$

Where:

κ = Solar sail characteristic acceleration.

P^* = Solar radiation pressure at 1 AU.

r^* = Distance from sun to sailcraft, where:

$r^* \equiv R_{IE} \equiv 1$ AU.

Again, a factor of two is included to account for the ideal sail reflectivity [19].

Substituting Equation 2.5 into Equation 2.4, the acceleration $\vec{a}$ of an ideal solar sail due to SRP can also be written as

$$\vec{a} = \kappa\left(\frac{R_{IE}}{r}\right)^2 \cos^2(\alpha)\,\hat{n} \tag{2.6}$$

Where:

$\kappa \left(\frac{R_{IE}}{r}\right)^2$ = Magnitude of acceleration of sailcraft at distance r from sun due to SRP.

α = Sail cone angle.

For a sailcraft orbiting Earth, generally $|\vec{a}|$ is taken as equal to κ because r is very close to R_{IE} [19]. However, for a sailcraft transiting in cislunar space, the magnitude of the acceleration will differ by 8% between the sailcraft's closest and furthest points from the sun. I consider this difference to be non-negligible and choose not to assume $|\vec{a}| = \kappa$.

The SRP acceleration may also be written in terms of its radial and transverse components [38]:

$$\vec{a} = a_r\,\hat{r} + a_t\,\hat{t} \tag{2.7}$$

Where:

a_r = Radial component of SRP acceleration, where:

$$a_r \equiv \kappa \left(\frac{R_{IE}}{r}\right)^2 \cos^3 \alpha$$

a_t = Transverse component of SRP acceleration, where:

$$a_t \equiv \kappa \left(\frac{R_{IE}}{r}\right)^2 \cos^2 \alpha \sin \alpha$$

Comparing sail designs. The characteristic acceleration, sail loading, and lightness number offer like comparison between different solar sail designs.

Characteristic acceleration. The characteristic acceleration (see Equation 2.5) is a sail's acceleration performance at Earth's distance from the sun. It can also be used to determine the size of the sail needed: if you know the necessary characteristic acceleration for the mission, the

desired payload mass, and the approximate efficiency, you can calculate the required sail area [19].

   Sail loading. Most of the terms in Equation 2.4 relate to the sailcraft's position and orientation with respect to the sun. Two terms that are inherent characteristics of the sailcraft itself are the sail area and mass. The solar sail acceleration has an inverse relationship with the sailcraft mass: the sailcraft must be extremely low mass to generate as large an acceleration as possible from the momentum captured from the incident and reflected photons. And the solar sail should have a very large area to capture as many photons as possible. The sail loading parameter σ is a standard sail performance metric that captures these two inherent characteristics; it is defined as the ratio of sail mass to sail area [19]:

$$\sigma = \frac{m}{A} \tag{2.8}$$

Where:

   σ = Sail loading parameter.

   Lightness number. The solar sail lightness number β is a dimensionless parameter and is defined as the ratio of the SRP acceleration to the solar gravitational acceleration. It can be written as [19]

$$\beta = \frac{\sigma^*}{\sigma} \tag{2.9a}$$

$$\sigma^* = \frac{L}{2\pi\,\mu_O\,c_0} \tag{2.9b}$$

Where:

β = Solar sail lightness number.

μ_O = Gravitational parameter of the sun.

The lightness number is a function of the sailcraft's reflectivity (captured in the sail efficiency η) and mass; hence the name [44].

Cone and clock angles. For an ideal solar sail, the sail normal vector $\hat{n}$ is defined in terms of the sail cone angle α and a sail clock angle δ, which together represent the sailcraft attitude:

$$\hat{n} = \cos\alpha\,\hat{r} + \sin\alpha\cos\delta\,\hat{p} + \sin\alpha\,\sin\delta\,\hat{p}\times\hat{r} \qquad (2.10)$$

Where:

δ = Sail clock angle.

$\hat{p}$ = Unit vector normal to orbital plane.

As previously stated, the sail cone angle α is the angle between $\hat{n}$ and $\hat{r}$. The sail clock angle is the angle between the projection of the sail normal and a reference direction onto a plane normal to the sun-line, as shown in Figure 2.5 [19]. For a sailcraft with one reflective side and one non-reflective side, the sail thrust vector $\hat{n}$ is constrained to be oriented away from the sun: $0° \leq \alpha \leq 90°$ [38].
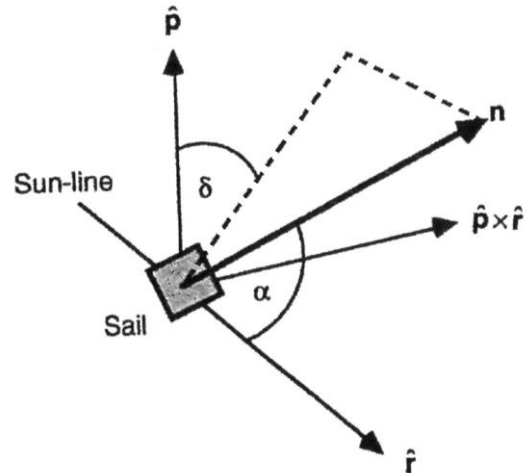
Figure 2.5 Cone Angle α and Clock Angle δ on Solar Sail. Adapted from [19].

Eclipse factor. Since the sailcraft has an equatorial orbit around Earth and is dependent on sunlight for propulsion, a model was created to estimate where the Earth's shadow is (Figure 2.6) and if the sailcraft is in it (Figure 2.7). It assumes the orbit has small eccentricity such that the distance from the center of Earth to the sailcraft $|\vec{r}_E|$ is approximately equal at opposition and at the edge of the umbra (the blue lines in Figure 2.7). This is a decent approximation at the initial low altitudes when the orbit is almost circular. However, the sailcraft's orbit quickly increases eccentricity as it raises orbit. This model assumes the sailcraft remains in the (x, y) plane of E and does not account for the z-direction.
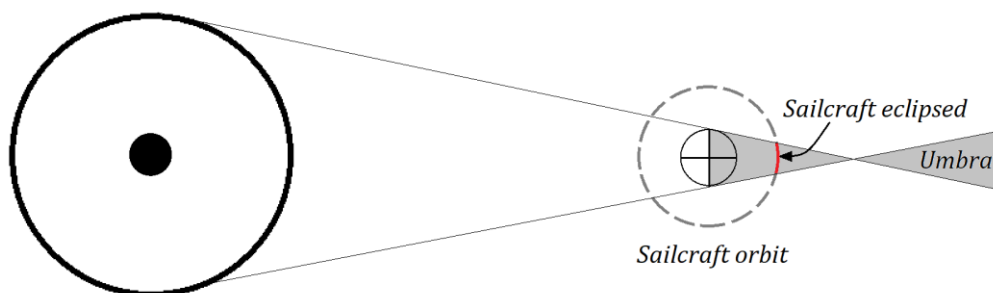
Figure 2.6 Top View of Portion of Sailcraft's Orbit Eclipsed by Earth's Umbra [n*ot to scale*].

Using the rules of similar triangles, the values of a, b, c, d as shown in Figure 2.7 are

given by

$$a = \frac{r_\oplus}{r_O} \frac{R_{IE}}{1 - r_\oplus/r_O} = 1.38 \times 10^6 \text{ km} \tag{2.11a}$$

$$b = \frac{r_\oplus (a - r_E)}{a} \tag{2.11b}$$

$$c = positive\ root\ of\ \left(1 + \frac{b^2}{(a-r_E)^2}\right)c^2 - \frac{2ab^2}{(a-r_E)^2}c + \left(\frac{a^2b^2}{(a-r_E)^2} - r_E^2\right) = 0 \tag{2.11c}$$

$$d = \frac{r_\oplus (a - c)}{a} \tag{2.11d}$$

Where:

$r_\oplus$ = Radius of the Earth.

r_O = Radius of the sun.

$\vec{r}_E$ = Sailcraft position vector from the center of the Earth.

$\vec{R}_{IE}$ = Earth position vector from the center of the sun.

Note a is a constant and b, c, d are dependent on the orbit's current height (i.e.,

sailcraft's distance from center of the Earth). Also of note, the value of a greatly exceeds Earth's

sphere of influence so the geometric diagram given is valid for the sailcraft anywhere in the

cislunar region.

The critical distance, r_{crit}, the point at which the orbiting sailcraft enters or exits Earth's

umbra is given by

$$r_{crit} = \sqrt{(R_{IE} + c)^2 + d^2} \tag{2.12}$$

If the sailcraft's distance from the sun exceeds r_{crit} then the sailcraft is in Earth's umbra.
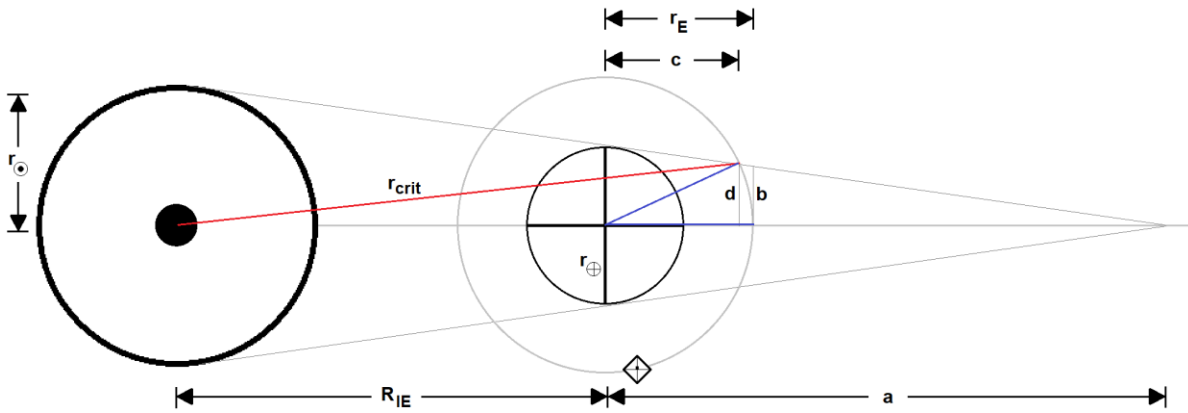
Figure 2.7 Top view of Geometric Diagram to Find r_{crit}, the point at which the orbiting sailcraft enters or exits Earth's umbra [*not to scale*].

Orbital Mechanics

This section is a brief explanation how orbits are defined and how they can be changed – both for general spacecraft and for sailcraft. It also details common reference frames in astrodynamics, orbital dynamics models, and several transfer orbits for sailcraft.

Define an orbit. An orbit is classified by its shape and further described by its orbital elements.

Orbit shapes. Boden states Keplerian spacecraft orbits may be classified as a circle, ellipse, parabola, or hyperbola [21]. There is also a special sub-type of hyperbolic orbit called a rectilinear orbit [19]. Figure 2.8 shows the orbits' respective shapes come from curves formed by the intersection of a plane and a right circular cone called conic sections [21].
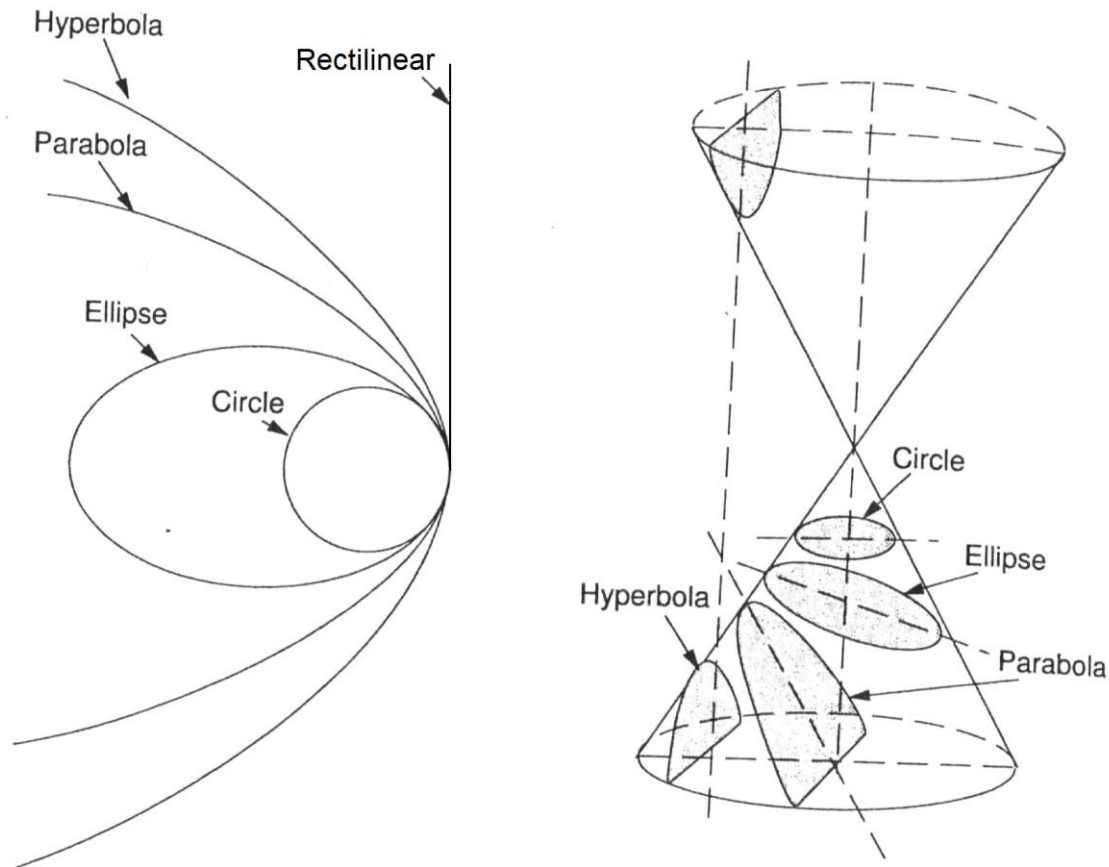
Figure 2.8 Source of Conic Section Orbits' Shapes. Adapted from [21].

Each type of conic section orbit is defined by its eccentricity value (or range of values), which is true for all objects in that type of orbit [21]. The orbit type and corresponding eccentricity are shown in the first and second columns, respectively, of Table 2.1. The table's third column shows for sailcraft specifically, the solar sail lightness number that would produce that type of orbit [19]. The fourth column denotes whether the orbit is a bound trajectory or an escape trajectory.

Table 2.1

Conic Section Orbits

Orbit Type	Eccentricity	Lightness Number	Note
Circular[a]	$e = 0$	$\beta = 0$	Bound trajectory
Elliptical	$0 < e < 1$	$0 < \beta < \frac{1}{2}$	Bound trajectory
Parabolic	$e = 1$	$\beta = \frac{1}{2}$	Escape trajectory
Hyperbolic[b]	$e > 1$	$\frac{1}{2} < \beta < 1$ or $\beta > 1$	Escape trajectory
Rectilinear[c]	$e \to \infty$	$\beta = 1$	Escape trajectory

Note. Adapted from [19]. Lightness Number = Solar Sail Lightness Number.
[a]A circular orbit is a special sub-type of elliptical orbit.
[b]For a lightness number of greater than unity (i.e., 1), the hyperbolic orbit inverts so that the sun occupies the opposite focus of the conic section.
[c]A rectilinear orbit is a special sub-type of hyperbolic orbit.

Parabolic and hyperbolic orbits are considered escape trajectories, whereas elliptical orbits (which includes circular orbits) are bound trajectories. A parabolic trajectory has the minimum amount of energy needed to escape the gravitational attraction of the primary body it orbits [21]. A hyperbolic trajectory has more than the minimum energy needed. The greater its speed, the less the trajectory looks like an arc curving toward the primary body and more like an arc curving away from the primary body. An elliptical orbit lacks sufficient energy to escape and, barring any outside disturbance forces, will trace the same path around the primary body in an inertial frame over time. Such disturbance forces may include atmospheric drag at lower altitudes and the perturbing gravitational force of Earth's oblateness [20]. The velocity V of a spacecraft in a circular orbit, tangential to the orbit, is simply [21]

$$V = \sqrt{\mu/s} \tag{2.13}$$

Where:

   V = Tangential velocity of a spacecraft in a circular orbit.

   μ = Primary body's gravitational parameter.

   s = Distance from center of primary to spacecraft.

   Orbital elements. A spacecraft's Keplerian elliptic orbit can be described by six classical

orbital elements [21]. Five of the elements are constants that describe the size, shape, and

orientation of the orbit, and the final element varies with time to locate the spacecraft along its

orbit at any particular time [20]. For a spacecraft orbiting Earth, its orbital elements are specified

with respect to the Earth-centered inertial (ECI) reference frame [20]. The ECI reference frame

has its origin at the center of Earth but does not rotate with Earth [20], [21]. The X-axis in the

equatorial plane and pointing to the vernal equinox, the Z-axis is along the Earth's polar axis of

rotation, and the Y-axis completes the right-hand set [20], [21].

   The six classical orbital elements, shown in Figure 2.9, are as follows. The semimajor

axis, a, and eccentricity, e, describe the size and shape of the ellipse, respectively. More

specifically, the semimajor axis, a, is half the sum of the radius of perigee and the radius of

apogee, where the perigee is the orbit's point of closest approach to Earth and the apogee is the

farthest point on the ellipse. The inclination, i, denotes the angle between the equatorial plane

and the orbital plane, which intersect along the line of nodes. The right ascension longitude of

the ascending node, Ω, is the angle from the vernal equinox to the ascending node. The argument

of perigee, ω, measures the angle from the ascending node eastward to perigee. Finally, the true

anomaly, θ, defines the angle from perigee to the spacecraft position, measured in the direction

of spacecraft motion [19]–[21].
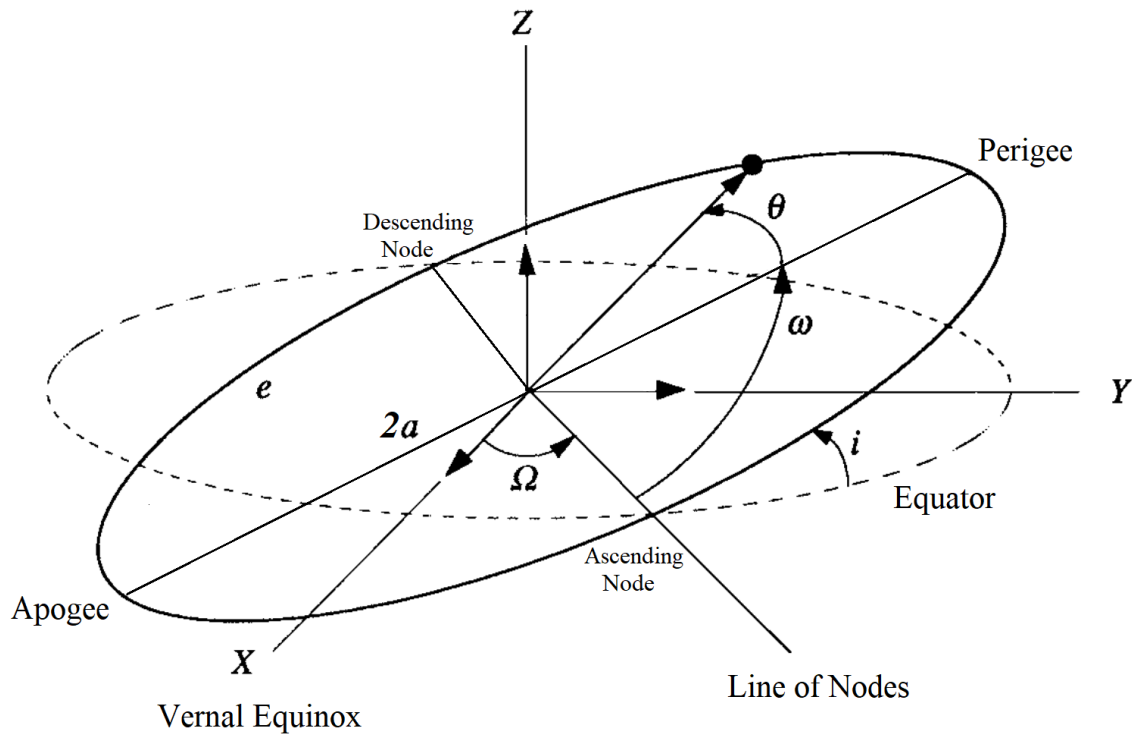
Figure 2.9 The Keplerian Classical Orbital Elements for a Spacecraft in Earth Orbit. Adapted from [20].

An orbit is called "prograde" if its inclination meets $0° \leq i < 90°$, and experiences

precession toward the west. A "polar" orbit has an inclination $i = 90°$. Lastly, a "retrograde"

orbit's inclination meets $90° < i < 180°$ and experiences precession toward the east [21].

Change an orbit. For a spacecraft orbiting a primary body, the total specific mechanical

energy (i.e., the sum of the kinetic and potential energy per unit mass) of the system is

conserved. Therefore, the spacecraft moves slowest at apogee because its potential energy is at a

maximum and its kinetic energy is at a minimum. Conversely, the spacecraft moves fastest at

perigee because its potential energy is at a minimum and its kinetic energy is at a maximum [21].

Changing the spacecraft's orbit requires changing the total energy or changing the direction of the spacecraft without changing the total energy. The total energy is a function of the semi-major axis. Thus, changing an orbit requires changing the semi-major axis or changing the direction of the spacecraft without changing the semi-major axis. Potential energy cannot be "added" to this system. However, by changing its velocity vector through what is known as a "ΔV burn", the spacecraft can gain or lose kinetic energy and thus change the total energy. A ΔV burn can also alter the spacecraft's direction without changing the kinetic and total energies [21].

Posigrade burns are those that increase the spacecraft's velocity, i.e., gain kinetic energy, and retrograde burns are those that slow the spacecraft and lose kinetic energy, as shown in Figure 2.10. Note, regardless of the burn type, the spacecraft will still pass through the burn point on subsequent orbits – until it makes another burn [45]. Therefore, "any maneuver changing the orbit of a space vehicle must occur at a point where the old orbit intersects the new orbit. If the orbits do not intersect, we must use an intermediate orbit that intersects both" [21].
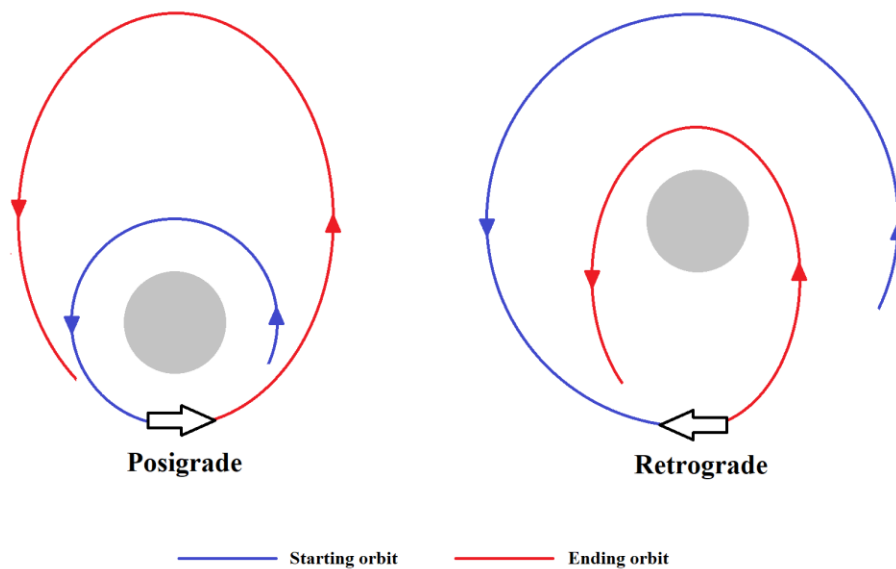
Figure 2.10 Posigrade and Retrograde Burns. Posigrade burns increase the spacecraft's velocity, boosting it to a higher orbit. Retrograde burns brake the spacecraft, slowing it to a lower orbit.

Changing orbital altitude. Changing the orbital altitude (also known as an "orbit transfer" or "orbit raising") requires changing at least the magnitude of the spacecraft's velocity vector [21]. Two examples of ΔV burns that change only the magnitude of the spacecraft's velocity are shown in Figure 2.11.
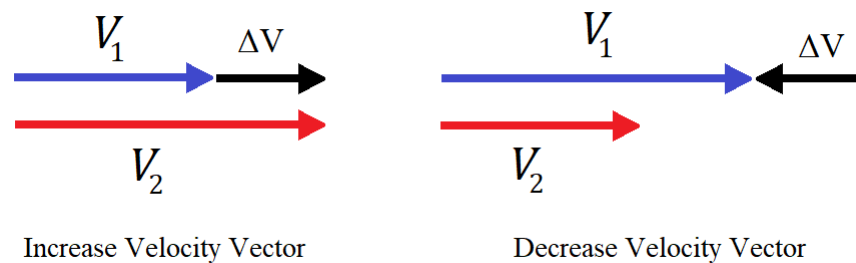
Figure 2.11 Example ΔV burns that Change Orbital Altitude. V_1 is the velocity before the burn and V_2 is the velocity after the burn.

To maneuver, a conventional chemical propulsion spacecraft uses propellant-based thrusters in short bursts for impulsive changes of velocity. The spacecraft's maneuverability is thus limited by the amount of its reaction-mass propellant and each maneuver comes at a cost. A common orbit transfer for chemical propulsion spacecraft is a Hohmann transfer. A Hohmann transfer to increase orbit consists of a high ΔV posigrade burn at perigee to add kinetic energy, increase the semi-major axis, and raise its orbit, followed by a high ΔV posigrade burn at apogee to circularize the higher orbit. A faster but even higher propulsion cost option is a one-tangent burn [21].

Even for a "low-thrust" orbit transfer, the spacecraft must make a series of burns around perigee and one or two burns at apogee to reach a higher (circular) orbit [21]. Thus, it would not

make sense to use the low-thrust orbit transfer approach with a sailcraft, considering the low magnitude SRP force that could be applied during to the limited time per period that it will be near apogee or perigee.

Instead, sailcraft maneuvers require changing the sail's attitude with respect to the sun or changing the sail's reflective properties, each of which produce a smaller "step change" in the sailcraft's acceleration than impulsive thrusters do [34]. The sailcraft may increase its orbital altitude by directing a component of the SRP force in the direction of its velocity vector [19]. These sailcraft maneuvers change the vector field but the sailcraft's trajectory remains continuous in both position and velocity and the state of the sailcraft remains the same. Thus sailcraft maneuvers are considered "zero cost" maneuvers [34].

Changing orbital plane inclination. Changing the orbital plane inclination (also known as "orbit cranking") requires changing at least the direction of the spacecraft's velocity vector [21]. Of note, thrust at ascending or descending nodes will rotate the orbital plane about the line of nodes [45]. The simple and combined plane changes described below apply to all spacecraft and are shown in Figure 2.12. This is followed by a description of a third method of changing the orbital plane inclination that is specific to sailcraft.

A simple plane change alters the inclination of the orbital plane *i* without altering the size or total energy of the orbit. In effect, the direction of the velocity vector is changed, and the magnitude is unchanged. Thus, the required ΔV maneuver must be perpendicular to the orbital plane. The ΔV expression is given by [21]

$$\Delta V = 2V_1 \sin(\Delta i / 2) \tag{2.14}$$

Where:

ΔV = Change in spacecraft velocity.

V_1 = Velocity before and after the ΔV burn.

Δi = Inclination angle change required.

Due to its orientation limitations, a sailcraft cannot direct the SRP force entirely perpendicular to

its orbital plane except if in a polar orbit of Earth.
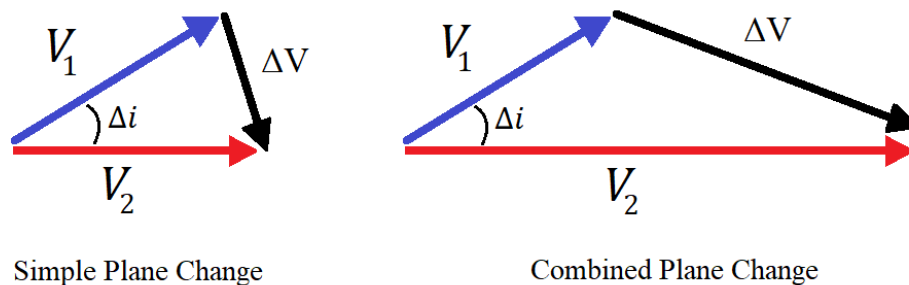
Figure 2.12 Simple and Combined Plane Changes. Example ΔV burns that would change the orbital plane inclination. V_1 is the velocity before the burn and V_2 is the velocity after the burn.

A combined plane change alters both the inclination and the size of the orbit. The

direction and the magnitude of the velocity vector is changed such that the overall ΔV maneuver

is not perpendicular to the orbital plane. The minimum ΔV required (assuming the plane change

combines a Hohmann transfer and a simple plane change) is given by [21]

$$\Delta V = \left(V_1{}^2 + V_2{}^2 - 2V_1 V_2 \cos \Delta i \right)^{1/2} \qquad (2.15)$$

Where:

V_2 = Velocity after the ΔV burn.

Note for both simple and combined plane changes that it is most energy-efficient to change inclination when V_1 is at a minimum, e.g., at apogee of an elliptic orbit [21]. Physically, even a small propulsive force from the spacecraft can greatly alter its inclination when at the end of a large lever arm. For a spacecraft that needs to both raise its orbit and change its inclination at some point during its mission, it would be most energy-efficient to raise its orbit as much as possible before changing its inclination because, again, V_1 would be at a minimum.

Sailcraft may change their orbital plane inclination by alternately directing a component of the SRP force above and below the ecliptic plane every half orbit. The sail cone and clock angles that maximize the out-of-plane SRP force and thus maximize the rate of change of inclination are [19]

$$\alpha^* = \tan^{-1}\left(1/\sqrt{2}\right) = 35.26° \tag{2.16a}$$

$$\delta^* = \begin{cases} 0° & (\cos(\omega + \theta) \geq 0) \\ 180° & (\cos(\omega + \theta) < 0) \end{cases} \tag{2.16b}$$

These specific cone and clock angles result in the following degrees of inclination change per orbit, Δi_p, given by [19]

$$\Delta i_p = 88.2\beta \tag{2.17}$$

Where:

Δi_p = Inclination change per orbit.

Reference frames and orbital dynamics models. Reference frames & orbital dynamics models bring the basics of how an orbit is defined into a larger context to understand where the spacecraft is and to track its movement.

Earth-centered inertial reference frame. The Earth-centered inertial (ECI) reference frame has its origin at the center of Earth but does not rotate with Earth [20], [21]. The X-axis in the equatorial plane and pointing to the vernal equinox, the Z-axis is along the Earth's polar axis of rotation, and the Y-axis completes the right-hand set, as shown in Figure 2.13 [20], [21]. Again, a satellite's or spacecraft's orbital elements are specified with respect to this frame. It is treated as inertial although the Earth rotates and revolves around the sun.
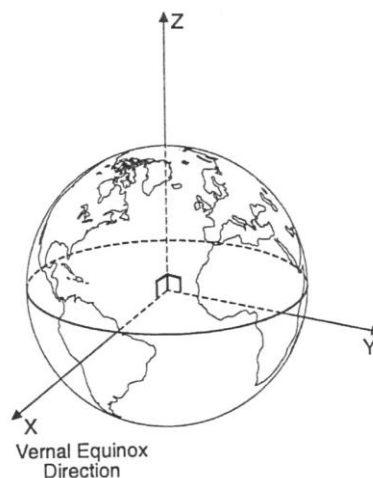
Figure 2.13 Earth-Centered Inertial Reference Frame [21].

Heliocentric ecliptic inertial reference frame. The heliocentric ecliptic inertial (HEI) reference frame has its origin at the center of the sun and is truly inertial within the context of the solar system. The Z-axis is normal to the ecliptic plane defined by the X- and Y-axis.

Radial–tangential–normal reference frame. A spacecraft's attitude can be described in a radial–tangential–normal (RTN) orbital reference frame fixed at the spacecraft's center of mass. As the spacecraft moves along its orbit, its reference frame moves with it. The X-axis points radially toward the primary body it orbits, the Y-axis is along the direction of flight (tangential to the orbit), and the Z-axis completes the set and is normal to the orbital plane [20], [38]. Roll, pitch, and yaw refer to rotations about these axes: roll is around the flight y-axis, pitch is around the normal z-axis, and yaw around the radial x-axis, as shown in Figure 2.14.
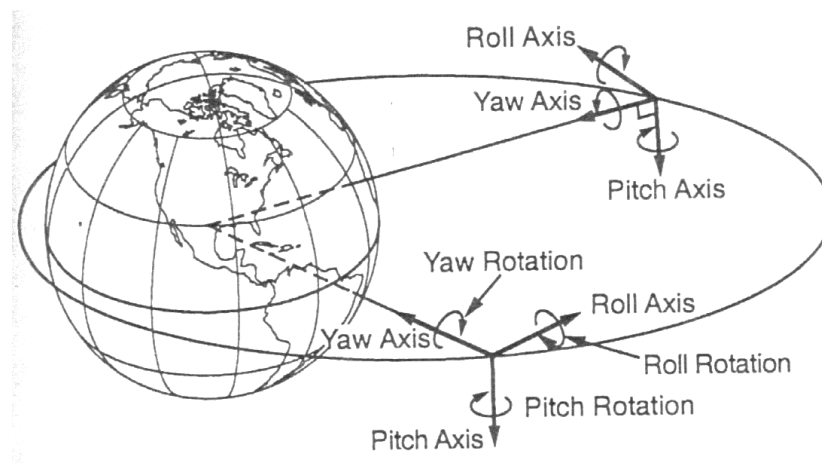
Figure 2.14 Spacecraft Roll, Pitch, and Yaw [21].

Rotating reference frames. Consider a particle *P* in motion relative to reference frame *B*, which is itself in motion relative to reference frame *A*, as shown in Figure 2.15.
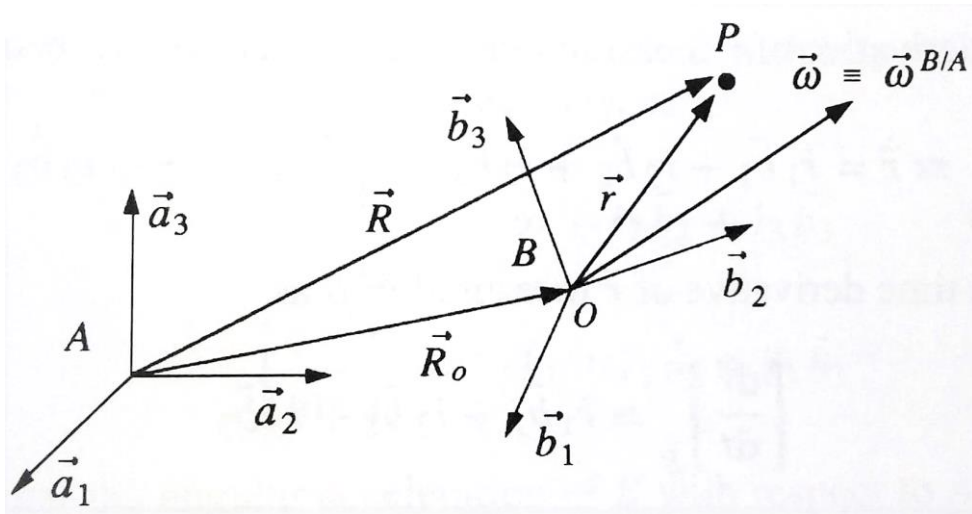
Figure 2.15 Rotating and Translating Reference Frames. A particle *P* moves relative to reference frame *B*, which is itself in motion relative to reference frame *A* [20].

The angular velocity of reference frame *B* with respect to reference frame *A* is defined as $\vec{\omega}^{B/A}$ and the position of the particle from an arbitrary point *O* of frame *B* is defined as $\vec{s}$. The particle's velocity with respect to the point *O* of *B* as seen from *A* can be given as [20]

$$\left\{\frac{d\vec{s}}{dt}\right\}_A = \left\{\frac{d\vec{s}}{dt}\right\}_B + \vec{\omega}^{B/A} \times \vec{s} \tag{2.18}$$

Where:

$\left\{\frac{d\vec{s}}{dt}\right\}_A$ = Rate of change of position vector $\vec{s}$ as seen from reference frame *B*.

$\left\{\frac{d\vec{s}}{dt}\right\}_B$ = Rate of change of position vector $\vec{s}$ as seen from reference frame *A*.

$\vec{\omega}^{B/A}$ = Angular velocity of reference frame *B* with respect to reference frame *A*.

$\vec{s}$ = Position of particle from an arbitrary point *O* of frame *B*.
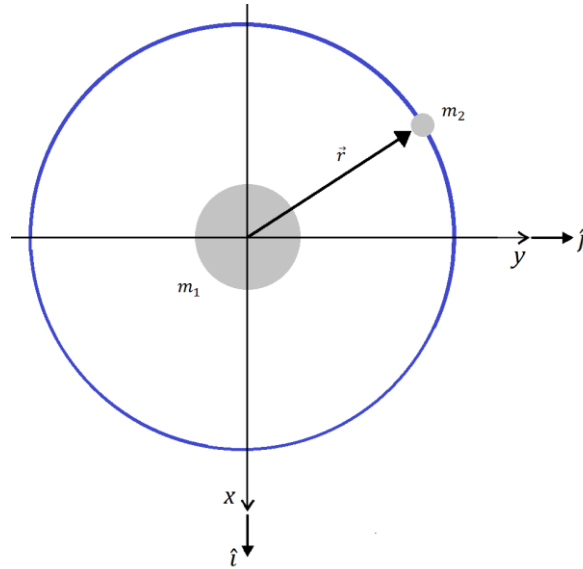
Figure 2.16 Restricted Two-Body Problem (R2BP). An infinitesimal mass m_2 in a circular orbit (blue line) around an inertially fixed primary body of mass m_1, with $m_1 \gg m_2$.

Restricted two-body problems. A restricted two-body problem (R2BP) is an infinitesimal mass m_2 in motion around an inertially fixed primary body of mass m_1, as shown in Figure 2.16. The position $\vec{r}$ of the mass m_2 relative to the center of the primary body can be expressed in Cartesian coordinates as

$$\vec{r} = x\,\hat{\imath} + y\,\hat{\jmath} + z\,\hat{k} \tag{2.19}$$

The physical model only considers the two masses and the gravitational force between them. If $m_1 \gg m_2$, as is the case for a planet or sun and a spacecraft, the force exerted by the infinitesimal mass on the primary body is assumed to be negligible. Energy and angular momentum are conserved for a two-body system [20]. The acceleration $\ddot{\vec{r}}$ of the infinitesimal mass is linearly dependent on the sum of the forces $\sum \vec{F}$ acting on the mass:

$$m_2 \, \ddot{\vec{r}} = \sum \vec{F} \tag{2.20}$$

From Equation 2.20, the equation of motion of the infinitesimal mass relative to the primary

body due to the gravitational attraction of the primary body is given by [19]

$$\ddot{\vec{r}} = -\mu \frac{\vec{r}}{r^3} \tag{2.21}$$

Where:

$\vec{r}$ = Position vector of the infinitesimal mass from the center of the primary body.

μ = Gravitational parameter of the two-body system, where:

$\mu = G(m_1 + m_2)$.

$\mu \approx Gm_1$ = Gravitational parameter of the primary body.

G = Gravitational constant.

Restricted three-body problems. A restricted three-body problem (R3BP) examines the

motion of an infinitesimal mass m in the gravitational field of two primary bodies of mass M_1

and M_2, as shown in Figure 2.17. The position of the mass m relative to the center of mass of the

two primary bodies can be written in Cartesian coordinates as

$$\vec{r} = x \, \hat{\imath} + y \, \hat{\jmath} + z \, \hat{k} \tag{2.22}$$

The physical model only considers the three masses and the gravitational force between them.

The force exerted by the infinitesimal mass on either of the primary bodies is assumed to be

negligible and the infinitesimal mass is assumed to move in the plane defined by the primary

bodies' orbits [20].
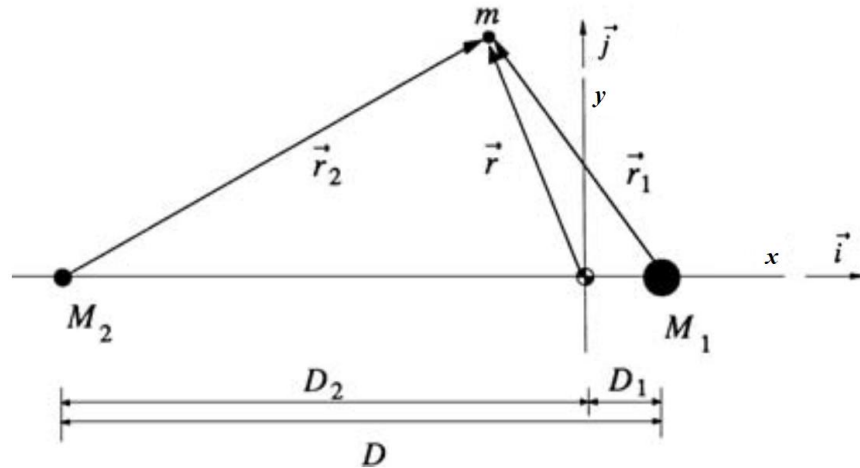
Figure 2.17 Restricted Three-Body Problem (R3BP). An infinitesimal mass m is in motion in the gravitational fields of two primary bodies of mass M_1 and M_2. Adapted from [20].

For a circular restricted three-body problem (CR3BP), the motion of the two primary

bodies is constrained to circular orbits around their center of mass, also known as their

barycenter. The system is assumed to rotate with a constant angular velocity [20]

$$\omega_b = \sqrt{G(M_1 + M_2)/D^3} \tag{2.23}$$

Where:

ω_b = Angular velocity of the system of two primary bodies.

M_1 = Mass of one primary body.

M_2 = Mass of other primary body.

D = Constant distance between the two primary bodies.

The equation of motion of the mass m relative to the barycenter due to the gravitational attraction of the two primary bodies is given by [20]

$$m\ddot{\vec{r}} = -\frac{GM_1 m}{r_1^3}\vec{r}_1 - \frac{GM_2 m}{r_2^3}\vec{r}_2 \tag{2.24}$$

Where:

m = Infinitesimal mass in orbit.

$r_1 = \sqrt{(x - \rho)^2 + y^2 + z^2}$ = Distance from M_1 to m.

$r_2 = \sqrt{(x + 1 - \rho)^2 + y^2 + z^2}$ = Distance from M_2 to m.

$\rho = M_2 / (M_1 + M_2)$ = Mass ratio of the system.

Common Transfer Orbits for Solar Sails

This section details several common transfer orbits for sailcraft, specifically those to increase orbital altitude. Sailcraft maneuvers require changing the sail's orientation to the sun or changing the sail's reflective properties [34]. This thesis focuses on maneuvers performed by re-orienting the sail.

Maximization. An efficient method to conduct orbit transfer maneuvers is to optimize the sail attitude to maximize the component of the SRP force in a given desired direction [19]. An arbitrary unit vector $\hat{q}$ is here defined to represent the desired direction [19]:

$$\hat{q} = \cos\tilde{\alpha}\,\hat{r} + \sin\tilde{\alpha}\cos\tilde{\delta}\,\hat{p} + \sin\tilde{\alpha}\sin\tilde{\delta}\,\hat{p} \times \hat{r} \tag{2.25}$$

Where:

$\hat{q}$ = Arbitrary unit vector.

$\tilde{\alpha}$ = Desired cone angle of arbitrary unit vector $\hat{q}$.

$\tilde{\delta}$ = Desired clock angle of arbitrary unit vector $\hat{q}$.

The SRP force component in the $\hat{q}$ direction is maximized for an ideal sailcraft if the sail clock

angle δ and the sail cone angle α respectively satisfy [19]

$$\delta = \tilde{\delta} \tag{2.26a}$$

$$\tan \alpha = \frac{-3+\sqrt{9+8\tan^2 \tilde{\alpha}}}{4 \tan \tilde{\alpha}} \tag{2.26b}$$

The desired cone angle $\tilde{\alpha}$ may lie between 0 and 90 degrees, with 0° being parallel (radial) to the

sun-line and 90° being perpendicular (transverse) to the sun-line, as shown in Figure 2.18.
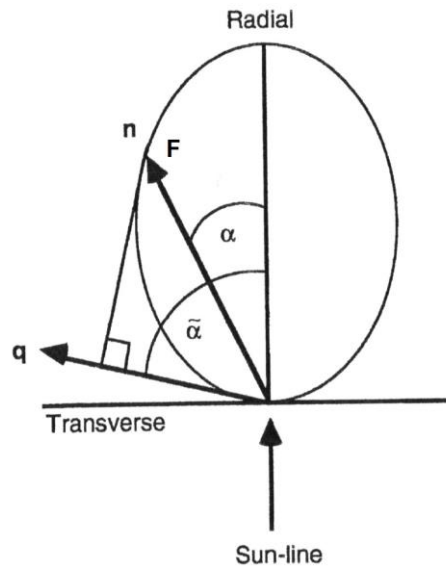
Figure 2.18 Optimization of the Sail Cone Angle [*top view*]. Adapted from [19].

The sail cone angle that maximizes the radial component of the SRP force on the sailcraft

is $\alpha = 0°$. The sail cone angle that maximizes the transverse component of the SRP force on an

ideal sailcraft is $\alpha = \tan^{-1}(1/\sqrt{2}) = 35.26°$ [20]. If α exceeds 35.26°, a component of the SRP

force is directed toward the sun, opposite the direction of motion, and the sailcraft will slow. To

raise the sailcraft's orbit quickly, the component of the SRP force should be maximized in the

direction of the sailcraft's velocity vector whenever possible [19].

Spiral trajectories. Spiral trajectories exploit a sailcraft's continuously thrusting

capabilities. This subsection explores three types of spiral trajectories available to sailcraft for

increasing orbital altitude: on-off switching, orbit rate steering, and logarithmic spiral

trajectories. There are additional orbit-raising methods that are more efficient than on-off

switching and orbit rate steering but add comparatively little efficiency for additional complexity

[19]. Due to their complexity, these additional methods are not considered in this thesis.

In general, the change in velocity ΔV for a spiral trajectory between two circular orbits is

approximately

$$\Delta V = |V_2 - V_1| \tag{2.27}$$

where V_1 and V_2 are given by Equation 2.13 [21].

On-off switching. On-off switching is the simplest method of sailcraft orbit

maneuvering. As the sailcraft moves away from the Sun in its orbit around Earth, the spacecraft

is oriented to maximize sail area perpendicular to the Sun, receiving maximum radiation pressure

to increase its orbital energy and therefore increase its altitude. As the spacecraft returns on the

other side of Earth, it is re-oriented as edge-on to the Sun, minimizing solar pressure, so the Sun

does not reduce its orbital energy [25]. In short, the sailcraft directly faces the sun as its 'on'

position and is oriented edgewise to the sun as its 'off' position, as shown in Figure 2.19 [19].

For Equation 2.4, $\hat{n} = \hat{r}$ when 'on' and $\hat{n} \perp \hat{r}$ when 'off'. This method requires two rapid 90°

rotations per orbit, assuming the sailcraft has a reflective coating on one side [19].

Figure 2.19 Orientation of Sailcraft For On-Off Switching. The sail faces the sun directly as its
'on' position and orients edgewise as its 'off' position [*top view*]. Adapted from [19].

The transverse thrust $\tilde{T}_t$ experienced by the sailcraft conducting on-off switching is thrust

transverse to the sailcraft's orbit around Earth, not transverse to the direction of SRP force. Its

magnitude is given by [19]

$$\tilde{T}_t(\theta_E) = \begin{cases} 0 & (0° \leq \theta_E < 180°) \\ \varepsilon \, m \, \kappa \left(\frac{R_{IE}}{r}\right)^2 \cos(\theta_E - 270°) & (180° \leq \theta_E < 360°) \end{cases} \tag{2.28}$$

Where:

$\tilde{T}_t$ = Transverse thrust due to SRP and controls.

θ_E = Angle between sun-Earth vector $\vec{R}_{IE}$ and Earth-sailcraft vector $\vec{r}_E$.

ε = Eclipse factor, where:

$\varepsilon = 0$ If the sailcraft is in umbra.

$\varepsilon = 1$ If the sailcraft is in sunlight.

Assuming the sailcraft has a relatively small sail area and does not accelerate quickly, then its radial thrust components approximately cancel over the course of one 'on' period. Thus, the actual thrust vector experienced by the sailcraft conducting on-off switching can be approximated as

$$\vec{\tilde{T}}\,(\theta_E) \approx \begin{cases} \vec{0} & (0° \leq \theta_E < 180°) \\ \varepsilon\, m\, \kappa \left(\frac{R_{IE}}{r}\right)^2 \hat{r} & (180° \leq \theta_E < 360°) \end{cases} \tag{2.29}$$

Where:

$\vec{\tilde{T}}$ = Actual thrust vector due to SRP and controls.

For the size of a solar sail that can fit in a CubeSat, this is a reasonable assumption. For a very large area solar sail, this would not be a reasonable assumption.

Orbit rate steering. A more complex method of orbit maneuvering, orbit rate steering varies the sail's attitude to the sun as it rotates around Earth. More specifically, the steering law directs the sailcraft to rotate at half the orbit rate, as shown in Figure 2.20. That is, the sail pitch rate is related to the orbit rate by [19]

$$\frac{d\alpha}{dt} = \frac{1}{2}\frac{d\theta_E}{dt} \tag{2.30}$$

Where:

$$\frac{d\alpha}{dt} = \text{Sail pitch rate.}$$

$$\frac{d\theta_E}{dt} = \text{Sailcraft orbit rate.}$$

With this method, the sailcraft can gain limited energy even when the solar sail is approaching

the sun. However, this method requires one rapid 180° rotation per orbit, assuming sailcraft has

reflective coating on one side. The maximum sail turning rate is a limiting factor for determining

the trajectory's efficiency [19].
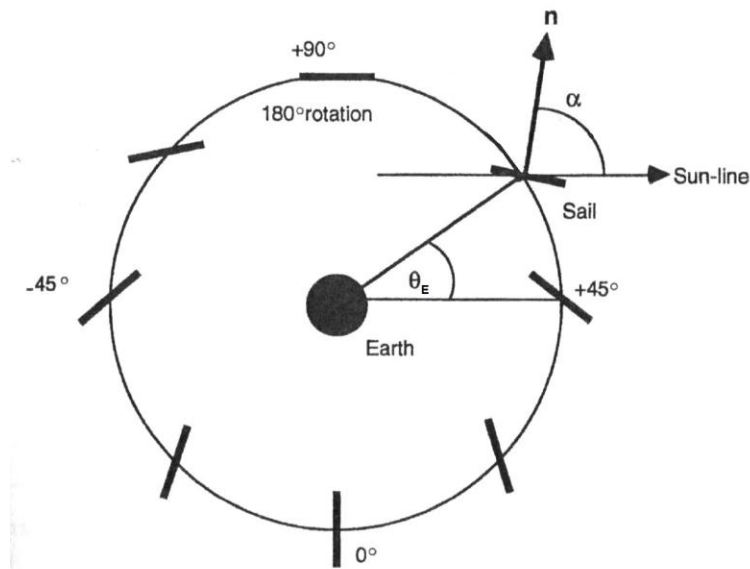
Figure 2.20 Orientation of Sailcraft For Orbit Rate Steering. The sail's attitude to the sun slowly varies as it rotates around Earth [*top view*]. Adapted from [19].

The transverse thrust experienced by the sailcraft conducting orbit rate steering is given

by [19]

$$\tilde{T}_t(\theta_E) = \varepsilon \, m \, \kappa \left(\frac{R_{IE}}{r}\right)^2 \left|\cos^3\left(45° + \frac{\theta_E}{2}\right)\right| \qquad (0° \leq \theta_E \leq 360°) \quad (2.31)$$

Logarithmic spiral trajectories. The main advantage of logarithmic spiral trajectories is that they offer exact solutions rather than numerical solutions to the sailcraft's equations of motion [25]. Each trajectory solution is characterized by the sail attitude being constant in an orbital reference frame [37]. That is, the sailcraft's velocity vector is at a fixed angle to the instantaneous radius vector, as shown in Figure 2.21 [19]. The constancy of the sail attitude means a very simple control law can produce a logarithmic spiral trajectory. In addition, the exact solutions do not require specific assumptions about the sail performance [37].
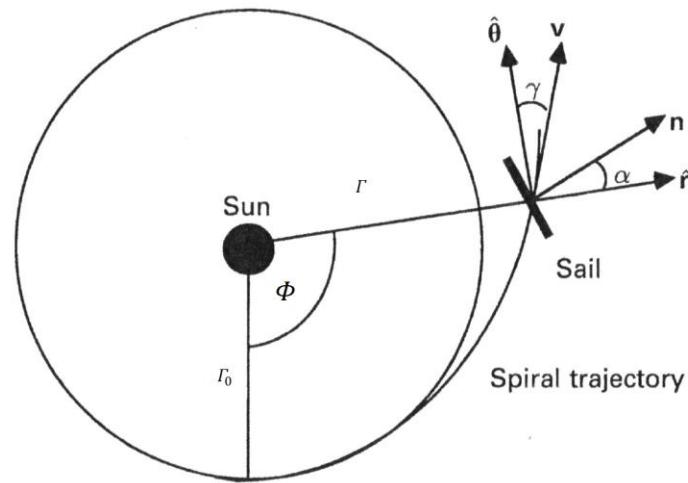
Figure 2.21 Orientation of Sailcraft For Logarithmic Spiral Trajectories. The sail's attitude to the sun is constant as it orbits [*top view*]. Adapted from [19].

The main disadvantage of logarithmic spiral trajectories is that they have poor flexibility, which makes some important mission scenarios infeasible [37]. Most egregiously, they do not offer continuous solutions for circle-to-circle orbit transfers, which results from the initial and

final solar sail velocity vectors not matching that of the initial and final orbits [19], [37]. Also, the logarithmic spiral trajectory literature focuses on heliocentric, not planet-centered, transfer orbits.

For logarithmic spiral trajectories in the ecliptic plane, the clock angle δ is 90°. The cone angle α determines the sailcraft's motion. One logarithmic spiral solution to the sun-centered equations of motion is

$$\Gamma(\theta) = \Gamma_0 \, e^{\Phi \tan \gamma} \tag{2.32}$$

Where:

Γ = Instantaneous radius of trajectory.

Γ_0 = Initial radius of trajectory.

Φ = Angle subtended by the arc between the instantaneous and initial radii.

γ = Spiral angle.

The spiral angle is the angle between the sail velocity vector and the transverse direction [19].

The relationship between the sail pitch angle α and the spiral angle γ can be approximated for small spiral angles as

$$\tan \gamma = \frac{2 \, \beta (\cos \alpha)^2 \sin \alpha}{1 - \beta (\cos \alpha)^3} \tag{2.33}$$

The relationship between the solar sail lightness number and the optimal sail pitch angle α^* that minimizes the transfer time is

$$\beta - \frac{2}{\cos \alpha^*} \frac{1-2\,(\tan \alpha^*)^2}{2-(\tan \alpha^*)^2} = 0 \qquad (2.34)$$

For a given lightness number, Equation 2.34 can be solved to obtain the required sail pitch angle. Then Equation 2.33 can use the given lightness number and sail pitch angle solution to find the ideal spiral angle [19].

To generate preliminary heliocentric solar sailing trajectories, McInnes recommends using a combination of simple logarithmic spiral trajectories and locally optimal sail-steering laws which maximize the instantaneous rate of change of selected sailcraft orbital elements [19].

Trajectory Planning and Design

This section describes the process of designing trajectories to complete a given mission, as well as several commonly used trajectory design programs.

Orbit planning process. Based on my literature review, I consider orbit planning and trajectory design two different, though related processes. Orbit planning comes before trajectory design to get a rough idea of the design space before getting more exact solutions. Wertz notes orbit planning has no absolute rules but offers the following orbit planning process framework for consideration [21]:

1. Establish orbit types

2. Determine orbit-related mission requirements

3. Assess applicability of specialized orbits

4. Evaluate whether single satellite vs. constellation is needed

5. Do mission orbit design trades

6. Assess launch and retrieval or disposal options

7. Evaluate constellation growth and replenishment (if applicable)

8. Create ΔV budget

9. Document work and iterate as needed.

Using Wertz's orbit planning process, I first divide the space mission into segments and establish an appropriate orbit type for each segment. For this thesis's selected case study of a solar sail starting in a circular orbit above Earth and then transiting toward the moon, the mission has three segments: a parking orbit around Earth to match conditions between the launch and transfer phases, a transfer orbit from Earth orbit to lunar vicinity, and a space-referenced orbit in the vicinity of the moon to deliver supplies. Of the three segments, this thesis focuses on the second one: the transfer orbit toward the moon.

The next two steps in the orbit planning process are to determine orbit-related mission requirements for each segment and to assess the applicability of specialized orbits for each segment. Requirements that affect transfer, parking, and space-referenced orbits include orbit decay rates and long term orbit stability, radiation and thermal environments, and accessibility by launch or upper stage vehicles (ΔV required) [21].

For simplicity, in the first two models, the sailcraft is assumed to start in a circular equatorial parking orbit around Earth at 1000 km altitude, which is a reasonable injection altitude by a commercial launch vehicle and where drag can be treated as negligible. In the third model, the sailcraft is assumed to start in a circular parking orbit around the E-M barycenter in the E-M plane of motion and with initial closest point of approach to Earth at 1000 km altitude. As the sailcraft maneuvers to raise its orbit, its perigee should not fall significantly below the initial altitude of 1000 km. The transfer orbit from Earth to the moon should minimize the transit time, while meeting the zero-propellant use constraint and physical limitations of the solar sail's

orientation. At some point during the mission, the sailcraft must orbit crank to match the moon's inclination from Earth's ecliptic.

Specialized parking orbits include geosynchronous, sun-synchronous, Molniya, and polar orbits but are not useful for the application of parking before transferring orbits [21]. Although the name seems to lend itself to solar sail missions, sun-synchronous orbits are generally for taking imagery of Earth's surface under consistent lighting conditions [45]. For its transfer orbit segment, the sailcraft must apply a continuously thrusting spiral trajectory to reach a higher orbit. For the space-referenced orbit around the moon, the specific orbital elements depend on the particular mission application. One possible specialized orbit for this segment would be NRHO if the sailcraft is to deliver supplies to NASA's Gateway.

Recall from the Limitations and Assumptions section in Chapter 1, the concept sailcraft is assumed to be self-sufficient in terms of sensing and navigating/correcting course. Therefore, it is assumed to have sun sensors, star cameras, computer star maps, and accelerometers to determine its location and orientation and an onboard computer to provide control signals to actuators. The sailcraft is assumed to not require uplink sensor data from Earth to navigate or adjust course nor downlink scientific sensor data, therefore none of its three orbit segments are limited by ground station coverage.

The fourth step is to choose a single satellite or constellation for the mission [21]. For the purpose of this thesis, a single spacecraft was chosen. Constellation missions are generally limited to science observation, telecommunications, and global positioning purposes which require satellite coverage at multiple places around Earth or coverage of one area by multiple satellites.

The fifth step in the process is to do design trades, evaluating the effects of different orbits on the mission as a whole. Start by assuming a circular orbit if applicable, conduct altitude and inclination trades, and evaluate the use of eccentric orbits. This process establishes a range of potential altitudes and inclinations, from which I can select one or more alternatives. Trades can also be done based on acceptable risk. For example, some orbit methods allow low orbit deployment for equipment checkout prior to raising orbit which can lower the mission risk [21].

Step six is to assess launch and retrieval or disposal options. How the mission begins and ends does affect the mission itself. The launch vehicle strongly contributes to the total mission cost and ultimately limits the amount of mass that can be placed in the desired orbit. Historically, retrieval and disposal of the spacecraft at the end of the mission was not generally considered important. However, the exponential increase in orbital debris has led to wider recognition of the importance of this design step. Options for the spacecraft at the end of its mission include a controlled reentry, burning up in the atmosphere, and on-orbit retrieval to refurbish and reuse spacecraft [21]. Placing the spacecraft in a graveyard orbit (above 36,100 km altitude) is the least desired since it only delays in the inevitable [46].

The seventh step is not applicable for this thesis and the final ninth step is not covered.

The eighth step is to create ΔV budget. For a conventional chemical propellant-based spacecraft, the ΔV budget is a large factor in the final cost of a space mission due to the cost of launching the propellant and storage tanks required for the mission [21]. For a sailcraft, the ΔV budget is more closely tied to the area and material selected for the solar sail. For this thesis, the total ΔV is the sum of the ΔV to go from Earth orbit to moon orbit and the ΔV to change inclination from the Earth's ecliptic to the moon. Minor attitude corrections made to follow the reference trajectory are assumed negligible, i.e., $\Delta V = 0$ for attitude corrections.

Trajectory design process. After completing the orbit planning process to outline mission constraints and restraints and to get an idea of acceptable values, I can move on to the trajectory design process to find specific trajectory solutions. It is important to note a trajectory is defined as "a set of states that satisfies a set of equations of motion" [35]. Various authors ([18], [31], [33], [35], [36], [47]) have used the following approximate framework for spacecraft trajectory design:

1. Set the mission constraints.

2. Determine the dynamical model to be used.

3. Define the objective of the controls problem.

4. Make an initial guess for the solution.

5. Generate possible trajectories.

6. Refine the solution set.

Wawrzyniak and Howell warn that general spacecraft trajectory design is already difficult, but that "generating solar sail trajectories in multi-body regimes is particularly challenging." [33]

Setting the mission constraints is the first step in the trajectory design process and is accomplished by completing all steps in the orbit planning process of the previous section.

The second step is to determine the dynamical or physical model to be used (in this case, CR3BP). From there I can select appropriate equations of motions to model the behavior of sailcraft in the E-M system. The ideal sailcraft's vector equation of motion in the E-M barycenter's rotating reference frame is given by [18], [19], [31], [33]

$$\ddot{\vec{r}}_b + 2\vec{\omega}_b \times \dot{\vec{r}}_b + \nabla U = \vec{a} \tag{2.35}$$

Where:

$\vec{r}_b$ = Position vector of sailcraft relative to the center of mass of the two primary bodies.

$\vec{\omega}_b$ = Angular velocity of the system's rotating reference frame with respect to the sun's inertial frame.

∇U = Gradient of a pseudo-potential that includes the centripetal acceleration and the gravity effects of the two primary bodies.

$\vec{a}$ = Acceleration of sailcraft due to SRP.

Note the units of the system are chosen such that the position vector, angular velocity, SRP acceleration, and sum of the primary bodies are dimensionless.

The third step in the trajectory design process is to define the objective of the controls problem. The objective is often chosen with minimizing the mission cost in mind: propellant-based spacecraft controls are designed to minimize the fuel needed and sailcraft controls are minimum time problems. In this thesis, the objective of the optimal control problem is to find the states $x(t) = [x \quad y \quad z \quad vx \quad vy \quad vz]^T$ and controls $u(t) = [u_x \quad u_y \quad u_z]^T = (\alpha, \delta)$ over time that abide by the dynamics in my chosen model (see Equation 2.35) while stabilizing the system and minimizing the transit time from Earth to the moon [31].

The fourth step is to make an initial guess for the solution, that is, the trajectory or trajectories that satisfy the equations of motion in Equation 2.35 and the controls objectives. The variables that require initial guess values will depend on the trajectory generation methods employed in the fifth step. For example, Vance et al. note the differential corrector method requires an initial guess for the orbital period and the initial conditions $x(t = 0)$ [36]. Wawrzyniak and Howell recommend the survey technique: "multiple grids of initial guesses are

created and then used to initialize a numerical solution technique for boundary-value problems that generates feasible trajectory options" [35].

Generating possible trajectories is the next step in the process. The possible trajectories are numerical solutions to the sailcraft's equations of motion, typically found through numerical integration, linearization relative to a known solution, or analytical approximations [33], [37]. Due to the complex and competing constraints on the sailcraft's trajectory, there is no single, simple trajectory solution. (The one exception is logarithmic spiral trajectories, which offer exact solutions, as previously discussed.) Instead, it is generally necessary to identify multiple possible trajectories in order to weigh the best option that meets most of the constraints. The additional simulated solutions comes at a non-negligible computational cost, though the cost can be "significantly" reduced via closed-form analytical solutions [37]. The following is a brief discussion of numerical solution methods.

One example of a numerical integration method is an initial-value problem. If one set of position and velocity states and its time is known – or given in the initial assumptions – the trajectory can be considered an initial-value problem. Then the solution can be found via explicit or implicit integration methods [35].

Investigating the motion of a sailcraft above the E-M ecliptic, Simo and McInnes found periodic solutions to the sailcraft's unusual orbit in two steps, using both linearization and analytical approximations. First, they linearized the system of nonlinear, nonautonomous ordinary differential equations of motion. Then they used a Laplace transform to derive a first-order analytical solution [18].

Heiligers et al. solved their sailcraft's optimal control problem numerically in two parts. The first part applied a "direct method based on pseudo-spectral transcription" in PSOPT, an

open source software tool written by V.M. Becerra [31]. The resulting non-linear programming problem was solved in the second step through IPOPT [48], an open source interior point method for large-scale problems [31].

Wawrzyniak and Howell investigated three common numerical strategies to generate sailcraft trajectories: shooting methods (also known as differential corrections processes), finite difference methods (FDMs), and collocation strategies but noted that other numerical tools do exist. The shooting methods compute trajectory variations relative to a reference solution to the sailcraft's nonlinear differential equations of motion: they linearize the reference solution, numerically integrate it, and then use a state transition matrix to linearly correct the trajectory's position and velocity states. Shooting methods may be described as single shooting or multiple shooting, depending whether the trajectory solution is one long arc or broken into multiple shorter arc segments for stability of the numerical process, respectively [33]. Vance et al. (2020) used single-shooting methods to generate sailcraft trajectories to access NASA's proposed Lunar Gateway's halo orbit [36].

FDMs take a more holistic approach to the trajectory generation process. A simple guess for the trajectory, such as a circular orbit or a static point, is discretized into a series of position vectors over time [33], [35]. FDMs are simple to understand and implement but are limited in local accuracy by the size of the time step between two consecutive position vectors. Wawrzyniak and Howell prefer the use of FDMs for time-dependent control profiles or for a "general understanding" of the design space from a "relatively quick" analysis [33].

Collocation methods discretize both the trajectory and control, and then deliver a solution for the discretized states simultaneously. Collocation methods minimize the difference between the derivative of a continuous approximating polynomial and the derivative from the equations

of motion at an intermediate point on an arc between time steps along the trajectory. Collocation methods are relatively insensitive to a poor initial guess and relatively accurate compared to other solution methods but are more complex due to their use of higher-degree polynomials. Wawrzyniak and Howell recommend the use of collocation methods for solving boundary value problems, including optimal control problems [33]. Collocation-based software includes DIDO [49], GPOPS [50], [51], and MATLAB's BVP*C functions (* = 4,5,6) [52], [53].

The final step in the trajectory design process is to refine the solution set. Refining the solution set may consist of conducting trade studies to identify among the trajectory solutions the best option that meets the mission constraints and control limitations. Or it may consist of adding complexity to the model, such as removing the assumption of a flat sail and modeling a sail that can billow. It may also consist of finding a less-accurate or low-fidelity solution in order to get a relatively quick idea of a possible solution(s) and then plugging it into a higher-accuracy or high-fidelity method to get a more exact solution [33].

A possible seventh step would be to automate the trajectory design process to quickly iterate steps 1 through 6 for new initial condition values or mission constraints. For example, Bosanac et al. developed a preliminary agile framework for trajectory design – and redesign – for low-thrust CubeSats transiting from Earth departure to lunar orbit. In the case the project timeline shifts, thus changing the departure conditions, their new trajectory design solutions still satisfy the mission and hardware requirements [47].

Trajectory design program options. NASA's Small Spacecraft Virtual Institute has a very useful list of software tools for the development of small spacecraft missions [54]. The following trajectory design programs are four examples of publicly available software from either NASA or the Open-Source community. This list is by no means restrictive.

SPICE. The Spacecraft Planet Instrument Camera-matrix Events (SPICE) Toolkit offers free trajectory design for small satellite and CubeSat missions [54]. The SPICE Toolkit is offered in several languages, including MATLAB. NASA's Planetary Science Division' s Navigation and Ancillary Information Facility built SPICE to assist NASA engineers from mission concept development through execution of planetary exploration missions and to assist NASA scientists in post-mission analysis of data from space-based scientific instruments. It has been used on such missions as Cassini, Mars Exploration Rover, and Deep Space Network communications [55].

GMAT. The General Mission Analysis Tool (GMAT) is a free, open source program from NASA Goddard Space Flight Center for designing, modeling, and optimizing spacecraft trajectories [54]. It stands alone but can be used in coordination with other programs such as Copernicus. GMAT is capable of modeling of both impulsive ΔV maneuvers and continuous thrust propulsion [56].

STK Astrogator. AGI Systems Tool Kit (STK) Astrogator is a popular extension of the for-pay STK program. It offers trajectory design for all phases of mission planning, from initial estimations to final high-fidelity solutions. It can develop, refine, optimize, and validate solutions for transfer, station-keeping, rendezvous, and proximity operations, as well as provide 3D visualization of the trajectory models in STK. It even enables users to create custom, repeatable workflows to automate regular tasks and data products [57]. The Astrogator's Guild publishes free scenarios and tutorials to use with the STK Astrogator program [54].

Trajectory Browser. NASA Ames Research Center's Trajectory Browser website lets the user search for trajectories based on the user's desired constraints, but it does not include Earth's moon as a possible destination. Instead, it focuses on other planets and near-Earth

asteroids and comets. It includes a visualizer to review and compare possible trajectories [54], [58].

Other options. The following are also common trajectory design programs but have restricted access. NASA Jet Propulsion Laboratory's Mission Analysis Low-Thrust Optimization program (MALTO) and Johnson Space Center's Copernicus Trajectory Design and Optimization System are only available to federal employees and contractors working on applicable projects. MALTO is an easy-to-use software tool for the preliminary design and optimization of low-thrust interplanetary trajectories [59]. Copernicus is a Python-based graphical user interface capable of solving a range of trajectory design and optimization problems. These include trajectories centered about any planet or moon in the solar system, trajectories influenced by two or more celestial bodies such as libration point trajectories (halo orbits), E-M and interplanetary transfers, and asteroid and comet missions [60].

Attitude Control and Design

Getting a spacecraft from point A to point B requires more than just a means of propulsion. An ADCS and a navigation subsystem are also needed for mission success. The ADCS includes sensors to determine orientation, actuators to change or maintain orientation, and digital control algorithms to process inputs from the sensors and to output commands to the actuators. These digital control algorithms can be complex to meet or at least balance the priority of multiple requirements: effecting the right orientation at the right time or at the right point along the spacecraft's trajectory to the desired accuracy. Doing so requires an information exchange with the navigation subsystem; correcting for disturbances; and ensuring spacecraft stability [21]. This section summarizes actuator hardware options. ADCS sensor options and the process to design attitude control algorithms for general spacecraft are not covered. The process

to design attitude control algorithms for sailcraft is covered in the Common Transfer Orbits for Solar Sails section since thrust vector controls are equivalent to attitude controls for a sailcraft.

The purpose of actuators is to change and maintain the orientation of the spacecraft [21]. For a sailcraft, the orientation is defined by the cone and clock angles [19]. I focused on actuators options that use no propellant since my concept sailcraft is supposed to use zero propellant; conventional propellant-based thrusters are summarized at the conclusion for comparison to the other options. It is also possible to have unintended disturbance torque sources that affect a sailcraft's attitude, e.g., a shift in the center of pressure due to uneven sail material degradation that results in increases in absorptivity [61].

Reaction and momentum wheels. Reaction and momentum wheels are heavy flywheels that spin faster or slower to change their momentum to create a control torque that forces the spacecraft to react by rotating. Reaction wheels may be at rest most of the time and only spin up/down when attitude changes are needed, whereas momentum wheels constantly spin rapidly to store momentum to stabilize one axis of the spacecraft. Both spin on a fixed axis relative to the spacecraft. An arrangement of three reaction/momentum wheels offer three-axis attitude control [62], [63].

Reaction wheels are the simplest and least expensive of all momentum exchange actuators but are limited compared to control moment gyros in terms of control torque capability. Reaction and momentum wheels may be used in combination with magnetic torquers in order to unload momentum without using thrust propellant to counter the de-spin effects [20]. Eterno offers simplified equations to size the spacecraft's reaction wheels based on the intended applications [21].

Control moment gyros. Control moment gyros (CMGs) are a more complicated version of a momentum wheel, though more power efficient. Like a momentum wheel, they are heavy flywheels that spin faster or slower to change their momentum to create a control torque, but they can also rotate on a single-gimbal axis or dual-gimbal axes relative to the spacecraft [62]. An arrangement of three single-axis CMGs offers three-axis attitude control. They have large control torque capability, which is good for agile satellites in LEO, large spacecraft, and fast slew maneuvers [20], [63].

Magnetic torquers. Magnetic torquers (also known as magnetorquers or torque bars) can be used directly for attitude control or for momentum unloading of reaction wheels that perform the attitude control. They offer momentum unloading without affecting the orbital motion. To function, the magnetic torquer is electrically energized to generate a magnetic dipole moment $\vec{M}$. The interaction between this magnetic dipole moment and Earth's magnetic field $\vec{B}$ produces a control torque vector $\vec{N}$ acting on the spacecraft. The relationship is given by

$$\vec{N} = \vec{M} \times \vec{B} \tag{2.36}$$

Three-axis magnetometers are required on the spacecraft to measure the Earth's magnetic field to inform the controls how much current is required to energize the magnetic torquer [20]. Magnetic torquers offer two-axis control at any time but effectively offer three-axis control over the course of one orbit [64]. However, the magnetic torquers would not work effectively far from Earth, e.g., by the moon [21].

Gimbaled control boom. Translating the sailcraft's center of mass location relative to its center of pressure location offers three-axis attitude control. A basic gimbaled control boom

articulates a tip-mounted mass within a hemisphere. A more complex gimbaled control boom

rotates as well as extends and retracts the control boom length [20]. Unfortunately, this actuator

has limited effect when the sail is edgewise to the sun. It is a less efficient option than control

vanes but it only requires one gimbal actuator near the center of mass rather than 4 actuators at

the spar tips, meaning less wiring mass and less hardware that can malfunction [19].

Tip vanes. Articulating reflective vanes located at the spar tips provide a small force yet

a large moment arm for control torques [19]. Putting two or four vanes at the spar tips, where

each vane has one or two degrees of freedom, offers three-axis attitude control. Tip vanes may be

used in combination with a gimbaled control boom, as shown in Figure 2.22 [20]. Tip vanes are

an effective control option regardless of the sail's orientation relative to the sun. However, the

actuators at the end of each spar present packing problems. They also must be accurately

controlled to avoid creating unintended disturbance torques [19].
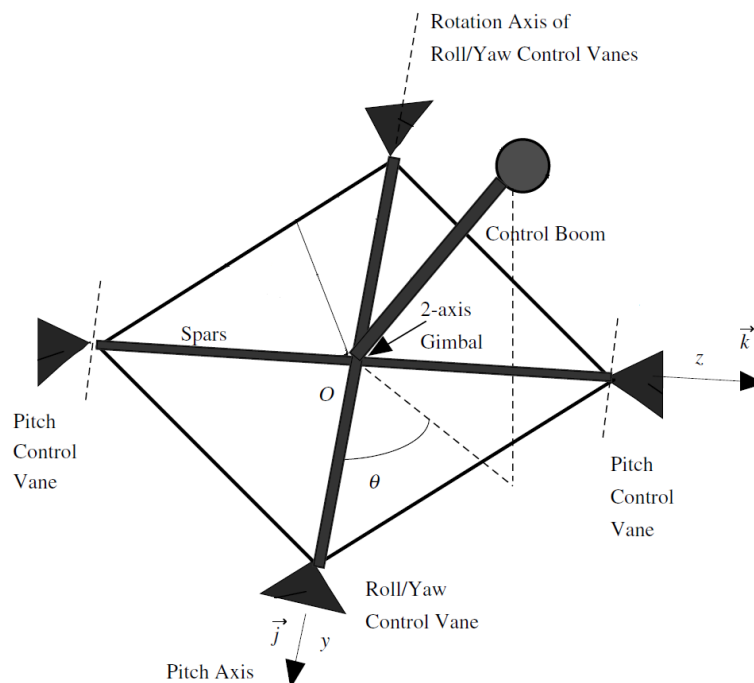
Figure 2.22 Sailcraft with Gimbaled Control Boom and Four Tip Vanes. Adapted from [20].

Sail translation. Reeling in lines may translate the sail across the sail structure, shifting the center of pressure relative to the center of mass [19]. Sail translation offers three-axis attitude control. However, this method has a limited effect when the sail is edgewise to the sun [19].

Reflectivity control devices. The application of voltage changes the optical properties of the reflectivity control devices (RCDs), generally located along the outer edges of a solar sail for maximum control torque capability. If voltage is applied to RCDs along one half of the solar sail and not applied to the other half, the sail will rotate. The side with non-zero voltage is the axis about which the sail will rotate [41]. This control method cannot rotate the sailcraft around the normal axis. For JAXA's IKAROS, the liquid crystal RCDs were specular-dominant when a voltage was applied and diffusive-dominant when it was off [24]. The University of Maryland and NASA have proposed a newer technology using polymer-dispersed liquid crystals that take on a diffuse state when a voltage is applied and a transparent state when it is off, in order to improve the sail's momentum change [41]. Mu et al. developed a method of designing RCD-based active controls [40]. Of the actuators listed in this section, RCDs are the only non-mechanical system, and are therefore not subject to mechanical failures.

Propellant-based thrusters. Propellant-based thrusters include conventional cold gas reaction jets and combustion thrusters. They are a propellant-dependent attitude control option, therefore limiting the mission lifetime. Lightweight pulsed-plasma thruster modules consume much less propellant than other thrusters and have a history of reliable spaceflight operation. They may be mounted at the sailcraft mast tips for short, efficient thrust corrections but present packing problems [20]. An arrangement of eight static thrusters offers three-axis attitude control [65].

State Space

  This section describes state-space models in the form of ordinary differential equations and their use in control theory. More detailed information about mathematical models of the sailcraft's motion is given in the next chapter.

  No mathematical model of a physical system is exact. Systems may be static or dynamic, causal or noncausal, time varying or time invariant, linear or nonlinear, finite dimensional or infinite dimensional [66]. However, in many cases a mathematical model based on a finite set of ordinary differential equations in state-space form can represent almost any physical system with relatively good accuracy. The control algorithm for a physical system is usually designed based on the state-space mathematical models, but it is applied to real-life systems whose behavior is only approximately described by such models. Success of such an approach is due to the presence of a feedback loop whose natural self-correcting properties provide robustness that can deal with imperfections in the mathematical model [67]. Control systems may have both feedforward and feedback control channels. The feedforward will ensure the system has the desired output, while the feedback loop will ensure the solution is stable.

  Consider a dynamic physical system described by a set of nonlinear differential equations in the vector form [20]

$$\dot{\boldsymbol{x}} = \boldsymbol{f}(\boldsymbol{x}, \boldsymbol{u}, t) \qquad\qquad (2.37)$$

Where:

  $\boldsymbol{x}$ = State vector and $\boldsymbol{x} = [x_1 \dots x_n]^{\mathrm{T}} \in \mathbb{R}^n$.

  $\boldsymbol{f}$ = Vector field and $\boldsymbol{f} = [f_1 \dots f_n]^{\mathrm{T}} \in \mathbb{R}^n$.

$\boldsymbol{u}$ = Control input vector and $\boldsymbol{u} = [u_1 \dots u_m]^\mathrm{T} \in \mathbb{R}^m$.

t = Time.

By assumption on the properties of the function $\boldsymbol{f}$, the initial conditions of the physical system at time t_0 and any subsequent control inputs (from some set of permissible inputs) uniquely determine the behavior of the system for all $t \geq t_0$ [20].

In many cases the system model (Equation 2.37) can be linear time-invariant:

$$\dot{\boldsymbol{x}} = \boldsymbol{A}\,\boldsymbol{x} + \boldsymbol{B}\,\boldsymbol{u} \tag{2.38a}$$

$$\boldsymbol{y} = \boldsymbol{C}\,\boldsymbol{x} \tag{2.38b}$$

Where:

$\boldsymbol{y}$ = Output vector and $\boldsymbol{y} = [y_1 \dots y_l]^\mathrm{T} \in \mathbb{R}^l$.

$\boldsymbol{A}$ = State matrix with dimensions $n \times n$.

$\boldsymbol{B}$ = Input matrix with dimensions $n \times l$.

$\boldsymbol{C}$ = Output matrix with dimensions $m \times n$.

Stability. Consider a nonlinear dynamic system described by $\dot{\boldsymbol{x}} = \boldsymbol{f}(\boldsymbol{x}, t)$. This system may represent a closed-loop model. An equilibrium point of this system is defined as a constant solution or a point $\boldsymbol{x}^*$ in the state-space that satisfies equation $\boldsymbol{f}(\boldsymbol{x}*, t) = 0$ for all t. An isolated equilibrium point $\boldsymbol{x}^*$ of this system is by definition Lyapunov stable if for any $\epsilon > 0$ there exists a real positive number $\delta(\epsilon, t_0)$ such that

$$\|\boldsymbol{x}(t_0) - \boldsymbol{x}^*\| \leq \delta \rightarrow \|\boldsymbol{x}(t) - \boldsymbol{x}^*\| \leq \epsilon \tag{2.39}$$

for all $t \geq t_0$ where $\|x\|$ denotes the Euclidean norm of x [11]. It is asymptotically stable if it is stable and any solution with an initial condition from δ-vicinity converges to the equilibrium point x^* as time t increases to infinity. It is proved that a linear system is stable if all eigenvalues of matrix A have non-positive real parts and no repeated eigenvalues on the imaginary axis [20].

In a globally asymptotically stable system, any solution converges to x^* from any initial conditions. A locally asymptotically stable system returns to x^* from certain small deviations in the vicinity of the equilibrium (e.g., a ball in a finite valley). In a marginally stable system, small deviations do not go far from x^* but also do not return to x^* (e.g., a ball on a flat floor). An unstable system lacks stability; small deviations from the equilibrium point will leave the vicinity of x^* entirely (e.g., a ball on a steep hill) [68].

Linear controllability. Consider a linear time invariant dynamic system described by

$$\dot{x} = A\,x + B\,u \tag{2.40}$$

Where:

$x \in \mathbb{R}^n$.

$u \in \mathbb{R}^m$.

This system is defined as controllable if there exists a control law input $u(t)$ that will transfer any state $x(t_0)$ to any other state $x(t_1)$ in finite time $t_1 > t_0$. The system is proved to be controllable if the following condition is satisfied: the $n \times nm$ controllability matrix (see Equation 2.41) has rank n [20]

$$[B \quad AB \quad A^2B \quad \cdots \quad A^{n-1}B] \tag{2.41}$$

It is important to note that, although the controllability is defined for open-loop time-dependent controls $\boldsymbol{u}(t)$, it allows for designing feedback to provide asymptotic stability of any feasible equilibrium $\boldsymbol{x}^*$ or trajectory $\boldsymbol{x}^*(t)$: $\boldsymbol{u} = -\boldsymbol{K}(\boldsymbol{x} - \boldsymbol{x}^*) + \boldsymbol{u}_{ff}$, where $\boldsymbol{u}_{ff} = B^+(\dot{\boldsymbol{x}}^* - \boldsymbol{A}\boldsymbol{x}^*)$ is the feedforward part of the control (here B^+ is a left pseudoinverse). The gain matrix $\boldsymbol{K}$ can be chosen such that closed loop system is asymptotically exponentially stable with any desired rate.

Observability. Consider a linear time invariant dynamic system described by $\dot{\boldsymbol{x}} = \boldsymbol{A}\,\boldsymbol{x} + \boldsymbol{B}\,\boldsymbol{u}$ and $\boldsymbol{y} = \boldsymbol{C}\,\boldsymbol{x}$ where $\boldsymbol{x} \in \mathbb{R}^n$, $\boldsymbol{u} \in \mathbb{R}^m$, $\boldsymbol{y} \in \mathbb{R}^l$. This system is defined as state observable at t_0 if the knowledge of the control input $\boldsymbol{u}(t)$ and the output $\boldsymbol{y}(t)$ over the time input $t_0 \leq t \leq t_1$ suffices to determine the state $\boldsymbol{x}(t_0)$. The linear time-invariant system is proved to be observable if the following condition is satisfied: the $nl \times n$ observability matrix (see Equation 2.42) has rank n [20]

$$\begin{bmatrix} C \\ AC \\ A^2C \\ \vdots \\ A^{n-1}C \end{bmatrix} \tag{2.42}$$

Observability establishes whether there is enough information from sensors to restore the state of the system uniquely. If the observability condition is fulfilled, then the state observers can be used to obtain the state of the system. In this thesis, I always assume that the state vector is available.

Summary

This chapter reviewed examples of previous work on solar sail missions as well as the basics of solar sails, orbital mechanics, and solar sails in orbit. It also covered trajectory design, attitude controls design, actuators, and state-space math. Using this background knowledge, the square sail was selected for this thesis due to its simplicity and its ability to turn rapidly in orbit raising maneuvers and spiral trajectories [19]. A specific sail material was not selected because it is beyond the scope of this thesis; the sail is modeled as an ideal sail. The reference trajectory is a logarithmic spiral trajectory because they offer exact solutions to the sailcraft's equations of motion. The trajectory design is modeled in MATLAB due to my familiarity with program, the capabilities of program, and its extensibility with the SPICE Toolkit. The objective of the controls problem is stabilization so that the sailcraft's actual position over time converges to the reference trajectory. A secondary objective is to minimize the time to follow the reference trajectory to the destination.

Chapter III
Mathematical Models

I build and explore three mathematical models in MATLAB around control designs to get the concept sailcraft from Earth orbit toward the moon: The Forward Euler model, the Earth-centered state-space model, and the Earth-moon (E-M) system-centered state-space model.

Forward Euler Model

The Forward Euler model is the simplest of the three models, describing a mass orbiting Earth. For simplicity, it does not include controls or SRP effects, nor does it attempt to orbit raise. The Forward Euler model was built to model the sailcraft's motion in a circular equatorial orbit around Earth due to gravity.

Research approach. Consider a sailcraft C in an ECI reference frame $E(O; x, y, z)$ of unit vectors $(\hat{e}_1, \hat{e}_2, \hat{e}_3)$, as shown in the left panel of Figure 3.1, where $\vec{r}_E$ and $\vec{v}$ are the sailcraft position vector and velocity vector, respectively, with respect to the Earth. The ECI reference frame is treated as sufficiently inertial for an Earth-orbiting spacecraft, although Earth technically rotationally accelerates around its axis and around the sun [21].

In the MATLAB simulations described in the next chapter the sailcraft is modeled to start from 1000 km altitude above Earth in an initially circular equatorial orbit. It has an initial tangential velocity necessary to maintain a circular orbit at that altitude. More specifically, its initial position is 7378 km from the center of Earth in the x-direction and its initial velocity is 0.441 km/min in the y-direction, as shown in the right panel of Figure 3.1. The sailcraft is supposed to maintain that orbit at that altitude.
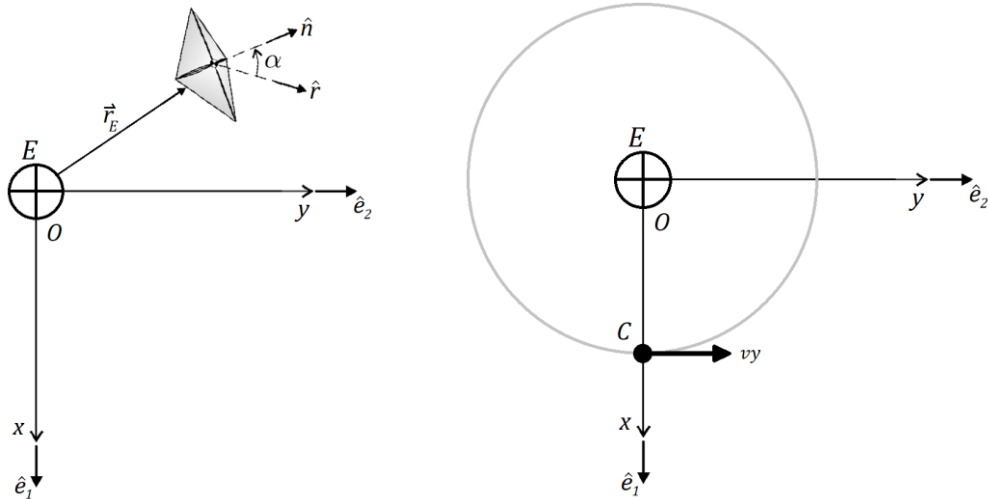
Figure 3.1 Left panel: Sailcraft in Reference Frame E, orbiting the Earth. SRP effects are ignored. Adapted from [38]. Right panel: Sailcraft Initial Conditions.

Limitations and assumptions. In addition to the limitations and assumptions in Chapter 1, the effects of SRP on the sailcraft are not considered in this model. The simplified physical model only involves the Earth and sailcraft and the gravitational force between them. The mass of the sailcraft is significantly less than the mass of the Earth so the center of mass of the Earth-sail system is assumed to be at the center of mass of the Earth [19]. Disturbing forces from astronomical bodies other than the Earth (e.g., Earth's moon) are neglected. The spacecraft's gravitational force on the Earth has a negligible effect on the Earth, therefore it can be treated as an R2BP.

Physical model. The sailcraft's position vector $\vec{r}_E$ can be expressed in E in Cartesian coordinates as

$$\vec{r}_E = x\,\hat{e}_1 + y\,\hat{e}_2 + z\,\hat{e}_3 \tag{3.1}$$

and the magnitude of the position vector or the distance of the sailcraft from Earth's center is

$$r_E = \sqrt{x^2 + y^2 + z^2} \tag{3.2}$$

The equation of motion in vector form of the infinitesimal solar sail orbiting a primary body

(Earth) in a R2BP and subject to Earth's gravity is [19]

$$\ddot{\vec{r}}_E = -\mu_\oplus \frac{\vec{r}_E}{r_E^3} \tag{3.3}$$

Where:

$\vec{r}_E$ = Position vector of the sailcraft from the center of the Earth.

$\mu_\oplus$ = Gravitational parameter of the Earth.

Note, $r_E{}^3$ is constant if the sailcraft is in a circular orbit; otherwise $r_E{}^3$ is time dependent.

State-space model. If I choose $\boldsymbol{x_1} = \vec{r}_E = [x \quad y \quad z]^T$ and $\boldsymbol{x_2} = \dot{\vec{r}}_E = \vec{v} =$

$[v_x \quad v_y \quad v_z]^T$ as the state variables, then the state-variable description of the linear system in

Equation 3.3 becomes:

$$\dot{x}_1 = x_2 \tag{3.4}$$

$$\dot{x}_2 = \frac{-\mu_\oplus}{r_E{}^3} x_1$$

Computationally, the sailcraft's position over time can be approximated using different

numerical methods. We need to obtain the discrete-time equation relating $\boldsymbol{x}(t_k)$ and $\boldsymbol{x}(t_{k+1})$

$$\boldsymbol{x}(t_{k+1}) = \boldsymbol{F}(\boldsymbol{x}(t_k)) \tag{3.5}$$

The simplest of them is the Euler method, which is a first order method of solving ordinary differential equations like that in Equation 3.3. The Euler method is basic and it is subject to error accumulation dependent on step size of time intervals. An appropriate step size must be selected to meet its stability criterion.

The first derivative with respect to time is approximately the difference between two subsequent steps divided by the time interval between the steps:

$$\dot{x} \approx \frac{x(t_{k+1}) - x(t_k)}{dt} \tag{3.6}$$

Using the approximation shown in Equation 3.6, Equation 3.4 can be rewritten as:

$$x_1(t_{k+1}) \approx x_1(t_k) + dt \cdot x_2(t_k) \tag{3.7}$$

$$x_2(t_{k+1}) \approx x_2(t_k) - \frac{\mu_\oplus}{r_E^3} dt \cdot x_1(t_k)$$

Where:

dt = Time interval.

t_k = Initial time step.

t_{k+1} = Subsequent time step, such that $t_k + dt = t_{k+1}$.

Note Equation 3.7 is a discretized time expression. For sufficiently small values of dt, Equation 3.7 behaves only approximately like Equation 3.5. In addition, I can assume r and x will change very little during dt and thus treat them as constants. With Equation 3.7, the sailcraft's orbital equation of motion is now in the desired computational form, which can be entered into MATLAB and used to simulate the sailcraft's position over time.

Earth-Centered State-Space Model

The Earth-centered state-space model is a step up in complexity from the first model, introducing SRP effects on the sailcraft. This model was built to model the sailcraft's motion as it increases its altitude from a circular equatorial orbit around Earth due to gravity, SRP, and ideal controls. The ideal controls are those for on-off switching, the most basic method of orbit raising for a sailcraft in a planet-centered orbit. On-off switching is an exact, "pre-made" thrust vector solution to increase altitude. This model also includes the eclipse factor model to account for the sailcraft being in periods of shadow.

Research approach. Consider a sailcraft C in an ECI reference frame $E(O; x, y, z)$ of unit vectors $(\hat{e}_1, \hat{e}_2, \hat{e}_3)$, as shown in Figure 3.2, where $\vec{r}_E$ and $\vec{v}$ are the sailcraft position vector and velocity vector, respectively, with respect to the Earth. In this model, the ECI reference frame is treated as semi-inertial: it is sufficiently inertial when describing the motion of the spacecraft around Earth and it is not inertial as the Earth translates due to acceleration in the truly inertial HEI reference frame $I(O; x, y, z)$ of unit vectors $(\hat{i}_1, \hat{i}_2, \hat{i}_3)$ [21].
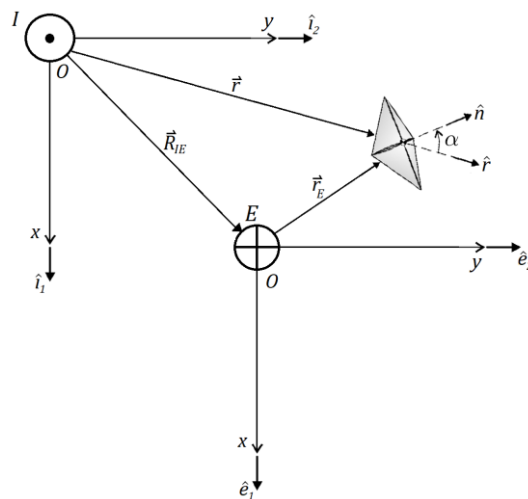
Figure 3.2 Sailcraft in Reference Frames E and I. The sailcraft orbits Earth, which orbits the sun. Adapted from [38].

As in the first model, the sailcraft is modeled to start from 1000 km altitude above Earth in an initially circular equatorial orbit. It has an initial tangential velocity necessary to maintain a circular orbit at that altitude. More specifically, its initial position is 7378 km from the center of Earth in the x-direction and its initial velocity is 0.441 km/min in the y-direction, as shown in the left panel of Figure 3.3. The sailcraft is supposed to raise its orbit using on-off switching.

The Earth is modeled to start 1 AU from the sun in a circular orbit in the ecliptic plane. It has an initial tangential velocity necessary to maintain a circular orbit at that distance. More specifically, its initial position is 149.6e6 km from the center of the sun in the x-direction and its initial velocity is nearly 1800 km/min in the y-direction, as shown in the right panel of Figure 3.3. The Earth maintains that circular orbit throughout the problem.
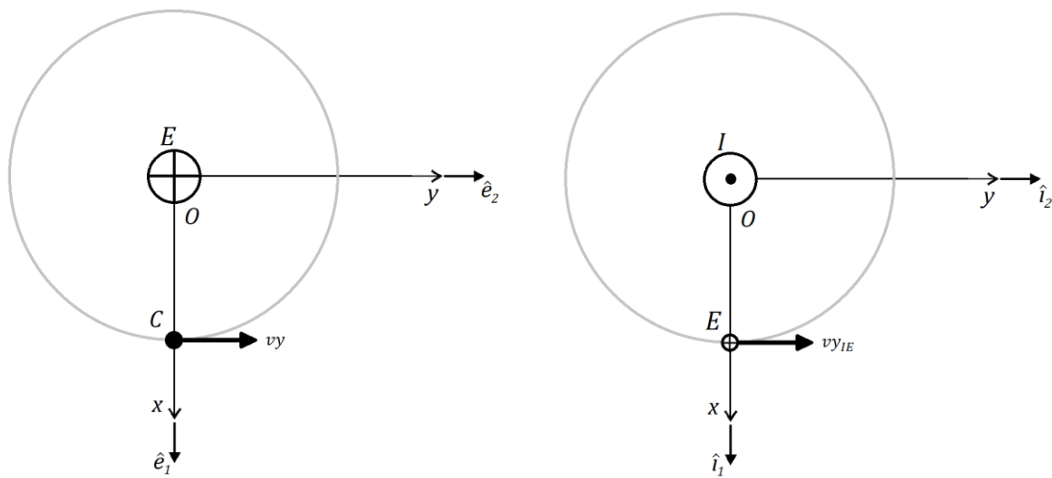
Figure 3.3 Left panel: Sailcraft Initial Conditions in *E*. Right panel: Earth Initial Conditions in *I*.

From Equation 2.4, it is clear I must know $\vec{r}$ in order to understand and model how the sailcraft moves due to SRP. As shown in the left panel of Figure 3.2, the sailcraft's position vector with respect to the sun is

$$\vec{r} = \vec{R}_{IE} + \vec{r}_E \tag{3.8}$$

Where:

$\vec{r}$ = Sailcraft inertial position vector from the center of the sun.

$\vec{R}_{IE}$ = Earth's position vector with respect to the sun.

Equation 3.8 offers a relatively easy way to find $\vec{r}$, as long as $\vec{R}_{IE}$ and $\vec{r}_E$ are known.

Adapting Equation 2.18, I can approximate the sailcraft as the particle C in motion relative to Earth's reference frame, which is itself in motion to the HEI reference frame. The sailcraft's velocity with respect to the origin of E as seen from I can be given as

$$\left\{ \frac{d\vec{r}_E}{dt} \right\}_I = \left\{ \frac{d\vec{r}_E}{dt} \right\}_E + \vec{\omega}^{E/I} \times \vec{r}_E \tag{3.9}$$

Where:

$\left\{ \frac{d\vec{r}_E}{dt} \right\}_I$ = Rate of change of position vector $\vec{r}_E$ as seen from reference frame I.

$\left\{ \frac{d\vec{r}_E}{dt} \right\}_E$ = Rate of change of position vector $\vec{r}_E$ as seen from reference frame E.

$\vec{\omega}^{E/I}$ = Angular velocity of reference frame E with respect to reference frame I.

Limitations and assumptions. The following limitations and assumptions are in addition to those in Chapter 1. In this model, I have two R2BPs. One is the same Earth-sailcraft system as in the first model: the simplified physical model only involves the Earth and sailcraft,

the gravitational force between them, and SRP. The mass of the sailcraft is significantly less than the mass of the Earth so the center of mass of the Earth-sail system is assumed to be at the center of mass of the Earth [19]. Disturbing forces from astronomical bodies other than the Earth (e.g., Earth's moon) are neglected. The spacecraft's gravitational force on the Earth has a negligible effect on the Earth.

The second R2BP considers the Earth orbiting the sun in an HEI reference frame. The simplified physical model only involves the Earth and sun and the gravitational force between them. The mass of the Earth is significantly less than the mass of the sun so the center of mass of the Earth-sun system is assumed to be at the center of mass of the sun [19]. Disturbing forces from astronomical bodies other than the sun (e.g., Earth's moon) are neglected. Earth's gravitational force on the sun has a negligible effect on the sun.

When on-off switching, the sail cone angle is assumed exactly $0°$ when 'on' (moving away from the sun) and $90°$ when 'off' (moving toward the sun). Ignoring disturbances, system is assumed uncontrollable only when approaching the sun.

Physical models. There are two physical models, one for each R2BP. The first solves for $\vec{r}_E$ and the second solves for $\vec{R}_{IE}$, in order to find $\vec{r}$ for Equation 3.8.

Sailcraft orbiting Earth, $\vec{r}_E$. The sailcraft's position vector relative to the Earth $\vec{r}_E$ can be expressed in E in Cartesian coordinates as

$$\vec{r}_E = x\,\hat{e}_1 + y\,\hat{e}_2 + z\,\hat{e}_3 \qquad (3.10)$$

and the magnitude of the position vector or the distance of the sailcraft from Earth's center is

$$r_E = \sqrt{x^2 + y^2 + z^2} \tag{3.11}$$

The equation of motion in vector form of the solar sail in an Earth-centered orbit (see Equation 3.12) was used to model the trajectory of a sailcraft in the vicinity of Earth. The equation of motion of a sailcraft is like Equation 2.21 but must include the acceleration due to SRP. The sailcraft is assumed an infinitesimal mass with an ideal solar sail under the gravitational attraction of a point mass (Earth) and subject to SRP [19]:

$$\ddot{\vec{r}}_E = -\mu_\oplus \frac{\vec{r}_E}{r_E{}^3} + \vec{a} \tag{3.12}$$

Where:

$\vec{r}_E$ = Position vector of the sailcraft from the center of the Earth.

$\mu_\oplus$ = Gravitational parameter of the Earth.

$\vec{a}$ = Additional acceleration of the sailcraft due to SRP.

If the sailcraft has thrust vector controls, Equation 3.12 can be rewritten as

$$\ddot{\vec{r}}_E = -\mu_\oplus \frac{\vec{r}_E}{r_E{}^3} + \frac{\vec{T}}{m} \tag{3.13}$$

Where:

$\vec{T}$ = Actual thrust vector due to SRP and other controls.

m = Mass of the sailcraft.

Note the thrust vector $\vec{T}$ is a function both of the SRP, which is itself a function of position $\vec{r}$, and of any controls acting on the sailcraft.

In this model, the sailcraft's thrust vector controls are those to perform on-off switching; therefore, the actual thrust vector is specifically that given in Equation 2.29. Finally, the comprehensive equation of motion of the solar sail in an Earth-centered orbit, which was used to model the trajectory of the sailcraft in the vicinity of Earth is

$$\ddot{\vec{r}}_E = -\mu_\oplus \frac{\vec{r}_E}{r_E{}^3} + \frac{\vec{T}(\theta_E)}{m} \tag{3.14}$$

Note, $r_E{}^3$ is time dependent because the sailcraft will attempt to raise its orbit, i.e., it is not in its initial circular orbit for long.

Earth orbiting sun, $\vec{R}_{IE}$. The Earth's position vector relative to the sun $\vec{R}_{IE}$ can be expressed in *I* in Cartesian coordinates as

$$\vec{R}_{IE} = x\,\hat{\imath}_1 + y\,\hat{\imath}_2 + z\,\hat{\imath}_3 \tag{3.15}$$

and the magnitude of the position vector or the distance of the Earth from the sun's center is

$$R_{IE} = \sqrt{x^2 + y^2 + z^2} \tag{3.16}$$

The equation of motion in vector form of the Earth in a sun-centered orbit (see Equation 3.17) was used to model the trajectory of the Earth around the sun. The equation of motion of a

sailcraft is like Equation 2.21. The Earth is assumed a point mass orbiting a primary body (sun) in a R2BP and subject to the sun's gravity [19]:

$$\ddot{\vec{R}}_{IE} = -\mu_O \frac{\vec{R}_{IE}}{R_{IE}{}^3} \tag{3.17}$$

Where:

$\vec{R}_{IE}$ = Position vector of the Earth from the center of the sun.

μ_O = Gravitational parameter of the sun.

Note $R_{IE}{}^3$ is considered constant since the Earth is approximated to have a circular orbit around the sun.

State-space models. There are two state-space models, one for each R2BP. The first solves for x and the second solves for Z, which contain $\vec{r}_E$ and $\vec{R}_{IE}$, respectively.

Sailcraft orbiting Earth, x. If I choose $x_1 = x$, $x_2 = y$, $x_3 = z$, $x_4 = v_x$, $x_5 = v_y$, $x_6 = v_z$ (i.e., the components of the sailcraft's position and velocity vectors with respect to the Earth) as the state variables, then the state-variable description of the linear system in Equation 3.14 becomes

$$\dot{x}_1 = x_4 \tag{3.18}$$

$$\dot{x}_2 = x_5$$

$$\dot{x}_3 = x_6$$

$$\dot{x}_4 = \frac{-\mu_\oplus}{r_E{}^3} x_1 + \frac{1}{m}\tilde{T}_1$$

$$\dot{x}_5 = \frac{-\mu_\oplus}{r_E{}^3} x_2 + \frac{1}{m}\tilde{T}_2$$

$$\dot{x}_6 = \frac{-\mu_\oplus}{r_E{}^3} x_3 + \frac{1}{m} \tilde{T}_3$$

Where:

$\tilde{T}_1 = \tilde{T}_x$ = Actual thrust control input vector component along x-axis.

$\tilde{T}_2 = \tilde{T}_y$ = Actual thrust control input vector component along y-axis.

$\tilde{T}_3 = \tilde{T}_z$ = Actual thrust control input vector component along z-axis.

If I define the state vector x using the state variables as elements:

$$x = [x_1 \quad x_2 \quad x_3 \quad x_4 \quad x_5 \quad x_6]^T \tag{3.19}$$

then the Equation 3.18 can be written as the state-space equation (and in the same format for a system with controls)

$$\dot{x} = Ax + B\tilde{T} = \begin{bmatrix} 0 & 0 & 0 & 1 & 0 & 0 \\ 0 & 0 & 0 & 0 & 1 & 0 \\ 0 & 0 & 0 & 0 & 0 & 1 \\ -\frac{\mu_\oplus}{r_E{}^3} & 0 & 0 & 0 & 0 & 0 \\ 0 & -\frac{\mu_\oplus}{r_E{}^3} & 0 & 0 & 0 & 0 \\ 0 & 0 & -\frac{\mu_\oplus}{r_E{}^3} & 0 & 0 & 0 \end{bmatrix} \begin{bmatrix} x_1 \\ x_2 \\ x_3 \\ x_4 \\ x_5 \\ x_6 \end{bmatrix} + \begin{bmatrix} 0 & 0 & 0 \\ 0 & 0 & 0 \\ 0 & 0 & 0 \\ \frac{1}{m} & 0 & 0 \\ 0 & \frac{1}{m} & 0 \\ 0 & 0 & \frac{1}{m} \end{bmatrix} \begin{bmatrix} \tilde{T}_1 \\ \tilde{T}_2 \\ \tilde{T}_3 \end{bmatrix} \tag{3.20}$$

Where:

A = State matrix.

B = Input matrix.

$\tilde{T}$ = Actual thrust control input vector, where:

$$\widetilde{T} = \vec{\widetilde{T}}\,(\theta_E) = \text{Actual thrust vector due to SRP and on-off switching controls.}$$

Note A in general depends on time t (time-varying) due to the r_E term slowly changing as the

sailcraft moves, but B does not depend on t (continuous time-invariant) [20]. In addition, $\widetilde{T}$

depends on t (continuous time-variant) due to the r and θ_E terms slowly changing as the sailcraft

moves.

The system in Equation 3.20 is nonlinear, dynamic, finite dimensional, and causal.

Technically it is time varying because the initial conditions of the sun, Earth, and sailcraft

positions affect the trajectory output. But it can be treated as time invariant because the $r_E{}^3$ term

over just a few orbits is almost constant.

Assuming that on the small time interval $[t_k, t_{k+1}]$ the matrix A is almost constant (due to

the slow orbital change), the solution of the Equation 3.20 can be rewritten as:

$$x(t_{k+1}) = e^{A(t_{k+1}-t_k)}\,x(t_k) + \int_{t_k}^{t_{k+1}} e^{A(t_{k+1}-\tau)}\,B\,\widetilde{T}(\tau)\,d\tau \qquad (3.21)$$

Where:

t_k = Initial time step.

t_{k+1} = Subsequent time step.

Since I have already mentioned the matrices A and $\widetilde{T}$ can be considered as constant

during a sufficiently small time interval dt, then Equation 3.21 can be approximated using the

first three terms in a Taylor series expansion of the exponential matrix [20] as:

$$x(t_{k+1}) \cong (I + A\,dt + 0.5\,A^2\,dt^2)\,x(t_k) + B\,\widetilde{T}(t_k)(I\,dt + 0.5\,A\,dt^2) \qquad (3.22)$$

Where:

I = Identity matrix.

dt = Time interval between t_k and t_{k+1}

Note Equation 3.22 is a discretized time expression. For sufficiently small values of dt, Equation 3.22 behaves like Equation 3.20. In addition, I can assume $x(t_k)$ and $\widetilde{T}(t_k)$ will change very little during dt and thus treat them as constants. Then, between steps, I update $x(t_k)$ and $\widetilde{T}(t_k)$. If $\widetilde{T}$ is set equal to zero, the open-loop system ensures a sailcraft starting in a circular orbit remains in the same circular orbit. Non-zero $\widetilde{T}$ values cause the sailcraft to alter its orbit: a closed-loop system. With Equation 3.22, the sailcraft's orbital equation of motion is now in the desired form, which can be entered into MATLAB and used to simulate the sailcraft's position over time.

Earth orbiting sun, Z. As for the sailcraft orbiting Earth, a state matrix is used to model the Earth orbiting the sun. The letter z is used to distinguish the Earth's state matrix from the sailcraft's state matrix. If I choose $z_1 = x_{IE}$, $z_2 = y_{IE}$, $z_3 = z_{IE}$, $z_4 = v_{x_{IE}}$, $z_5 = v_{y_{IE}}$, $z_6 = v_{z_{IE}}$ (i.e., the components of the Earth's position and velocity vectors with respect to the sun) as the state variables, then the state-variable description of the linear system in Equation 3.17 becomes:

$$\dot{z}_1 = z_4 \tag{3.23}$$

$$\dot{z}_2 = z_5$$

$$\dot{z}_3 = z_6$$

$$\dot{z}_4 = \frac{-\mu_O}{R_{IE}{}^3} z_1$$

$$\dot{z}_5 = \frac{-\mu_O}{R_{IE}{}^3} z_2$$

$$\dot{z}_6 = \frac{-\mu_O}{R_{IE}{}^3} z_3$$

If I define the state vector Z using the state variables as elements:

$$Z = [z_1 \quad z_2 \quad z_3 \quad z_4 \quad z_5 \quad z_6]^T \tag{3.24}$$

then the Equation 3.23 can be written as the state-space equation

$$\dot{Z} = A_{IE}Z = \begin{bmatrix} 0 & 0 & 0 & 1 & 0 & 0 \\ 0 & 0 & 0 & 0 & 1 & 0 \\ 0 & 0 & 0 & 0 & 0 & 1 \\ -\frac{\mu_O}{R_{IE}{}^3} & 0 & 0 & 0 & 0 & 0 \\ 0 & -\frac{\mu_O}{R_{IE}{}^3} & 0 & 0 & 0 & 0 \\ 0 & 0 & -\frac{\mu_O}{R_{IE}{}^3} & 0 & 0 & 0 \end{bmatrix} \begin{bmatrix} z_1 \\ z_2 \\ z_3 \\ z_4 \\ z_5 \\ z_6 \end{bmatrix} \tag{3.25}$$

Where:

A_{IE} = State matrix of Earth relative to sun.

Note A_{IE} does not depend on t (continuous time-invariant) because R_{IE} is constant.

Using the state transition matrix of A_{IE}, Equation 3.25 can also be rewritten as:

$$\mathbf{Z}(t_{k+1}) = e^{\mathbf{A}_{IE}(t_{k+1}-t_k)} \, \mathbf{Z}(t_k) \tag{3.26}$$

Note Equations 3.25 and 3.26 are both continuous time expressions.

Since $\mathbf{A}_{IE}$ is constant during time interval dt, Equation 3.26 can be approximated using the first three terms in a Taylor series expansion of the exponential matrix [20] as:

$$\mathbf{Z}(t_{k+1}) \cong \left(\mathbf{I} + \mathbf{A}_{IE} \, dt + 0.5 \, \mathbf{A}_{IE}^{\,2} \, dt^2\right) \mathbf{Z}(t_k) \tag{3.27}$$

Note Equation 3.27 is a discretized time expression. For sufficiently small values of dt, Equation 3.27 behaves like Equation 3.25. In addition, I can assume $\mathbf{Z}(t_k)$ will change very little during dt and thus treat it as a constant. Then, between steps, I update $\mathbf{Z}(t_k)$. With Equation 3.27, the Earth's orbital equation of motion is now in the desired form, which can be entered into MATLAB and used to simulate the Earth's position over time.

Control approach. The control goal is stabilization to the desired trajectory: that the system output $\vec{r}_E$, which is the sailcraft's actual position at time t, converges quickly to the desired output $\vec{R}$.

The main approach to spacecraft guidance and control in this thesis is that the desired output, which is the reference position, $\vec{R}$ is chosen to satisfy the model close to the spacecraft's natural motion in the gravity field but modified so that the reference trajectory slowly spirals out from Earth toward the moon, as shown in Equation 3.28 below.

$$\ddot{\vec{R}} = -\mu_{\oplus} \frac{\vec{R}}{r_E^{\,3}} + N_1 \, \vec{R} \tag{3.28}$$

Where:

$\vec{R}$ = Sailcraft reference position vector.

If R^3 is approximately equal to $r_E{}^3$, this equation looks like the equation describing natural motion in Earth's gravity field, except for the last term. The addition of the last term $N_1 \vec{R}$ allows the circular reference orbit $\vec{R}$ to spiral out with the rate regulated by the parameter N_1. Thus, the disturbing term makes the circular orbit a little bit unstable, turning it into a spiral outward instead. For simplicity, the disturbing term is assumed to be a linear function of the $\vec{R}$ vector only. The coefficient N_1 is a scalar and is assumed small so that large thrust is not required to effect the reference trajectory, which means the spiral deviation from a circle is also small. The spiral reference trajectory defines the intended change in orbit.

The difference between the two positions is the position error $\vec{e}$, defined as

$$\vec{e} \equiv \vec{r}_E - \vec{R} \qquad (3.29)$$

If stabilization is achieved, then the sailcraft's actual position over time (i.e., its actual trajectory) converges the reference trajectory, i.e., $\vec{r}_E \rightarrow \vec{R}$ and $\vec{e} \rightarrow \vec{0}$.

In order to rewrite Equation 3.29 in terms of $\vec{e}$ and $\vec{u}$ only, first let the actual thrust vector be given as

$$\vec{T}(f) = m N_1 \vec{r}_E + m \vec{u}(t) \qquad (3.30)$$

Where:

$\vec{u}$ = Acceleration control input vector.

Then the position error equation of motion is the difference between Equations 3.14 (with

Equation 3.30 substituted in) and 3.28:

$$\ddot{\vec{e}} = \ddot{\vec{r}}_E - \ddot{\vec{R}} = -\mu_\oplus \frac{\vec{e}}{r_E{}^3} + N_1 \vec{e} + \vec{u}(t) \tag{3.31}$$

If I choose $e_1 = e_x$, $e_2 = e_y$, $e_3 = e_z$, $e_4 = e_{vx}$, $e_5 = e_{vy}$, $e_6 = e_{vz}$ (i.e., the

components of the errors in the sailcraft's position and velocity vectors with respect to the Earth)

as the state variables and $u_1 = u_x$, $u_2 = u_y$, $u_3 = u_z$ (i.e., the error control components), then

the state-variable description of the linear system in Equation 3.31 becomes:

$$\dot{e}_1 = e_4 \tag{3.32}$$

$$\dot{e}_2 = e_5$$

$$\dot{e}_3 = e_6$$

$$\dot{e}_4 = \frac{-\mu_\oplus}{r_E{}^3} e_1 + N_1 e_1 + u_1$$

$$\dot{e}_5 = \frac{-\mu_\oplus}{r_E{}^3} e_2 + N_1 e_2 + u_2$$

$$\dot{e}_6 = \frac{-\mu_\oplus}{r_E{}^3} e_3 + N_1 e_3 + u_3$$

If I define the state vector $\boldsymbol{e}$ using the state variables as elements:

$$\boldsymbol{e} = [e_1 \quad e_2 \quad e_3 \quad e_4 \quad e_5 \quad e_6]^T \tag{3.33}$$

then the Equation 3.32 can be written as the state-space equation

$$\dot{e} = Ae + Bu \tag{3.34}$$

$$\dot{e} = \begin{bmatrix} 0 & 0 & 0 & 1 & 0 & 0 \\ 0 & 0 & 0 & 0 & 1 & 0 \\ 0 & 0 & 0 & 0 & 0 & 1 \\ -\dfrac{\mu_\oplus}{r_E{}^3} + N_1 & 0 & 0 & 0 & 0 & 0 \\ 0 & -\dfrac{\mu_\oplus}{r_E{}^3} + N_1 & 0 & 0 & 0 & 0 \\ 0 & 0 & -\dfrac{\mu_\oplus}{r_E{}^3} + N_1 & 0 & 0 & 0 \end{bmatrix} \begin{bmatrix} e_1 \\ e_2 \\ e_3 \\ e_4 \\ e_5 \\ e_6 \end{bmatrix} + \begin{bmatrix} 0 & 0 & 0 \\ 0 & 0 & 0 \\ 0 & 0 & 0 \\ 1 & 0 & 0 \\ 0 & 1 & 0 \\ 0 & 0 & 1 \end{bmatrix} \begin{bmatrix} u_1 \\ u_2 \\ u_3 \end{bmatrix}$$

Where:

A = State matrix.

B = Input matrix.

u = Acceleration control input vector.

Note A depends on time t (time-varying) due to the $r_E{}^3$ term slowly changing as the sailcraft

moves, but B does not depend on t (continuous time-invariant) [20].

For this model, a linear control algorithm is assumed:

$$u = -K\,e \tag{3.35}$$

Where:

K = Control gain matrix.

Matrix $\mathbf{K}$ is a slowly changing, almost constant matrix. The job of this control $\mathbf{u}$ is to make the state error $\mathbf{e}$ go to zero. The effectively linear $-\mathbf{K}\,\mathbf{e}$ term ensures stability. Substituting Equation 3.35 into Equation 3.34, I reach the desired state-space form for stability analysis:

$$\dot{\mathbf{e}} = (\mathbf{A} - \mathbf{B}\,\mathbf{K})\,\mathbf{e} \qquad (3.36)$$

$$\dot{\mathbf{e}} = \begin{bmatrix} 0 & 0 & 0 & 1 & 0 & 0 \\ 0 & 0 & 0 & 0 & 1 & 0 \\ 0 & 0 & 0 & 0 & 0 & 1 \\ -\frac{\mu_\oplus}{r_E^{\,3}} + N_1 - K_{11} & -K_{12} & -K_{13} & -K_{14} & -K_{15} & -K_{16} \\ -K_{21} & -\frac{\mu_\oplus}{r_E^{\,3}} + N_1 - K_{22} & -K_{23} & -K_{24} & -K_{25} & -K_{26} \\ -K_{31} & -K_{32} & -\frac{\mu_\oplus}{r_E^{\,3}} + N_1 - K_{33} & -K_{34} & -K_{35} & -K_{36} \end{bmatrix} \begin{bmatrix} e_1 \\ e_2 \\ e_3 \\ e_4 \\ e_5 \\ e_6 \end{bmatrix}$$

The eigenvalues λ_i of the $(\mathbf{A} - \mathbf{B}\,\mathbf{K})$ matrix can be assigned to make the system in Equation 3.36 asymptotically stable. Here, again, I used an assumption that the slow change of $\frac{\mu_\oplus}{r_E^{\,3}}$ allows me to assume that $\mathbf{A}$ is a constant matrix.

Earth-Moon System-Centered State-Space Model

The Earth-moon (E-M) system-centered state-space model is another step up in complexity from the second model. It also accounts for SRP effects, but it starts in an E-M system-centered rotating reference frame rather than an Earth-centered semi-inertial reference frame. Rather than assuming another exact thrust vector solution, I develop an LQR controller to limit the sailcraft's trajectory error from a reference logarithmic spiral trajectory toward the moon. For reasons to be explained in the Discussion section, this model does not include the eclipse factor model and therefore does not account for the sailcraft being in periods of shadow.

Research approach. Consider a sailcraft C moving in the vicinity of – and subject to the gravitational field of – the Earth and moon as a CR3BP. Understanding the motion of a

spacecraft in the vicinity of the Earth and moon is rather complex, even when simplified to a

CR3BP. The sailcraft is in a rotating reference frame $B(O; x, y, z)$ of unit vectors ($\hat{b}_1$, $\hat{b}_2$, $\hat{b}_3$), as

shown in Figure 3.4, where $\vec{r}_b$ and $\vec{v}$ are the sailcraft position vector and velocity vector,

respectively, with respect to the E-M barycenter origin. In this model, the E-M system-centered

rotating (BCR) reference frame B is not treated as inertial or even semi-inertial. Constrained to

rotate in circular orbits around their center of mass, the E-M system rotates with a constant

angular velocity $\omega_b\,\hat{b}_3$ in the truly inertial HEI reference frame $I(O; x, y, z)$ of unit vectors ($\hat{i}_1$, $\hat{i}_2$,

$\hat{i}_3$). The constant angular velocity ω_b given by [20]

$$\omega_b = \sqrt{G(M_1 + M_2)/D^3} \qquad (3.37)$$

Where:

   ω_b = Angular velocity of E-M system.

   M_1 = Mass of the Earth.

   M_2 = Mass of the moon.

   D = Constant distance between the Earth and moon.

Figure 3.4 Sailcraft in Reference Frames *B* and *I*. The sailcraft moves in relation to the Earth-moon system, which orbits the sun. Adapted from [20], [38].

The sailcraft is modeled to start 12052 km from the E-M barycenter in an initially circular orbit around the E-M system's center of mass. It has an initial tangential velocity necessary to maintain a circular orbit at that distance. More specifically, its initial position is 7378 km from the center of the Earth in the x-direction and its initial velocity is in the y-direction, as shown in the left panel of Figure 3.5. The sailcraft is supposed to raise its orbit via a LQR control algorithm to follow a reference logarithmic spiral trajectory.

The E-M system is modeled to start 1 AU from the sun in a circular orbit in the ecliptic plane. It has an initial tangential velocity necessary to maintain a circular orbit at that distance. More specifically, its initial position is 149.6e6 km from the center of the sun in the x-direction and its initial velocity is nearly 1800 km/min in the y-direction, as shown in the right panel of Figure 3.5. The E-M system maintains that circular orbit around the sun throughout the problem.

Figure 3.5 Left panel: Sailcraft Initial Conditions in B. Right panel: E-M System Initial Conditions in I.

From Equation 2.4, it is clear I must know $\vec{r}$ in order to understand and model how the sailcraft moves due to SRP. As shown in Figure 3.4, the sailcraft's position vector with respect to the sun is

$$\vec{r} = \vec{R}_{IB} + \vec{r}_b \tag{3.38}$$

Where:

$\vec{r}$ = Sailcraft inertial position vector from the center of the sun.

$\vec{R}_{IB}$ = E-M barycenter's position vector from the center of the sun.

Equation 3.38 offers a relatively easy way to find $\vec{r}$, as long as $\vec{R}_{IB}$ and $\vec{r}_b$ are known.

Adapting Equation 2.18, I can approximate the sailcraft as the particle C in motion relative to the BCR reference frame which is itself in motion to the HEI reference frame. The sailcraft's velocity with respect to the origin of B as seen from I can be given as

$$\left\{\frac{d\vec{r}_b}{dt}\right\}_I = \left\{\frac{d\vec{r}_b}{dt}\right\}_B + \vec{\omega}^{B/I} \times \vec{r}_b \tag{3.39}$$

Where:

$\vec{\omega}^{B/I}$ = Angular velocity of the E-M system in motion around the sun.

Note $\vec{\omega}^{B/I}$ is different from ω_b, which is the angular velocity of the Earth and moon around their center of mass in the sun's inertial reference frame.

Limitations and assumptions. The following limitations and assumptions are in addition to those in Chapter 1. In this model, I have one R2BP and one CR3BP. The R2BP considers the E-M system (treated as one body) orbiting the sun in an HEI reference frame. The simplified physical model only involves the E-M system, the sun, and the gravitational force between them. The mass of the E-M system is significantly less than the mass of the sun so the center of mass of the Earth-moon-sun system is assumed to be at the center of mass of the sun [19]. Disturbing forces from astronomical bodies other than the sun are neglected. The E-M system's gravitational force on the sun has a negligible effect on the sun.

The CR3BP considers the sailcraft orbiting the E-M system in a BCR reference frame. The simplified physical model only involves the E-M system and sailcraft, the gravitational force between them, and SRP. The mass of the sailcraft is significantly less than the mass of the E-M system so the barycenter of the Earth-moon-sail system is assumed to be at the center of mass of the E-M system [19]. Disturbing gravitational forces from astronomical bodies other than the

Earth and moon (e.g., the sun) are neglected. The spacecraft's gravitational force on the E-M system has a negligible effect on the E-M system. The Earth and moon are constrained to circular orbits and the sailcraft is assumed to move in the plane defined by the Earth's and moon's orbits.

For a sailcraft, this CR3BP system is time-dependent due to the sun's relative motion around the Earth–Moon system. Over the course of each synodic lunar period (about 29 days), "the direction of the photons impinging on the solar sail changes, which influences the magnitude and/or direction of the available solar sail acceleration over time" [32]. Vance et al. offer a detailed comparison of CR3BP and CR4BP (adding the sun as a fourth body in the system) model accuracy. They have a worthwhile discussion on the limitations of the CR3BP model for a sailcraft in the E-M system due to the perturbing "effects of the earth-moon eccentricity along with solar gravity" [36]. For the purposes of this thesis, the CR3BP model is sufficient for the desired low-fidelity model.

Physical models. There are four physical models, three for the CR3BP and one for the R2BP. The first solves for $\vec{r}_b$ and the fourth solves for $\vec{R}_{IB}$, to find $\vec{r}$ for Equation 3.38. The second defines the sailcraft's reference trajectory $\vec{R}$ and the third defines the error $\vec{e}$ between the actual and reference trajectories for use in the LQR control algorithm.

Sailcraft orbiting Earth-moon barycenter, $\vec{r}_b$. The sailcraft's position vector relative to the E-M barycenter $\vec{r}_b$ can be expressed in B in Cartesian coordinates as

$$\vec{r}_b = x\,\hat{b}_1 + y\,\hat{b}_2 + z\,\hat{b}_3 \tag{3.40}$$

and the magnitude of the position vector or the distance of the sailcraft from the E-M barycenter

is

$$r_b = \sqrt{x^2 + y^2 + z^2} \tag{3.41}$$

The sailcraft is assumed an infinitesimal mass with an ideal solar sail under the gravitational

attraction of two significant masses (the Earth and the moon) and subject to the gravitational

potential $U(\vec{r}_b)$ whose gradient gives the gravitational force [19]:

$$\nabla U(\vec{r}_b) = \dot{\vec{\omega}}_b \times \vec{r}_b + \vec{\omega}_b \times (\vec{\omega}_b \times \vec{r}_b) - \frac{GM_1}{r_1{}^3}\vec{r}_1 - \frac{GM_2}{r_2{}^3}\vec{r}_2 \tag{3.42a}$$

$$\nabla U(\vec{r}_b) = \dot{\vec{\omega}}_b \times \vec{r}_b + \vec{\omega}_b \times (\vec{\omega}_b \times \vec{r}_b) - \frac{\mu_1}{r_1{}^3}\vec{r}_1 - \frac{\mu_2}{r_2{}^3}\vec{r}_2 \tag{3.42b}$$

Where (assuming that the equations have already been written in standard non-dimensional form

[19]):

$\vec{r}_b$ = Position of spacecraft with respect to the E-M barycenter.

$\vec{r}_1$ = Sailcraft position vector from Earth, where:

$r_1 = \sqrt{(x - \rho)^2 + y^2 + z^2}$

$\vec{r}_2$ = Sailcraft position vector from the moon, where:

$r_2 = \sqrt{(x + 1 - \rho)^2 + y^2 + z^2}$

$\rho = M_2 / (M_1 + M_2)$ = Mass ratio of E-M system.

μ_1 = Gravitational parameter of Earth.

μ_2 = Gravitational parameter of the moon.

The equation of motion in vector form of the solar sail in an E-M system-centered orbit (see

Equation 3.43) was used to model the trajectory of a sailcraft in the vicinity of the E-M system.

The equation of motion of a sailcraft is like Equation 2.35. The equation of motion in vector

form of the solar sail in a reference frame rotating with constant angular velocity $\vec{\omega}_b$ can be

written as [18]

$$\ddot{\vec{r}}_b = -2\vec{\omega}_b \times \dot{\vec{r}}_b - \nabla U(\vec{r}_b) + \vec{a} \tag{3.43}$$

Where:

$\vec{a}$ = Additional acceleration due to the thrust.

If the sailcraft has thrust controls, Equation 3.43 can be rewritten using the substitution

for $\nabla U(\vec{r}_b)$ from Equation 3.42b:

$$\ddot{\vec{r}}_b = -2\vec{\omega}_b \times \dot{\vec{r}}_b - \vec{\omega}_b \times (\vec{\omega}_b \times \vec{r}_b) - \frac{\mu_1}{r_1^3}\vec{r}_1 - \frac{\mu_2}{r_2^3}\vec{r}_2 + \frac{\vec{T}}{m} \tag{3.44}$$

Where:

$\vec{T}$ = Actual thrust vector due to SRP and controls.

m = Mass of the sailcraft.

Note the actual thrust vector $\vec{T}$ is a function both of the SRP, which is itself a function of position

$\vec{r}$, and of any controls acting on the sailcraft.

Equation 3.43 may be rewritten again in standard non-dimensional form. From [20], the nondimensionalized, nonlinear equations of motion of the sailcraft subject to gravitational acceleration by the E-M system, inertial acceleration, and control acceleration are

$$\ddot{x} - 2\dot{y} - x = -\frac{(1-\rho)(x-\rho)}{r_1{}^3} - \frac{\rho\,(x+1-\rho)}{r_2{}^3} + \tilde{u}_x \tag{3.45a}$$

$$\ddot{y} + 2\dot{x} - y = -\frac{(1-\rho)y}{r_1{}^3} - \frac{\rho\,y}{r_2{}^3} + \tilde{u}_y \tag{3.45b}$$

$$\ddot{z} = -\frac{(1-\rho)\,z}{r_1{}^3} - \frac{\rho\,z}{r_2{}^3} + \tilde{u}_z \tag{3.45c}$$

Where:

(x, y, z) = Coordinates of the actual position vector at time t_k.

$\tilde{u}_x$ = Actual control acceleration component along x-axis.

$\tilde{u}_y$ = Actual control acceleration component along y-axis.

$\tilde{u}_z$ = Actual control acceleration component along z-axis.

Note that time is in units of $1/\omega_b$ and the z-axis equation is decoupled from the in-plane equations of motion. The terms $-2\dot{y}$ and $2\dot{x}$ are the Coriolis accelerations and the terms $-x$ and $-y$ are the centrifugal accelerations [20].

Reference trajectory, $\vec{R}$. The reference trajectory is a pre-determined logarithmic spiral trajectory. The sailcraft's reference position is where the sailcraft is supposed to be if it follows the reference trajectory perfectly. The reference trajectory is the series of reference positions over time and the two terms are used interchangeably. The sailcraft's reference position $\vec{R}$ with respect to the E-M barycenter can be expressed in B in Cartesian coordinates as

$$\vec{R} = X\,\hat{b}_1 + Y\,\hat{b}_2 + Z\,\hat{b}_3 \tag{3.46}$$

and the magnitude of the reference position vector from the E-M barycenter is

$$R = \sqrt{X^2 + Y^2 + Z^2} \tag{3.47}$$

Note the use of capitalization to distinguish between terms for the sailcraft's actual position over time and the sailcraft's desired position over time.

The equation of motion in vector form of the sailcraft's reference position (see Equation 3.48) was used to model the reference trajectory around the E-M system. The reference trajectory starts with a circular orbit around the E-M barycenter, is disturbed by a small term to form instead a slow logarithmic spiral out from Earth toward the moon, and is subject to a control acceleration to follow the desired path:

$$\ddot{\vec{R}} = -2\vec{\omega}_b \times \dot{\vec{R}} - \vec{\omega}_b \times (\vec{\omega}_b \times \vec{R}) - \frac{\mu_1}{R_1{}^3}\vec{R}_1 - \frac{\mu_2}{R_2{}^3}\vec{R}_2 + \Delta\vec{o} + \frac{\vec{T}^*}{m} \tag{3.48}$$

Where:

$\vec{R}$ = Sailcraft reference position vector.

$\vec{R}_1$ = Reference trajectory position vector from Earth.

$\vec{R}_2$ = Reference trajectory position vector from the moon.

$\Delta\vec{o}$ = Disturbing term from circular orbit to cause a logarithmic spiral out, where:

$\Delta\vec{o} = N_1\vec{R} + N_2\dot{\vec{R}}$

$\vec{T}^*$ = Thrust vector to follow the reference trajectory.

Note the reference thrust vector $\vec{T}^*$ is a function both of the SRP, which is itself a function of position $\vec{r}$, and of the controls acting on the sailcraft. The disturbing term makes circular orbit a little bit unstable, turning it into a logarithmic spiral outward instead. For simplicity, the disturbing term is assumed to be a linear function of the $\vec{R}$ and $\dot{\vec{R}}$ vectors. The disturbing term in the second model was similar but this third model adds the derivative term for more flexibility in the solutions. The coefficients N_1 and N_2 are scalars and are assumed small so that large thrust is not required to effect the reference trajectory, which means the logarithmic spiral deviation from a circle is also small.

Equation 3.48 may be rewritten in standard non-dimensional form. From [20], the nondimensionalized, nonlinear equations of motion of the reference trajectory subject to gravitational acceleration by the E-M system, inertial acceleration, the disturbing term, and control acceleration are

$$\ddot{X} - 2\dot{Y} - X = -\frac{(1-\rho)(X-\rho)}{R_1^{\,3}} - \frac{\rho\,(X+1-\rho)}{R_2^{\,3}} + N_1 X + N_2 \dot{X} + u_x^* \tag{3.49a}$$

$$\ddot{Y} + 2\dot{X} - Y = -\frac{(1-\rho)Y}{R_1^{\,3}} - \frac{\rho\,Y}{R_2^{\,3}} + N_1 Y + N_2 \dot{Y} + u_y^* \tag{3.49b}$$

$$\ddot{Z} = -\frac{(1-\rho)\,Z}{R_1^{\,3}} - \frac{\rho\,Z}{R_2^{\,3}} + N_1 Z + N_2 \dot{Z} + u_z^* \tag{3.49c}$$

Where:

(X, Y, Z) = Coordinates of the reference trajectory position vector at time t_k.

u_x^* = Reference control acceleration component along x-axis.

u_y^* = Reference control acceleration component along y-axis.

u_z^* = Reference control acceleration component along z-axis.

The time is in units of $1/\omega_b$ and the z-axis equation is decoupled from the in-plane equations of motion. The terms $-2\dot{Y}$ and $2\dot{X}$ are the Coriolis accelerations and the terms $-X$ and $-Y$ are the centrifugal accelerations [20].

Sailcraft position error, $\vec{e}_{out}$. The difference between the sailcraft's actual position and its desired or reference position is the sailcraft position error, defined as

$$\vec{e}_{out} \equiv \vec{r}_b - \vec{R} \tag{3.50}$$

Where:

$\vec{e}_{out}$ = Sailcraft position error.

The sailcraft position error $\vec{e}_{out}$ relative to the E-M barycenter can be expressed in B in Cartesian coordinates as

$$\vec{e}_{out} = e_x \, \hat{b}_1 + e_y \, \hat{b}_2 + e_z \, \hat{b}_3 \tag{3.51}$$

and the magnitude of the position error is

$$e_{out} = \sqrt{e_x{}^2 + e_y{}^2 + e_z{}^2} \tag{3.52}$$

I can treat $R_1{}^3$ as approximately equal to $r_1{}^3$ and $R_2{}^3$ as approximately equal to $r_2{}^3$ because the sailcraft actual trajectory is assumed to have only small deviations from the reference trajectory. Using this assumption and subtracting Equation 3.49a-c from Equation

3.45a-c, the nondimensionalized, nonlinear equations of motion of the error subject to

gravitational acceleration by E-M system, inertial acceleration, the disturbing term, and control

acceleration are

$$\ddot{e}_x - 2\dot{e}_y - e_x = -\frac{(1-\rho)e_x}{r_1{}^3} - \frac{\rho\, e_x}{r_2{}^3} - N_1 X - N_2 \dot{X} + u_x \tag{3.53a}$$

$$\ddot{e}_y + 2\dot{e}_x - e_y = -\frac{(1-\rho)e_y}{r_1{}^3} - \frac{\rho\, e_y}{r_2{}^3} - N_1 Y - N_2 \dot{Y} + u_y \tag{3.53b}$$

$$\ddot{e}_z = -\frac{(1-\rho)\, e_z}{r_1{}^3} - \frac{\rho\, e_z}{r_2{}^3} - N_1 Z - N_2 \dot{Z} + u_z \tag{3.53c}$$

Where:

u_x = Error control acceleration component along x-axis.

u_y = Error control acceleration component along y-axis.

u_z = Error control acceleration component along z-axis.

The time is in units of $1/\omega_b$ and the z-axis equation is decoupled from the in-plane equations of

motion. The terms $-2\dot{e}_y$ and $2\dot{e}_x$ are the Coriolis accelerations and the terms $-e_x$ and $-e_y$ are

the centrifugal accelerations [20].

Earth-moon barycenter orbiting sun, $\vec{R}_{IB}$. The E-M barycenter's position vector $\vec{R}_{IB}$

relative to the sun can be expressed in I in Cartesian coordinates as

$$\vec{R}_{IB} = x\, \hat{\imath}_1 + y\, \hat{\imath}_2 + z\, \hat{\imath}_3 \tag{3.54}$$

and the magnitude of the position vector or the distance of the E-M barycenter from the sun's

center is

$$R_{IB} = \sqrt{x^2 + y^2 + z^2} \tag{3.55}$$

The equation of motion in vector form of the E-M barycenter in a sun-centered orbit (see Equation 3.56) was used to model the trajectory of the E-M barycenter around the sun. The E-M system is assumed a point mass orbiting a primary body (sun) in a R2BP and subject to the sun's gravity [19]:

$$\ddot{\vec{R}}_{IB} = -\mu_O \frac{\vec{R}_{IB}}{R_{IB}^3} \tag{3.56}$$

Where:

μ_O = Gravitational parameter of the sun.

Note R_{IB}^3 is considered constant since the system is approximated to have a circular orbit around the sun.

State-space models. There are four state-space models, three for the CR3BP and one for the R2BP. The first solves for x and the fourth solves for Z, which contain $\vec{r}_b$ and $\vec{R}_{IB}$, respectively. The second defines the reference trajectory X and the third defines the error e between the actual and reference trajectories for use in the LQR control algorithm.

Sailcraft orbiting Earth-moon barycenter, x . If I choose $x_1 = x$, $x_2 = y$, $x_3 = z$, $x_4 = v_x$, $x_5 = v_y$, $x_6 = v_z$ (i.e., the components of the sailcraft's actual position and velocity vectors with respect to the E-M barycenter) as the state variables, then the state-variable description of the linear system in Equations 3.45a-c becomes:

$$\dot{x}_1 = x_4 \tag{3.57}$$

$$\dot{x}_2 = x_5$$

$$\dot{x}_3 = x_6$$

$$\dot{x}_4 = 2x_5 + x_1 - \frac{(1-\rho)(x_1-\rho)}{r_1{}^3} - \frac{\rho\,(x_1+1-\rho)}{r_2{}^3} + \frac{1}{m}\tilde{T}_1$$

$$\dot{x}_5 = -2x_4 + x_2 - \frac{(1-\rho)x_2}{r_1{}^3} - \frac{\rho\,x_2}{r_2{}^3} + \frac{1}{m}\tilde{T}_2$$

$$\dot{x}_6 = -\frac{(1-\rho)\,x_3}{r_1{}^3} - \frac{\rho\,x_3}{r_2{}^3} + \frac{1}{m}\tilde{T}_3$$

Where:

$\tilde{T}_1 = \tilde{T}_x$ = Actual thrust control input vector component along x-axis.

$\tilde{T}_2 = \tilde{T}_y$ = Actual thrust control input vector component along y-axis.

$\tilde{T}_3 = \tilde{T}_z$ = Actual thrust control input vector component along z-axis.

If I define the state vector x using the state variables as elements:

$$x = [x_1 \quad x_2 \quad x_3 \quad x_4 \quad x_5 \quad x_6]^T \tag{3.58}$$

then the Equation 3.57 can be written as the state-space equation:

$$\dot{x} = f(x) + B\,\tilde{T} \tag{3.59}$$

Where:

$\tilde{T}$ = Actual thrust control input vector and $f(x)$ includes all other terms.

Note $\tilde{T}$ is the sailcraft's actual thrust vector due to SRP and control inputs. The mathematical

format in Equation 3.58 makes physical sense because the actual trajectory of the sailcraft is the

nearly Keplerian equations of motion due to gravity plus an additional term due to the SRP

(including any controls) acting on the solar sail.

Reference trajectory, X. If I choose $X_1 = X$, $X_2 = Y$, $X_3 = Z$, $X_4 = VX$, $X_5 = VY$,

$X_6 = VZ$ (i.e., the components of the reference trajectory's position and velocity vectors with

respect to the E-M barycenter) as the state variables, then the state-variable description of the

linear system in Equations 3.49a-c becomes:

$$\dot{X}_1 = X_4 \tag{3.60}$$

$$\dot{X}_2 = X_5$$

$$\dot{X}_3 = X_6$$

$$\dot{X}_4 = 2X_5 + X_1 - \frac{(1-\rho)(X_1-\rho)}{R_1{}^3} - \frac{\rho\,(X_1+1-\rho)}{R_2{}^3} + N_1 X_1 + N_2 X_4 + \frac{1}{m}T_1{}^*$$

$$\dot{X}_5 = -2X_4 + X_2 - \frac{(1-\rho)X_2}{R_1{}^3} - \frac{\rho\,X_2}{R_2{}^3} + N_1 X_2 + N_2 X_5 + \frac{1}{m}T_2{}^*$$

$$\dot{X}_6 = -\frac{(1-\rho)\,X_3}{R_1{}^3} - \frac{\rho\,X_3}{R_2{}^3} + N_1 X_3 + N_2 X_6 + \frac{1}{m}T_3{}^*$$

Where:

$T_1^* = T_x^* =$ Reference thrust control input vector component along x-axis.

$T_2^* = T_y^* =$ Reference thrust control input vector component along y-axis.

$T_3^* = T_z^* =$ Reference thrust control input vector component along z-axis.

If I define the state vector X using the state variables as elements:

$$X = [X_1 \quad X_2 \quad X_3 \quad X_4 \quad X_5 \quad X_6]^T \qquad (3.61)$$

then the Equation 3.60 can be written as the state-space equation

$$\dot{X}(t) = f(X) + \Delta o + B\, T^* \qquad (3.62)$$

Where:

Δo = Disturbing term from circular orbit to cause a logarithmic spiral out, where:

$$\Delta o = N_3 X = \begin{bmatrix} 0 & 0 & 0 & 0 & 0 & 0 \\ 0 & 0 & 0 & 0 & 0 & 0 \\ 0 & 0 & 0 & 0 & 0 & 0 \\ N_1 & 0 & 0 & N_2 & 0 & 0 \\ 0 & N_1 & 0 & 0 & N_2 & 0 \\ 0 & 0 & N_1 & 0 & 0 & N_2 \end{bmatrix} \begin{bmatrix} X_1 \\ X_2 \\ X_3 \\ X_4 \\ X_5 \\ X_6 \end{bmatrix}$$

N_3 = Reference trajectory matrix.

T^* = Reference thrust control input vector.

Note T^* is the desired thrust vector for the sailcraft to follow the reference trajectory. The mathematical format of Equation 3.62 makes physical sense because the reference trajectory that the sailcraft should follow is, again, nearly Keplerian. The Δo term accounts for the deviations from the Keplerian orbit in the form of a logarithmic spiral and the T^* term accounts for the sail's desired thrust controls to follow the reference spiral trajectory exactly. Since coefficients N_1 and N_2 are small scalars, then N_3 is a small, constant matrix.

Sailcraft error state vector, e . To parallel the sailcraft position error defined in Equation 3.50, the sailcraft error state vector can be defined as

$$e = x - X \tag{3.63}$$

Where:

e = Sailcraft error state vector.

x = Actual state vector.

X = Desired state vector.

That is,

$$[e]_i = [x]_i - [X]_i \ \forall \ i \tag{3.64}$$

Note that the error state vector e represents errors in position and velocity; the position error $\vec{e}_{out}$ only represents errors in position.

If I choose $e_1 = e_x$, $e_2 = e_y$, $e_3 = e_z$, $e_4 = e_{vx}$, $e_5 = e_{vy}$, $e_6 = e_{vz}$ (i.e., the components of the errors in the sailcraft's position and velocity vectors with respect to the E-M barycenter) as the state variables, then the state-variable description of the linear system in Equation 3.53a-c becomes:

$$\dot{e}_1 = e_4 \tag{3.65}$$

$$\dot{e}_2 = e_5$$

$$\dot{e}_3 = e_6$$

$$\dot{e}_4 = 2e_5 + e_1 - \frac{(1-\rho)e_1}{r_1{}^3} - \frac{\rho \, e_1}{r_2{}^3} - N_1 X - N_2 \dot{X} + \frac{1}{m} T_1$$

$$\dot{e}_5 = -2e_4 + e_2 - \frac{(1-\rho)e_2}{r_1{}^3} - \frac{\rho \, e_2}{r_2{}^3} - N_1 Y - N_2 \dot{Y} + \frac{1}{m} T_2$$

$$\dot{e}_6 = -\frac{(1-\rho)\,e_3}{r_1{}^3} - \frac{\rho\,e_3}{r_2{}^3} - N_1 Z - N_2 \dot{Z} + \frac{1}{m} T_3$$

Where:

$T_1 = T_x$ = Error thrust control input vector component along x-axis.

$T_2 = T_y$ = Error thrust control input vector component along y-axis.

$T_3 = T_z$ = Error thrust control input vector component along z-axis.

$[X \quad Y \quad Z \quad \dot{X} \quad \dot{Y} \quad \dot{Z}]^T = [X_1 \quad X_2 \quad X_3 \quad X_4 \quad X_5 \quad X_6]^T$ = Reference trajectory state

vector.

Or, substituting Equations 3.57 and 3.60 into Equation 3.64, the state-variable description can be

written as

$$\dot{e}_1 = e_4 \tag{3.66}$$

$$\dot{e}_2 = e_5$$

$$\dot{e}_3 = e_6$$

$$\dot{e}_4 = 2e_5 + e_1 - \frac{(1-\rho)e_1}{r_1{}^3} - \frac{\rho\,e_1}{r_2{}^3} + \frac{1}{m}\tilde{T}_1 - N_1 X_1 - N_2 X_4 - \frac{1}{m}T_1{}^*$$

$$\dot{e}_5 = -2e_4 + e_2 - \frac{(1-\rho)e_2}{r_1{}^3} - \frac{\rho\,e_2}{r_2{}^3} + \frac{1}{m}\tilde{T}_2 - N_1 X_2 - N_2 X_5 - \frac{1}{m}T_2{}^*$$

$$\dot{e}_6 = -\frac{(1-\rho)\,e_3}{r_1{}^3} - \frac{\rho\,e_3}{r_2{}^3} + \frac{1}{m}\tilde{T}_3 - N_1 X_3 - N_2 X_6 - \frac{1}{m}T_3{}^*$$

If I define the state vector $\boldsymbol{e}$ using the state variables as elements:

$$\boldsymbol{e} = [e_1 \quad e_2 \quad e_3 \quad e_4 \quad e_5 \quad e_6]^T \tag{3.67}$$

then the Equation 3.66 can be written as the state-space equation

$$\dot{e} = f(e + X) - f(X) + B\,\tilde{T} - N_3\,X - B\,T^* \tag{3.68}$$

This state-space equation will be further manipulated in the Controls subsection.

Earth-moon barycenter orbiting sun, Z. A state matrix is used to model the E-M barycenter orbiting the sun. The letter Z is used to distinguish the E-M barycenter's state matrix from the sailcraft's state matrix. If I choose $Z_1 = X_{IB}$, $Z_2 = Y_{IB}$, $Z_3 = Z_{IB}$, $Z_4 = V_{X_{IB}}$, $Z_5 = V_{Y_{IB}}$, $Z_6 = V_{Z_{IB}}$ (i.e., the components of the E-M barycenter's position and velocity vectors with respect to the sun) as the state variables, then the state-variable description of the linear system in Equation 3.56 becomes:

$$\dot{Z}_1 = Z_4 \tag{3.69}$$

$$\dot{Z}_2 = Z_5$$

$$\dot{Z}_3 = Z_6$$

$$\dot{Z}_4 = \frac{-\mu_O}{R_{IB}{}^3} Z_1$$

$$\dot{Z}_5 = \frac{-\mu_O}{R_{IB}{}^3} Z_2$$

$$\dot{Z}_6 = \frac{-\mu_O}{R_{IB}{}^3} Z_3$$

If I define the state vector $\mathbf{Z}$ using the state variables as elements:

$$\mathbf{Z} = [Z_1 \quad Z_2 \quad Z_3 \quad Z_4 \quad Z_5 \quad Z_6]^T \tag{3.70}$$

then the Equation 3.69 can be written as the state-space equation

$$\dot{Z} = A_{IB}Z = \begin{bmatrix} 0 & 0 & 0 & 1 & 0 & 0 \\ 0 & 0 & 0 & 0 & 1 & 0 \\ 0 & 0 & 0 & 0 & 0 & 1 \\ -\frac{\mu_O}{R_{IB}^3} & 0 & 0 & 0 & 0 & 0 \\ 0 & -\frac{\mu_O}{R_{IB}^3} & 0 & 0 & 0 & 0 \\ 0 & 0 & -\frac{\mu_O}{R_{IB}^3} & 0 & 0 & 0 \end{bmatrix} \begin{bmatrix} Z_1 \\ Z_2 \\ Z_3 \\ Z_4 \\ Z_5 \\ Z_6 \end{bmatrix} \tag{3.71}$$

Where:

A_{IB} = State matrix of Earth relative to E-M system barycenter.

Note A_{IB} does not depend on t (continuous time-invariant) because R_{IB} is constant.

Using the state transition matrix of A_{IB}, Equation 3.71 can also be rewritten as:

$$Z(t_{k+1}) = e^{A_{IB}(t_{k+1}-t_k)} Z(t_k) \tag{3.72}$$

Note Equations 3.71 and 3.72 are both continuous time expressions.

Since A_{IB} is constant during time interval dt, Equation 3.72 can be approximated using the first three terms in a Taylor series expansion of the exponential matrix [20] as:

$$Z(t_{k+1}) \cong \left(I + A_{IB}\, dt + 0.5\, A_{IB}^2\, dt^2\right) Z(t_k) \tag{3.73}$$

Note Equation 3.73 is a discretized time expression. For sufficiently small values of dt, Equation 3.73 behaves like Equation 3.71. In addition, I can assume $\mathbf{Z}(t_k)$ will change very little during dt and thus treat it as a constant. Then, between steps, I update $\mathbf{Z}(t_k)$. With Equation 3.73, the E-M system's orbital equation of motion is now in the desired form, which can be entered into MATLAB and used to simulate the E-M system's position over time.

Control models. This subsection describes the control goal selected for this model and the initial control design as well as an LQR control design. A linear control algorithm is assumed, and the system is modeled as a standard linear feedback control system. The control model is designed to make the system asymptotically stable.

Control goal. The control goal for this thesis is stabilization: that the system output $y(t)$ converges quickly to the desired output Y. The system output is the sailcraft's actual position at time t:

$$y(t) = \vec{r}_b = [x_1 \quad x_2 \quad x_3]^T \tag{3.74}$$

The desired output is the reference position, defined in advance via trajectory design:

$$Y = \vec{R} = [X_1 \quad X_2 \quad X_3]^T \tag{3.75}$$

The difference between the two output positions is the output error, also known as the position error, defined in vector notation as

$$\vec{e}_{out} = y(t) - Y = \vec{r}_b - \vec{R} \tag{3.76}$$

and in state-space as

$$\boldsymbol{e_{out}} = \begin{bmatrix} 1 & 0 & 0 & 0 & 0 & 0 \\ 0 & 1 & 0 & 0 & 0 & 0 \\ 0 & 0 & 1 & 0 & 0 & 0 \end{bmatrix} \boldsymbol{x} - \begin{bmatrix} 1 & 0 & 0 & 0 & 0 & 0 \\ 0 & 1 & 0 & 0 & 0 & 0 \\ 0 & 0 & 1 & 0 & 0 & 0 \end{bmatrix} \boldsymbol{X} \qquad (3.77)$$

If stabilization is achieved, then the sailcraft's actual position over time (i.e., its actual trajectory) converges to the reference trajectory:

$$y(t) \to Y \text{ and } \vec{e}_{out} \to \vec{0} \text{ and } \boldsymbol{e_{out}} \to \boldsymbol{0} \qquad (3.78)$$

The sailcraft follows the reference path exactly for

$$y(t) = Y \text{ and } \vec{e}_{out} = \vec{0} \text{ and } \boldsymbol{e_{out}} = \boldsymbol{0} \qquad (3.79)$$

However, the sailcraft's position relative to the reference trajectory is not the only factor in the stability of its path. If the sailcraft's actual instantaneous velocity is very different from the reference velocity for that position, the sailcraft will not follow the reference path for very long. Therefore, the overall error, i.e., the sailcraft error state vector $\boldsymbol{e}$, should also go to zero.

Initial control design. I can treat $R_1{}^3$ as approximately equal to $r_1{}^3$ and $R_2{}^3$ as approximately equal to $r_2{}^3$ because the sailcraft actual trajectory is assumed to have only small deviations from the reference trajectory. Using this assumption and subtracting Equation 3.44 from Equation 3.48, the position error equation of motion in vector form is

$$\ddot{\vec{e}} = \ddot{\vec{r}}_b - \ddot{\vec{R}} = -2\vec{\omega}_b \times \dot{\vec{e}} - \vec{\omega}_b \times (\vec{\omega}_b \times \vec{e}) - \frac{\mu_1}{r_1{}^3}\vec{e}_1 - \frac{\mu_2}{r_2{}^3}\vec{e}_2 - N_1\vec{R} - N_2\dot{\vec{R}}_1 + \frac{\vec{T}}{m} - \frac{\vec{T}^*}{m} \quad (3.80)$$

Where:

$\vec{e}_1$ = Difference in sailcraft's actual and desired position vectors from the Earth.

$\vec{e}_2$ = Difference in sailcraft's actual and desired position vectors from the moon.

Note, vectors $\vec{e}_1$ and $\vec{e}_2$ are different from the scalars e_1 and e_2 in Equations 3.65 through 3.67.

To rewrite Equation 3.80 in terms of $\vec{e}$ and $\vec{u}$ only, first let the actual thrust vector $\vec{T}$ be given as

$$\vec{T} = m\,N_1\vec{r}_b + m\,N_2\,\dot{\vec{r}}_b + m\,\vec{u}(t) \tag{3.81}$$

Then, substituting Equation 3.81 into Equation 3.80, the error equation of motion is

$$\ddot{\vec{e}} = -2\vec{\omega}_b \times \dot{\vec{e}} - \vec{\omega}_b \times (\vec{\omega}_b \times \vec{e}) - \frac{\mu_1}{r_1{}^3}\vec{e}_1 - \frac{\mu_2}{r_2{}^3}\vec{e}_2 + N_1\,\vec{e} + N_2\,\dot{\vec{e}} + \vec{u}(t) - \frac{\vec{T}^*}{m} \tag{3.82}$$

For the purposes of this thesis, a linear control algorithm is assumed. I can choose a linear control given by

$$\vec{u}(t) = f(\vec{e}) + \frac{\vec{T}^*}{m} \tag{3.83}$$

where $f(\vec{e})$ is a linear function of $\vec{e}$ described above and such that $f(0) = 0$. So, when the position error $\vec{e}$ is zero (i.e., when the sailcraft is on the reference trajectory), the controls instruct the sailcraft to follow the reference trajectory thrust vector controls. Substituting Equation 3.83 into Equation 3.82, the error equation of motion can be written as

$$\ddot{\vec{e}} = -2\vec{\omega}_b \times \dot{\vec{e}} - \vec{\omega}_b \times (\vec{\omega}_b \times \vec{e}) - \frac{\mu_1}{r_1{}^3}\vec{e}_1 - \frac{\mu_2}{r_2{}^3}\vec{e}_2 + N_1\,\vec{e}\, + N_2\,\dot{\vec{e}} + f(\vec{e}\,) \qquad (3.84)$$

Finally, the expression is only in terms of the position error $\vec{e}$, though the $f(\vec{e}\,)$ value is unknown.

The same process can be followed in state-space form. To design a control algorithm that ensures the stability of the system, I must write the system in the format of Equation 2.40. Here, the system refers to the set of differential equations that describe the equations of motion for the error state vector $\boldsymbol{e}$. To rewrite Equation 3.68 in the format of Equation 2.40 in terms of $\boldsymbol{e}$ and $\boldsymbol{u}$ only, first let the actual thrust control input vector $\widetilde{\boldsymbol{T}}$ be given as

$$\widetilde{\boldsymbol{T}} = -\,\boldsymbol{K}\,\boldsymbol{e} + m\,\boldsymbol{N_3}\boldsymbol{X} + \boldsymbol{T}^* \qquad (3.85)$$

Where:

$\boldsymbol{K}$ = Control gain matrix.

Note $\boldsymbol{K}$ is a slowly changing, almost constant matrix. The job of this control $\widetilde{\boldsymbol{T}}$ is to compensate for the $\Delta\boldsymbol{o} + \boldsymbol{T}^*$ terms in the reference trajectory and to make the error state vector $\boldsymbol{e}$ go to zero. The effectively linear $-\boldsymbol{K}\,\boldsymbol{e}$ term ensures stability and the $m\boldsymbol{N_3}\boldsymbol{X} + \boldsymbol{T}^*$ terms exist for the sailcraft to follow the desired path, like feedback and feed forward controls, respectively.

As a check on my work, I confirm the actual thrust control input vector $\widetilde{\boldsymbol{T}}$ simplifies to the reference thrust control input vector $\boldsymbol{T}^*$ when the error state vector $\boldsymbol{e} = \boldsymbol{0}$ (i.e., when the sailcraft's actual position and velocity match that of the reference trajectory). Substituting Equation 3.85 into Equation 3.59 and letting $\boldsymbol{e} = \boldsymbol{0}$, I obtain

$$\dot{x} = f(x) - BK\,e + mBN_3X + B\,T^* = f(x) + IN_3X + B\,T^* \qquad (3.86)$$

If $e = 0$, then $x = X$ and Equation 3.86 can be written as

$$\dot{x} = f(X) + N_3X + B\,T^* \qquad (3.87)$$

which is the same right-hand side as Equation 3.62. This relationship makes physical sense because, when the error state vector e is zero, the controls instruct the sailcraft to move along the trajectory subject to three conditions: the nearly Keplerian equations of motion due to gravity, the disturbing term that forms the desired spiral trajectory, and the reference thrust control input vector T^*. Also, the state-space form Equation 3.85 is equivalent to the vector form Equation 3.81 with the 3.83 substitution.

Next, substituting Equation 3.85 into Equation 3.68, the error state vector's state-space equation is

$$\dot{e} = f(e + X) - f(X) - BKe + IN_3X + B\,T^* - N_3X - B\,T^* \qquad (3.88)$$

which simplifies to

$$\dot{e} = f(e + X) - f(X) - BKe \qquad (3.89)$$

or even more simply to

$$\dot{e} = A\,e - BKe = (A - BK)e \tag{3.90}$$

Where:

A = System matrix.

Note A is a slowly changing, almost constant matrix. It technically depends on time t (continuous time-variant) due to the r_b term slowly changing as the sailcraft moves. However, A is changing so slowly that I can assume A is constant and use a constant matrix approach as opposed to a time-dependent matrix approach. Over time, I will need to correct K a little bit as I go, after A has changed enough.

Finally, Equation 3.90 is in the form of Equation 2.40, the desired state-space form for stability analysis. For the error to go to zero, the matrix pair (A, B) should be controllable. This system is said to be controllable if the following condition is satisfied: the $n \times nm$ controllability matrix (see Equation 2.41) has rank n. If the system is controllable, then it can be stabilized [20]. The eigenvalues of the $(A - BK)$ matrix can be assigned to make the system in Equation 3.90 asymptotically stable. The system is stable, and the error converges to zero when the eigenvalues λ_i for $A - BK$ have negative real parts.

LQR control design. Matrices A and B are determined by the physical models but K should be assigned. To choose K, one can solve for the problem of assigning eigenvalues λ_i of the matrix $A - BK$ that will ensure my error state vector e goes to zero and as a result the system for the tracking error is asymptotically stable. Another method is to apply the LQR method. Applying LQR can make the system in Equation 3.90 asymptotically stable and show the error is

converging to zero even though the controls are "turned off" when sailcraft approaches sun periodically.

First, I must solve the algebraic Ricatti equation for P [20]:

$$0 = A^T P + PA - PBR^{-1}B^T P + Q \tag{3.91}$$

Where:

P = Solution matrix to Q and R, where:

$P > 0$ and $P = P^T$

Q = State weighting matrix; $Q \geq 0$.

R = Control input weighting matrix; $R > 0$.

Next, I use the P solution to solve for K:

$$K = R^{-1}B^T P \tag{3.92}$$

Then I use the K solution to solve for the acceleration control input vector u:

$$u = -Ke \tag{3.93}$$

Lastly, I confirm this u solution will minimize the linear quadratic performance index J:

$$J = \frac{1}{2}\int_0^\infty (x^T Q x + u^T R u)\, dt \tag{3.94}$$

In this kind of optimal control problem, minimizing the index balances driving the error to zero quickly against not requiring a very large u to do so. I must avoid very large u values since the solar sail is limited in how much control thrust it can apply at once.

Alternate control design. The following alternate control design approach was considered but not completed.

1. Establish actual initial conditions (e.g., position and velocity) at t_1

2. Determine desired trajectory based on the logarithmic spiral reference trajectory at each t_k

3. Begin loop

4. Determine the error between the actual initial conditions and the desired initial conditions based on the reference trajectory at t_k

5. Determine the force required to effect the desired end conditions at t_{k+1}. Adjust the controls to generate the desired force

6. Model the sailcraft's movement from the actual initial position at t_k to the actual end position at t_{k+1}

7. Repeat loop for the next time interval.

Chapter IV
Simulation Results

This chapter details the results from the three mathematical models' simulations of the sailcraft's movement in MATLAB: The Forward Euler model, the Earth-centered state-space model, and the E-M system-centered state-space model.

Forward Euler Model

The Forward Euler model was built to model the sailcraft's motion in a circular equatorial orbit around Earth due only to gravity, not due to controls or SRP effects. The sailcraft starts in an initially circular equatorial orbit in the (x, y) plane of the ECI reference frame E. Its initial position is 1000 km altitude above Earth and initial speed is 441 km/min, the tangential velocity required to maintain a circular orbit at that altitude. The Forward Euler approximation (see Equation 3.7) is used as the update formula in the MATLAB simulations of the sailcraft position.

The total elapsed simulation time was 5000 minutes, with updates at 0.01-minute intervals, to limit error accumulation without adding too much computing time. Figure 4.1 shows the sailcraft's apparent position over time. Although modeled to maintain orbit, the sailcraft appeared to spiral outward as it orbited the Earth due to significant and rapid error accumulation in the Forward Euler approximation method, even with very short time intervals. The model of the orbit was numerically unstable due to the error accumulation, which increasingly impacted the sailcraft's apparent position over time. Over the total elapsed simulation time of 5000 minutes (83 hours), the magnitude of the sailcraft's position vector changed from 7378 to 9406 km, a fictional increase of 2028 km.
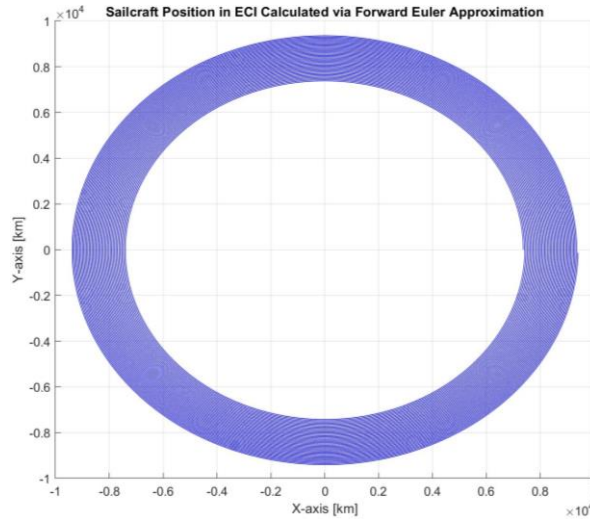
Figure 4.1 Apparent Position Over Time of Sailcraft Relative to Earth, Forward Euler Method. 2D rendering in (*x*, *y*) plane of *E*.

Earth-Centered State-Space Model

The Earth-centered state-space model was built to model the sailcraft's motion as it increases its altitude from a circular equatorial orbit around Earth due to gravity, SRP, and ideal controls, with the eclipse factor considered. The ideal controls are those for on-off switching, an exact thrust vector solution to increase altitude. The sailcraft starts in an initially circular equatorial orbit in the (*x*, *y*) plane of the semi-inertial ECI reference frame *E*, which is in orbit around the sun in the (*x*, *y*) plane of the truly inertial HEI reference frame *I*. The sailcraft's initial position is 1000 km altitude above Earth and initial speed is 441 km/min, the tangential velocity required to maintain a circular orbit at that altitude. Two different update formulae are used in the MATLAB simulations of the sailcraft position: matrix multiplication in state-space form (see Equation 3.22) with and without SRP and controls. That is, two models were built; one with $\boldsymbol{T} = 0$ and one with non-zero $\boldsymbol{T}$ substituted in the $\dot{\boldsymbol{x}} = \boldsymbol{Ax} + \boldsymbol{BT}$ system for updating spacecraft position and velocity.

Open-loop system, $\dot{x} = Ax$. The simplified model of the open-loop system does not

include SRP or controls. Figure 4.2 shows the block diagram.
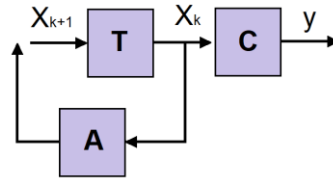
Figure 4.2 Open-Loop System Block Diagram.

The total elapsed simulation time was 5000 minutes, with updates at 0.01-minute

intervals, to limit error accumulation without adding too much computing time. The simulation

time of 5000 minutes was chosen as long enough to see the start of trends and short enough that

the computer was not excessively tied up running the simulations, especially when trouble-

shooting mistakes. The sailcraft was modeled at 10 kg and the sail area was not specified

because SRP was not considered. The position update formula used in the simulation was the

matrix multiplication in state-space form in Equation 3.22 with $T = 0$. Figure 4.3 shows the

spacecraft position over time, tracing the same circular orbit each time, even after 47 orbits.
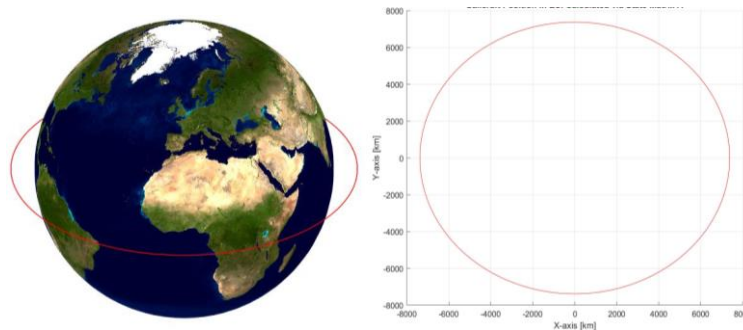
Figure 4.3 Position Over Time of Sailcraft Relative to Earth, State Matrix A Method. Left panel: 3D rendering of orbit around Earth. Right panel: 2D rendering in (x, y) plane of semi-inertial ECI reference frame E.

Figure 4.4 shows the sailcraft's position over time relative to the sun in the HEI reference frame *I*, as the sailcraft orbits the Earth. The sailcraft motion appears to zigzag from bottom right to top left as the sailcraft orbits the Earth and overall orbits the sun. The same update formula used to model the sailcraft in orbit around the Earth was adapted to model the Earth around the sun, and the two were combined to obtain the sailcraft relative to the sun. In *I*, the Earth and sailcraft start at a maximum value in the x-direction and move in an overall circular orbit around the sun. It does not account for adjustments that must be made for the ECI reference frame to change from a semi-inertial reference frame (as initially assumed) to a rotating, translating reference frame in *I*.
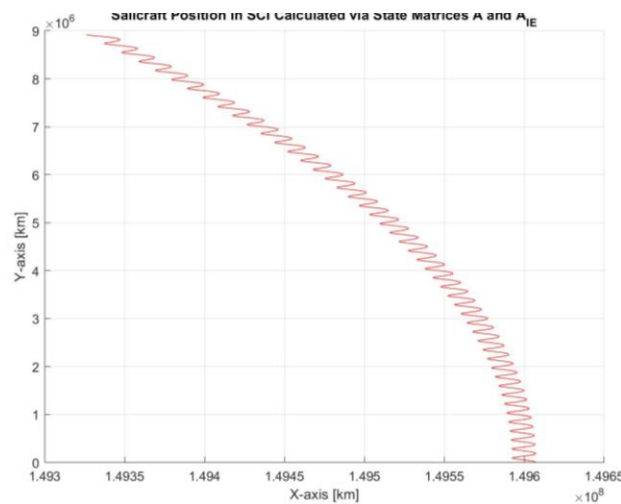
Figure 4.4 Position Over Time of Sailcraft Relative to Sun, State Matrices A and A_{IE} Method. 2D rendering in (*x*, *y*) plane of HEI reference frame *I*. Note the total simulation time is <1% of a year so the plot does not immediately appear overall circular.

Closed-loop system, $\dot{x} = Ax + B\widetilde{T}$. The simplified model of the closed-loop system includes the SRP and controls. Figure 4.5 shows the block diagram.
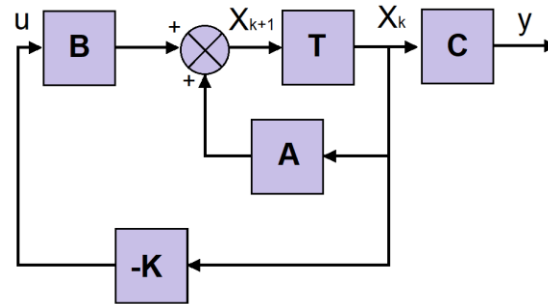
Figure 4.5 Closed-Loop System Block Diagram.

The research goal investigated a sailcraft with 25 m^2 sail area and 5 kg mass, a realistic size for a CubeSat-based sailcraft with a small payload. However, finding the elapsed time for a sailcraft with 25 m^2 sail area and 5 kg mass to reach 240,000 km from Earth was beyond the capability of my computer. As a result, two sets of simulations were run: one for a realistic-sized sailcraft with 25 m^2 sail area and 5 kg mass and one for a "super" sailcraft with 10,000 m^2 sail area and 10 kg mass. For clarity, the two sets are labeled by their respective sailing loading value. Simulations modeled the trajectories over 72,000 minutes (50 days) or until the sailcraft reached 240,000 km, whichever was first.

The total elapsed simulation time was 72,000 minutes (50 days), with updates at 0.01-minute intervals, to limit error accumulation without adding too much computing time. The position update formula used in the simulations was the matrix multiplication in state-space form in Equation 3.22 with nonzero T accounting for SRP and the simplest on-off switching method. Figures 4.6 and 4.7 show the spacecraft position over time, spiraling outward from Earth in the (x, y) plane of ECI reference frame E. The realistic-sized sailcraft with the larger sail loading value raised its orbit by less than 250 km in 50 days. The "super" sailcraft with the smaller sail loading value raised its orbit by 120,000 km in the same amount of time. The perigee of the two

trajectories was near $x = 0$ in E, which corresponds to the region of the orbit where the sailcraft is moving away from the sun and reaches maximum tangential acceleration from on-off switching.

Figure 4.6 3D Rendering of Sailcraft Trajectory Relative to Earth. Sailcraft trajectory in equatorial Earth orbit in (x, y) plane of semi-inertial ECI reference frame E, calculated via state matrix A method. Left panel: $\sigma = 0.2$. Right panel: $\sigma = 1{,}000$.

Figure 4.7 also shows the two sailcraft's trajectories with the eclipse factor considered (*red*) and without the eclipse factor (*blue*). I was curious how much the eclipse factor affected the sailcraft's spiral orbit. Note in the left panel of Figure 4.7 that both trajectories were plotted but the blue plot overlaps the red plot. In the right panel of Figure 4.7, the eclipse factor makes a very noticeable difference in the direction of the overall trajectory of the sailcraft with small σ and a noticeable difference in the major axis length. The direction of the small σ trajectory with the eclipse factor (which appears to "tilt" left) is due partly to the change in the sun's relative position to the Earth over the total elapsed time period. More specifically, the orbit's major axis remains normal to the sun-line so as the sun-line slowly rotates, the major axis also slowly changes direction within the orbital plane [19]. It is also due in part to the larger r values as the sailcraft moves away from the sun which means the radial components of its thrust do not cancel out over the duration of one orbit's 'on' mode. More investigation is required to check if there are additional factors.

For the small σ trajectory without the eclipse factor, since the Earth's shadow is not considered to block the last portion of the sailcraft's 'on' mode for on-off switching, the sailcraft can continue to accelerate due to SRP for a few extra moments each orbit. Over time, the additional thrust produces a longer trajectory in the direction of positive x values, producing the shape shown in terms of length and direction.
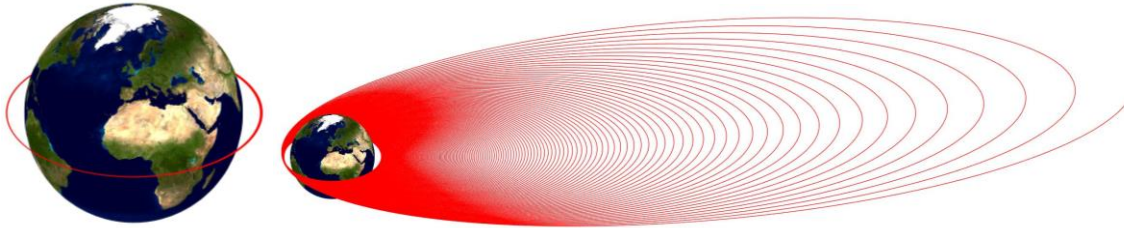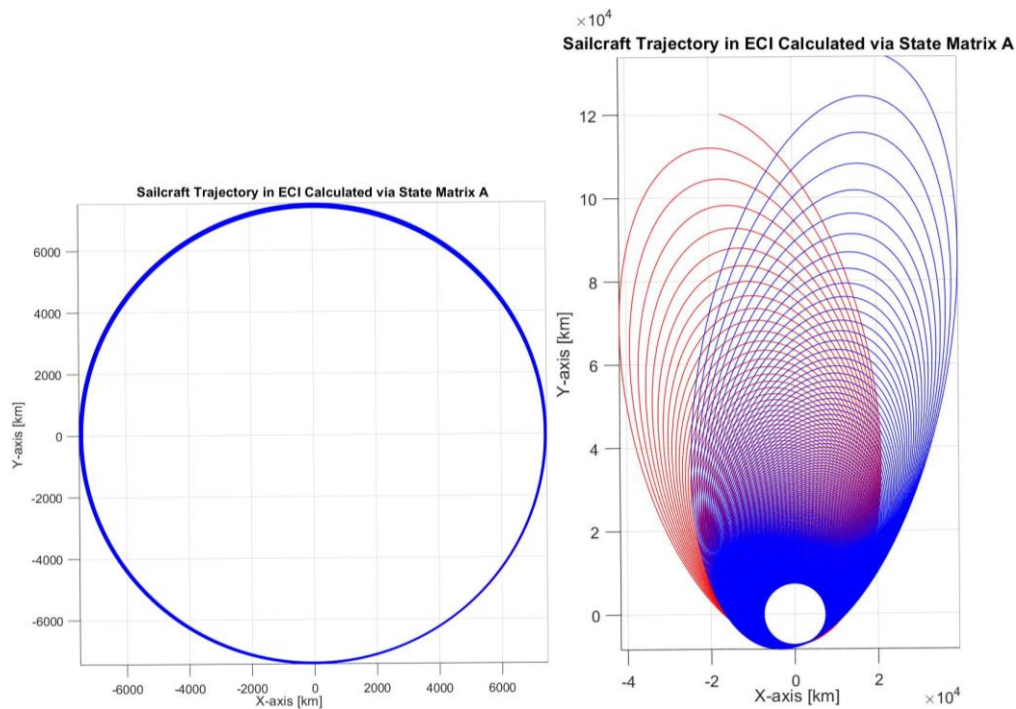

Figure 4.7 2D Rendering of Sailcraft Trajectory Relative to Earth. Sailcraft trajectory in equatorial Earth orbit in (x, y) plane of semi-inertial ECI reference frame E, calculated via state matrix A method. Left panel: $\sigma = 0.2$. Right panel: $\sigma = 0.001$. Both show trajectory with eclipse factor (*red*) and without eclipse factor (*blue*). In the left panel, the blue plot overlaps the red plot.

Figure 4.8 shows the two sailcraft's distance from Earth over time with the eclipse factor considered. The perigee and apogee in the large σ plot both increase over time, with apogee increasing faster. Each subsequent orbit is very slightly larger than the previous one such that the sinusoidal plot line instead appears as a solid block of color. In the small σ plot the perigee

decreases very slightly (so slightly it appears nearly constant) while the apogee increases

exponentially over time. The sinusoidal plot line is distinguishable over the full elapsed time. As

discussed, the sailcraft accelerates the fastest at perigee so the troughs appear very narrow

compared to the crests over equally spaced time intervals.
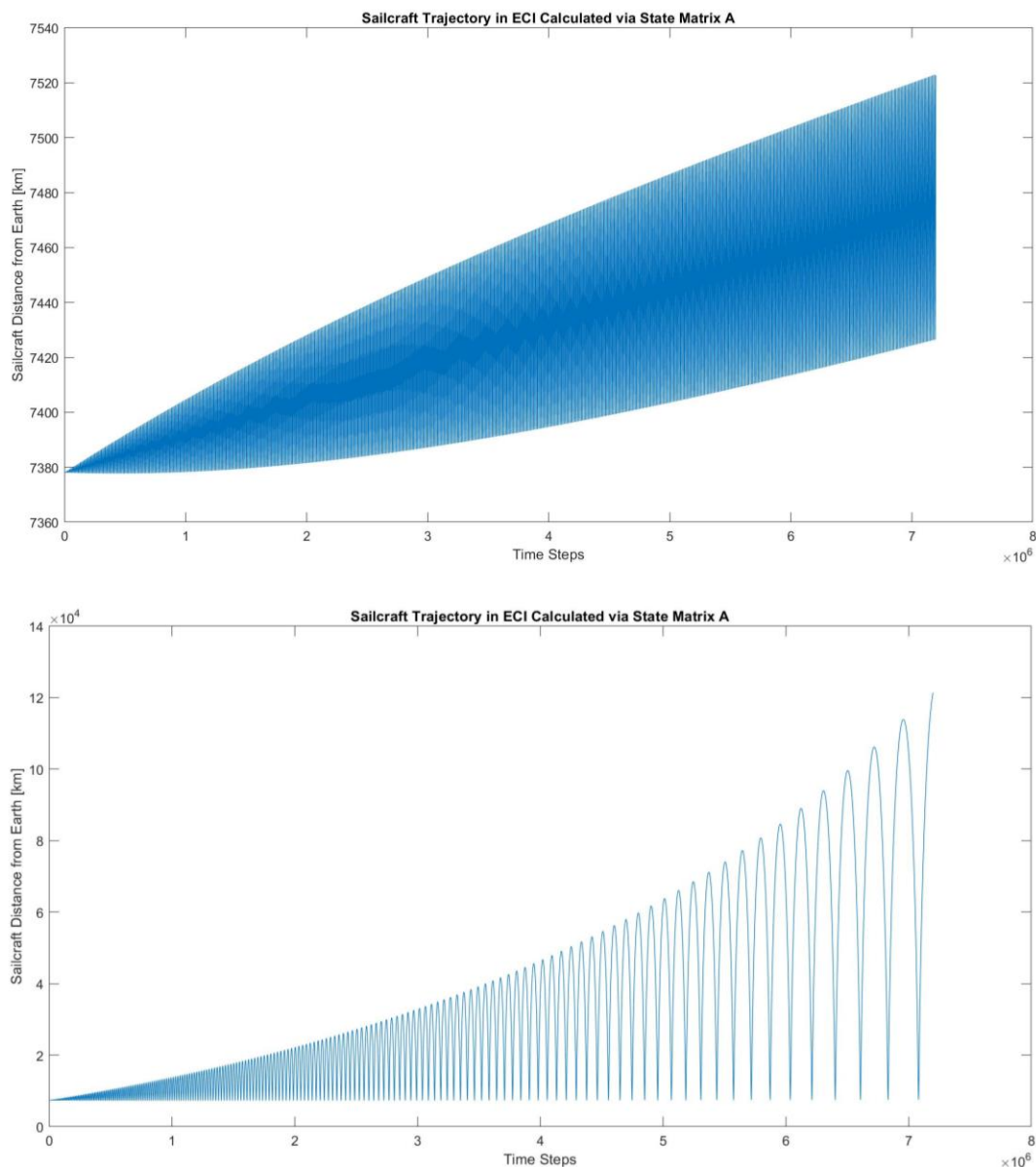
Figure 4.8 Sailcraft Distance from Earth Over Time, With Eclipse Factor. Magnitude of sailcraft trajectory in equatorial Earth orbit in E, calculated via state matrix A method. Top panel: $\sigma = 0.2$. Bottom panel: $\sigma = 0.001$.

Figure 4.9 shows the two sailcraft's magnitude of SRP acceleration (from Equation 2.4) over time, which does not consider the eclipse factor. In the large σ plot, similar to Figure 4.8 top panel, the sinusoidal plot over the total elapsed time appears as a solid block of color whose maximum and minimum values do not perceptibly change over time. Therefore, the large σ plot is instead shown over the first 10,000 time steps (100 minutes) so information can be extracted. Each orbit appears to last about 1,050 time steps (10.5 minutes).

For the small σ plot, the maximum values increase but at a slower rate than the minimum values decrease over time. If the sailcraft spirals out from Earth in the net direction of positive x values (since the eclipse factor is not considered), the distance from the sun at consecutive apogees increases. The SRP acceleration is inversely proportional to the square of the sailcraft's distance from the sun. Thus, the minimum acceleration value exponentially decreases over time.
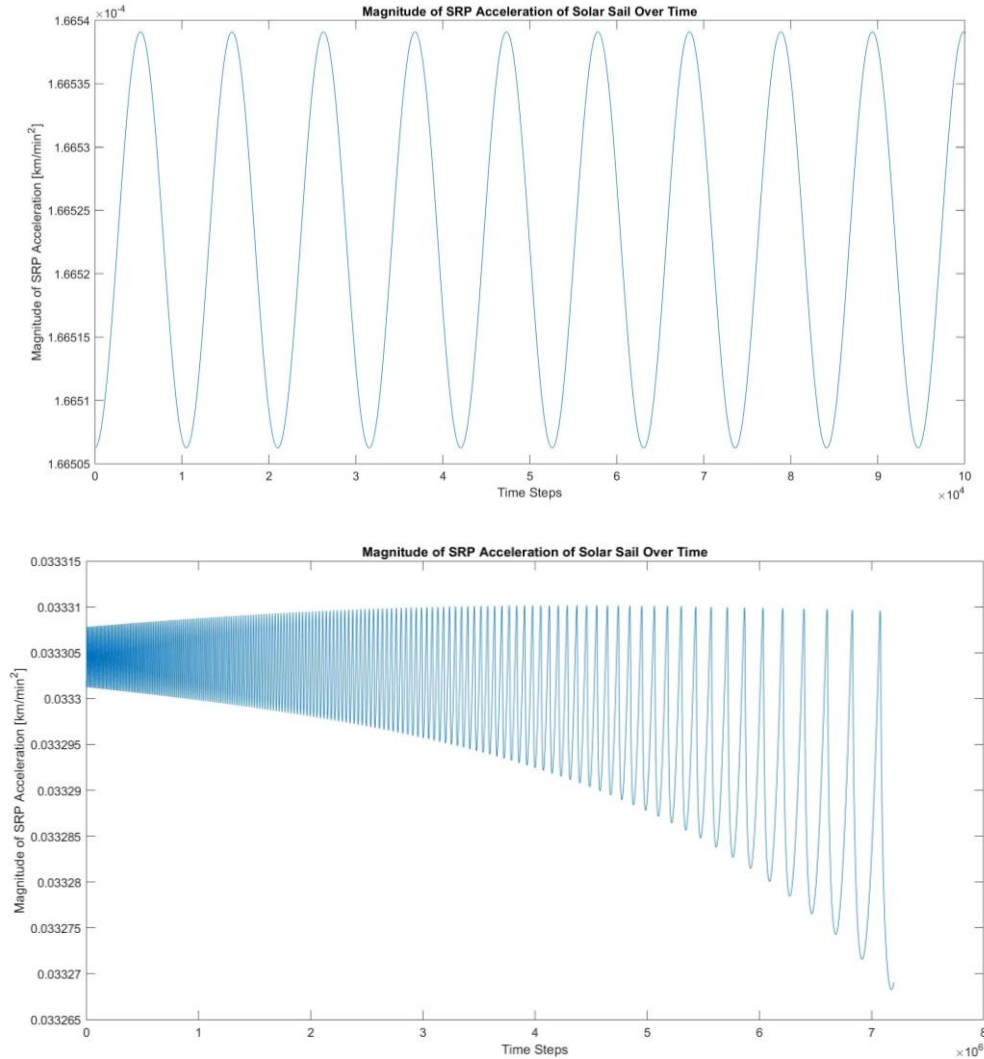
Figure 4.9 SRP Acceleration Over Time, Without Eclipse Factor. Magnitude of sailcraft acceleration due to SRP, calculated via Equation 2.4. Top panel: $\sigma = 0.2$ for the first 10,000 time steps. Bottom panel: $\sigma = 0.001$ for the full 7,200,000 time steps.

Figure 4.10 shows the two sailcraft's actual thrust vectors in the (x, y) plane with the eclipse factor considered (*blue*) and without the eclipse factor (*red*). The actual thrust vector is that experienced by the sailcraft due to SRP and on-off switching controls. Note in the top left and bottom left panels of Figure 4.10 that both trajectories were plotted but the red plot appears to completely overlap the blue plot. The large and small sail loading value plots have the approximately same wedge shape but very different value scales. The connecting plot lines are

included to indicate the thrust vector alternates between zero and non-zero values as the sailcraft switches between 'off' and 'on' steering modes, but the plots are ultimately discontinuous. The wedge shape is mostly because the Earth and sailcraft moved relative to the sun during this time and partly because the sailcraft's orbit became more elliptical.

In the top right and bottom right panels, which are detail views of the respective left panels, it is seen that the plots without the eclipse factor correspond to a larger actual thrust vector. As discussed above, this is because the sailcraft continues to accelerate due to SRP for a few extra moments each orbit. This is unrealistic for an equatorial orbit, especially at lower altitudes, since the Earth's shadow does exist and must be accounted for. However, this is important to consider if later models expand to include non-eclipsing orbits.
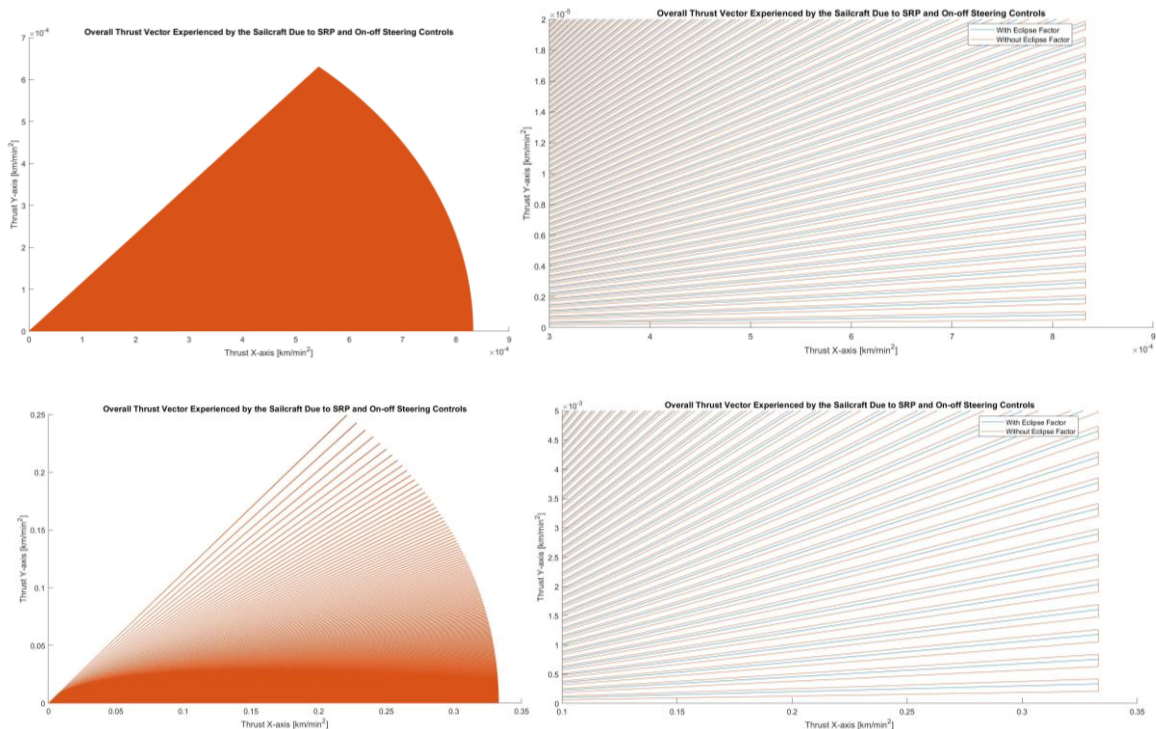
Figure 4.10 Sailcraft Thrust Vector. Actual thrust vector experienced by the sailcraft in the (x, y) plane of E due to SRP and on-off switching controls. Top left panel: $\sigma = 0.2$, overall thrust vector. Top right panel: $\sigma = 0.2$, detail view of thrust vector. Bottom left panel: $\sigma = 0.001$, overall thrust vector. Bottom right panel: $\sigma = 0.001$, detail view of thrust vector. The four panels

show the respective trajectory with eclipse factor (*blue*) and without eclipse factor (*red*), but the red plot overlaps the blue plot in places.

Figure 4.11 shows the sailcraft's position over time relative to the sun in the HEI reference frame *I*, as the sailcraft orbits the Earth. Over the total elapsed time and at this distance scale, the sailcraft's zigzag motion that was noted in Figure 4.4 as the sailcraft orbits the Earth and overall orbits the sun instead appears as a smooth curve. The same update formula used to model the sailcraft in orbit around the Earth was adapted to model the Earth around the sun, and the two were combined to obtain the sailcraft relative to the sun. It also does not account for adjustments that must be made for the ECI reference frame to change from a semi-inertial reference frame (as initially assumed) to a rotating, translating reference frame.
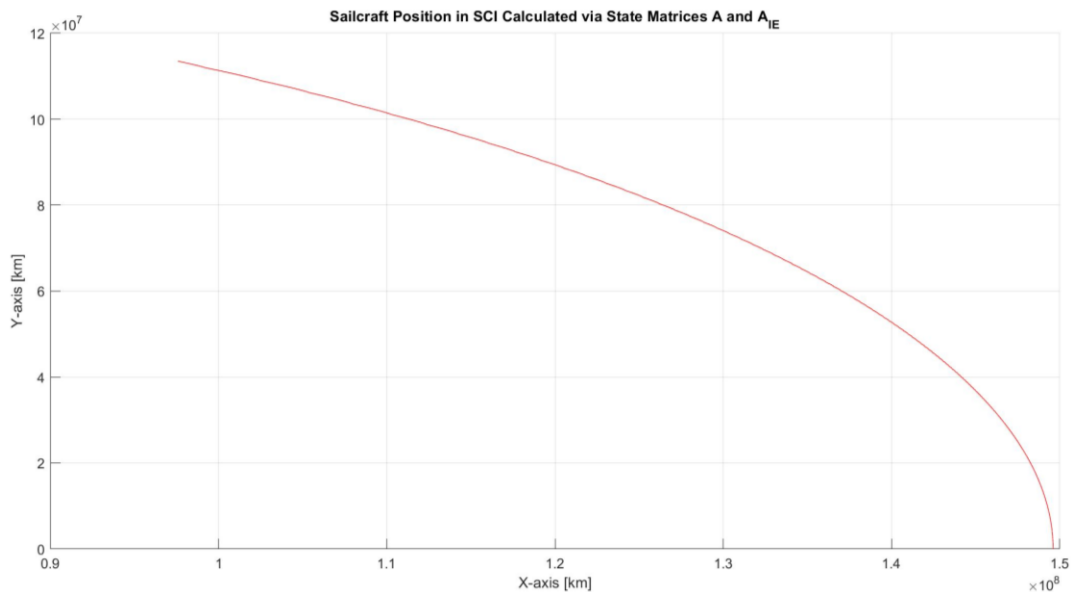
Figure 4.11 2D Rendering of Sailcraft Trajectory Relative to Sun, $\sigma = 0.001$. Sailcraft trajectory around sun in (x, y) plane of HEI reference frame *I*, calculated via state matrices *A* and *A_{IE}*. The plot of the sailcraft trajectory around sun for $\sigma = 0.2$ appears identical at this scale and is not shown to avoid redundancy.

Figure 4.12 compares the critical distance r_{crit} and the sailcraft's distance to the sun r over time. The sailcraft is eclipsed by Earth's shadow when the sun-sailcraft distance r (*red*) exceeds the critical distance r_{crit} (*blue*). From the detail plot of the small σ value, it is seen that the critical distance on one edge of Earth's shadow is increasingly different than that on the other edge. Thus, that the eclipse factor model is a good approximation at the initial low altitudes when the orbit is almost circular is an incomplete approximation. The eclipse factor model is a good approximation only if the sail area is also sufficiently small. A large sail area will cause the sailcraft to gain altitude so quickly that the assumption that $|\vec{r}_E|$ is approximately equal at opposition and at the edge of the umbra may be a poor approximation.
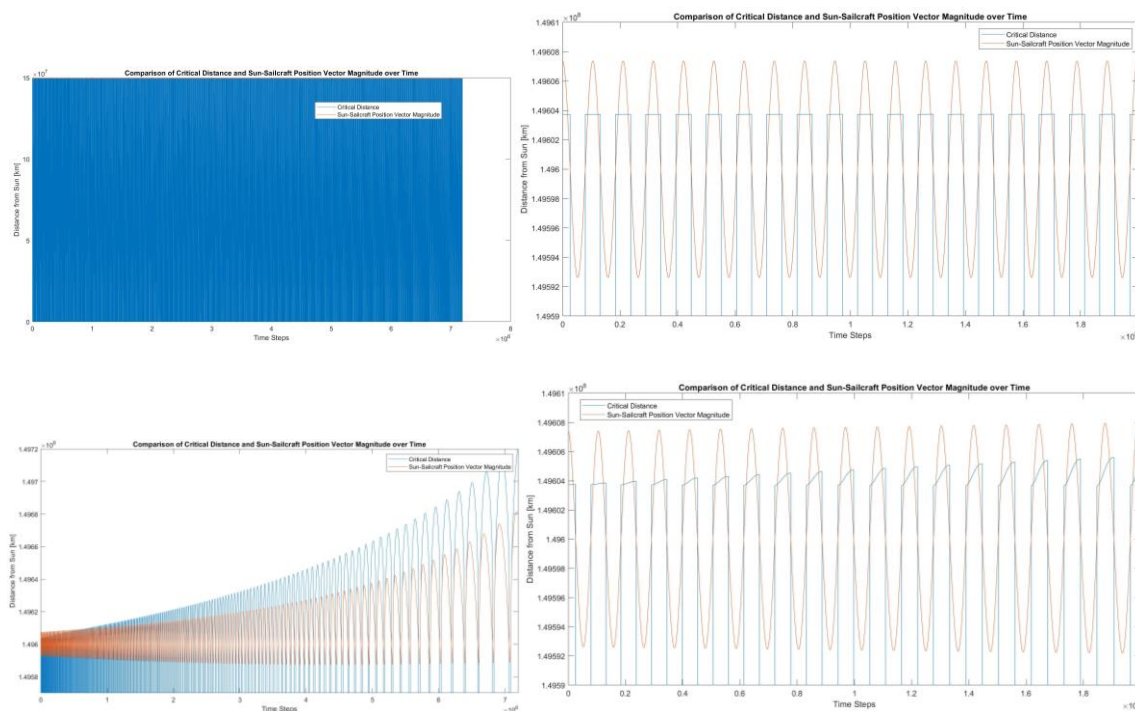
Figure 4.12 Comparison of Critical Distance r_{crit} and Sun-Sailcraft Distance r Over Time. The four panels show the sailcraft is eclipsed by Earth's shadow when the sun-sailcraft distance (*red*) exceeds the critical distance (*blue*). Top left panel: $\sigma = 0.2$, overall. Top right panel: $\sigma = 0.2$, detail view. Bottom left panel: $\sigma = 0.001$, overall. Bottom right panel: $\sigma = 0.001$, detail view.

Earth-Moon System-Centered State-Space Model

From Equation 3.66, the values of matrices A and B are:

$$A = \begin{bmatrix} 0 & 0 & 0 & 1 & 0 & 0 \\ 0 & 0 & 0 & 0 & 1 & 0 \\ 0 & 0 & 0 & 0 & 0 & 1 \\ (1 - \frac{1-\rho}{r_1{}^3} - \frac{\rho}{r_2{}^3}) & 0 & 0 & 0 & 2 & 0 \\ 0 & (1 - \frac{1-\rho}{r_1{}^3} - \frac{\rho}{r_2{}^3}) & 0 & -2 & 0 & 0 \\ 0 & 0 & (-\frac{1-\rho}{r_1{}^3} - \frac{\rho}{r_2{}^3}) & 0 & 0 & 0 \end{bmatrix}$$ (4.1a)

$$B = \begin{bmatrix} 0 & 0 & 0 \\ 0 & 0 & 0 \\ 0 & 0 & 0 \\ \frac{1}{m} & 0 & 0 \\ 0 & \frac{1}{m} & 0 \\ 0 & 0 & \frac{1}{m} \end{bmatrix}$$ (4.1b)

Substituting Equations 4.1a and 4.1b into Equation 3.90, I obtain

$$A - BK =$$ (4.2)

$$\begin{bmatrix} 0 & 0 & 0 & 1 & 0 & 0 \\ 0 & 0 & 0 & 0 & 1 & 0 \\ 0 & 0 & 0 & 0 & 0 & 1 \\ (1 - \frac{1-\rho}{r_1{}^3} - \frac{\rho}{r_2{}^3}) - \frac{K_{11}}{m} & -\frac{K_{12}}{m} & -\frac{K_{12}}{m} & -\frac{K_{14}}{m} & 2 - \frac{K_{15}}{m} & -\frac{K_{16}}{m} \\ -\frac{K_{21}}{m} & (1 - \frac{1-\rho}{r_1{}^3} - \frac{\rho}{r_2{}^3}) - \frac{K_{22}}{m} & -\frac{K_{23}}{m} & -2 - \frac{K_{24}}{m} & -\frac{K_{25}}{m} & -\frac{K_{26}}{m} \\ -\frac{K_{31}}{m} & -\frac{K_{32}}{m} & (-\frac{1-\rho}{r_1{}^3} - \frac{\rho}{r_2{}^3}) - \frac{K_{33}}{m} & -\frac{K_{34}}{m} & -\frac{K_{35}}{m} & -\frac{K_{36}}{m} \end{bmatrix}$$

I did not have sufficient time to find solutions for this model. Instead, the following is the process I would follow if I had more time.

1. Assign values for the small scalar coefficients N_1 and N_2.

2. Check the matrix pair (A, B) are controllable using Equation 2.41.

3. Assign the eigenvalues λ_i for $(\boldsymbol{A} - \boldsymbol{BK})$ matrix to have negative real parts to make the system asymptotically stable. In MATLAB, $\boldsymbol{K} = acker(\boldsymbol{A}, \boldsymbol{B}, \boldsymbol{W})$ where the elements of $\boldsymbol{W}$ are the desired eigenvalues with Re $\lambda_i < 0$.

4. Assign values for the $\boldsymbol{Q}$ and $\boldsymbol{R}$ matrices.

5. Solve the algebraic Ricatti equation for $\boldsymbol{P}$ using Equation 3.91.

6. Use the $\boldsymbol{P}$ solution to solve for $\boldsymbol{K}$ using Equation 3.92.

7. Use the $\boldsymbol{K}$ solution to solve for $\boldsymbol{u}$ using Equation 3.93.

8. Confirm this $\boldsymbol{u}$ solution will minimize the linear quadratic performance index J using Equation 3.94.

9. Iterate as needed.

Chapter V
Discussion, Conclusions, and Recommendations

Discussion

This section discusses the key results and potential implications from the three mathematical models' simulations of the sailcraft's movement in MATLAB: The Forward Euler model, the Earth-centered state-space model, and the E-M system-centered state-space model.

Forward Euler model. The Forward Euler model was selected for its simplicity, as a starting point to formulate the sailcraft movement model. Its weaknesses in terms of numerical stability were well-known. I expected a rapid accumulation of error, but I did not expect quite so significant an accumulation of error: over the total elapsed simulation time of 5000 minutes (83 hours), with updates at 0.01-minute intervals, the magnitude of the sailcraft's apparent position vector changed from 7378 to 9406 km, a fictional increase of 2028 km. Even after shortening the update intervals, the error accumulation was still rapid and comparatively significant.

These errors signaled an important warning that I kept in mind as I worked on each subsequent model: how well does the math model represent the physical model? For example, yes, I ultimately wanted the sailcraft to spiral outward from the Earth to the moon but in this model, it was appearing to spiral outward when it was supposed to be maintaining altitude. Next, I adapted the Forward Euler model to the Earth-centered open-loop model. Although the Forward Euler model provided useless results data, it was useful as a foundation for a more complicated state-space model, which was its purpose all along.

Earth-centered state-space model. The Earth-centered state-space model was selected for the simplicity of the on-off switching as an orbit raising method. Its simplicity made the process easier when formulating the sailcraft movement model in state space.

One key takeaway was seeing plainly that the math model matters. The Earth-centered open-loop model Figure 4.3 looks like what Forward Euler Figure 4.1 should have looked like. When T was equal to zero in Equation 3.22, the sailcraft stayed in the same circular orbit, tracing the same path over and over- what the first model should have done if it did not accumulate all those errors. The difference was that the Forward Euler method was numerically unstable but the Earth-centered state-space model as an open loop was stable, even though they were modeling the same thing: spacecraft in two body problem orbiting Earth with no SRP effects and no controls.

Upon review, this model had two major issues: the actual thrust equation (Equation 2.29) has an error and the eclipse factor model is flawed. In addition, the model is a state feedback closed loop. With sensors for spacecraft position and acceleration, the model would be an output feedback closed loop. Ultimately, the model should be built for what would actually be on the spacecraft.

I calculated the approximate actual thrust expression (see Equation 2.29) from the tangential thrust expression (see Equation 2.28), thinking that the radial thrust components approximately cancel over the course of one 'on' period for a small sail area. I then ran a simulation that plotted both Equation 2.28 and 2.29 to check how close the approximation was. After many orbits, the two appeared very similar plots. The only visible difference being that, depending which part of the orbit, one may be slightly greater than the other. More specifically, for $0 \leq \theta_E < \pi$, the two plots matched since $\tilde{T} = 0$ there. From $\pi < \theta_E < \sim \frac{7}{4}\pi$, the curved trajectory of 2.29 was very slightly closer to Earth than that of 2.28. From $\sim \frac{7}{4}\pi < \theta_E < 2\pi$, the curved trajectory of 2.29 was very slightly farther from Earth than that of 2.28. Due to the apparent similarities between the two plots, I elected to use the Equation 2.29 expression as my

main model since it was simpler to input in MATLAB. However, I was incorrect: the radial

thrust components do not cancel; the x-components of the radial thrust approximately cancel, but

the y-components do not. I now fear I forgot the difference between thrust transverse to the orbit

and thrust transverse to the sun-line and I do not recall whether I mistakenly used $\hat{r}$ for

$\hat{\vec{T}}_{transverse}$ in the model for 2.28.

Even if the actual thrust equation were corrected to be a good approximation of the

transverse thrust, it would only be accurate for small orbit eccentricity. The on-off switching

equations must change for elliptic orbits, including those of a sailcraft attempting to increase its

altitude toward the moon. At the start, in the initial circular orbit, each 'on' and 'off' period was

roughly 50% of the time. The way I set up the r_{crit} expression, the critical distance from the sun,

in MATLAB, I did not account for the fact the sailcraft accelerating in one direction meant its

apogee increased in a perpendicular direction. So, MATLAB was simulating that the 'off' period

length increased with each orbit, which explains the increasingly shorter thrust durations that

look like the fanned pages of a book in Figure 4.10. Lastly, my MATLAB model seemed to have

an issue with not using enough significant figures so $r_{crit} = norm(r(:, k))$ and the eclipse

factor was always 1. I did not have time to fix the eclipse factor model issues, so the third model

ignores the eclipse factor and simply assumes the sailcraft is in sunlight 100% of the time. One

way I did consider fixing it was to ignore θ_E and instead check if $r(t_{k+1}) > r(t_k)$ then the

sailcraft is moving away from the sun.

Earth-moon system-centered state-space model. The E-M system-centered state-space

model was selected to develop a linear control algorithm, one of the simplest types of controls,

that would limit the error from the reference trajectory. The reference trajectory was selected as a

logarithmic spiral to offer an exact reference solution. This model does not include the eclipse factor model and therefore does not account for the sailcraft being in periods of shadow.

A thrust vector control solution (see Equation 3.85) was developed for this model to minimize error from the reference trajectory. The solution has both feedforward and feedback control channels, which respectively ensure the system has the desired output and the solution is stable. The feedback loop's natural self-correcting properties provide robustness that can deal with imperfections in the third mathematical model. The preliminary results suggest Equation 4.2 may have control gain matrix K values that will result in all eigenvalues of $(A - BK)$ having non-positive real parts. These two equations are the significant result of the study and my contribution to previous solar sail controls research.

One limitation of this method is that A is a slowly changing, almost constant matrix, not a true constant matrix, due to the r_b term slowly changing as the sailcraft moves. Thus, K has to be periodically updated, after A has changed enough. The question then becomes how much change in A is enough and what is the impact of the error K introduces between its updates.

Conclusions

To address the two problems described in the first chapter, this thesis considered the technical feasibility of solar sail propulsion as a possible low-cost alternative in missions that are suitable for conventional propulsion spacecraft, specifically uncrewed missions to the vicinity of the moon. This thesis investigated orbit raising methods for sailcraft, the trajectory design process, and zero-propellant attitude control actuator options; explored multiple thrust vector control designs for a sailcraft to transit from Earth to the moon; and described the results from such transit simulations.

The analysis of this mission concept's technical feasibility had two focus topics: stable control design and reasonable trajectory mechanics. The initial findings from the third mathematical model indicate designing stable controls for the sailcraft's mission is indeed feasible. However, the technical feasibility relating to sailcraft's orbital mechanics is less straightforward. The two specified tasks that the sailcraft carry a small payload and be CubeSat-based (i.e., the sail area must fit inside a CubeSat) are physically at odds with the implied task that the sailcraft reach the moon in a reasonable amount of time. The sailcraft needs to be lightweight to be effective, yet also with a large enough sail to transit in a reasonable amount of time. Here, a reasonable amount of time is not to exceed 300 days. With the applications of pre-emplacing supplies or communications relays in mind, a delivery time on the order of months to almost a year is acceptable. Delivery times to the moon exceeding a year would likely be excessive and undesired.

Although the second model was incomplete, it offers a very rough estimate of the sailcraft's performance. The intended sailcraft of sail area 25 m^2 and 5 kg would not be an effective sailcraft to carry a small payload toward the moon because it cannot raise its orbit in a reasonable period of time via on-off switching. The "super" sailcraft of sail area 10,000 m^2 and 10 kg may be effective for this purpose, but it is implausible for such a large sail area to fit inside a CubeSat-sized volume as intended. By improving the model and optimizing the orbit raising method, it may be possible to find a sail area between the two extremes that can effectively carry payloads to higher orbits within a reasonable time period and fit within a CubeSat. It is highly recommended such changes to the model and control designs be attempted prior to relaxing the mission constraints.

The answers to the three research questions are summarized below.

What are simple control methods to increase altitude via solar sail propulsion?

Simple sailcraft control methods to increase altitude include maximization of a component of the SRP force in a given direction, on-off switching, orbit rate steering, logarithmic spiral trajectories, and LQR controls to limit the trajectory error from a reference trajectory.

What is the relationship between thrust vector control design, attitude control design, and trajectory planning and design for a sailcraft? For any spacecraft?

For a sailcraft, thrust vector control design and attitude control design are effectively the same thing because the sail's attitude to the sun determines its thrust vector. The nature of acceleration due to SRP is both a boon and a challenge to the sailcraft and its trajectory design. The acceleration is effectively constant, dependent only on sailcraft distance from the sun, orientation to the sun, and any periods of eclipse. However, it cannot be switched on and off as easily as chemical propulsion to make large, sudden changes to its orbit.

For trajectory planning and design, the biggest differences between a sailcraft and any spacecraft lie in the desired orbit types, launch and retrieval or disposal options, ΔV budget, and the objective of the controls problem. Those differences are directly related to their thrust vector and attitude control design capabilities and limitations. A conventional chemical propulsion spacecraft is generally matched with a high thrust, short duration ΔV budget, a control objective to minimize the fuel needed, and has a wider array of usable orbit types, and its thrust vector and attitude control designs reflect this. A sailcraft's thrust vector control design strictly limits permissible solutions for the trajectory design. For example, for a sailcraft with one reflective side and one non-reflective side, the sail thrust vector $\hat{n}$ is constrained to be oriented away from

the sun, which immediately removes from consideration any orientations toward the sun, which make up half of all possible solutions for any given moment.

Does control theory offer a reasonable linearized solution method for a sailcraft to traverse from LEO to the vicinity of the moon?

This thesis's research is not complete enough to decidedly answer whether control theory offers a reasonable linearized solution method. However, the initial findings from the third model, which is a linearized solution method, suggest it may be reasonable. Equation 3.85 offers a robust-looking thrust vector control solution to minimize error from the reference trajectory and Equation 4.2 appears to have matrix K values that will result in all eigenvalues of $(A - BK)$ having non-positive real parts. More work is required to compare the limits of the solution's robustness against likely disturbances, to confirm the eigenvalues' non-positive real parts, and to verify there are no repeated eigenvalues on the imaginary axis, in order to prove the stability of the system.

Recommendations

Recommendations for future work include improving the sailcraft and system stability, employing higher-fidelity models, altering the control models and goals, estimating the launch limits and cost and risk, testing the controls with hardware, and considering end-of-mission options.

Stability. One could confirm the matrix pair (A, B) are controllable, prove the stability of the system, and show that the error converges to zero even though the controls are effectively turned off periodically when the sailcraft is approaching the sun. Two options here are to use a Lyapunov function to show it is asymptotically stable or to do a V transform: If $V <= 0$, then the trajectory is stable.

Future work could include both ensuring the inherent stability of the sailcraft's physical design and adding more robust controls to counter disturbances. Ideally, the sailcraft would be statically stable, with the center of mass between the sun and the center of pressure. If a statically stable sailcraft is disturbed from its neutral sun-pointing orientation, a restoring torque is naturally generated that counters the disturbance. For a sailcraft that is not statically stable, any disturbance from its neutral orientation would instead be amplified [20]. A statically stable sailcraft does not require a robust attitude control design to counter the disturbance torques. However, it may still require controls to prevent the sailcraft from oscillating indefinitely around the neutral orientation from which is was disturbed. Other stability problems include modeling the impact of sail attitude stability, sail trajectory stability, precession, nutation, and thrust vector pointing performance on the mission completion, and selecting which to control for and which controls to optimize. Confirm the optimization tradeoffs chosen through test simulations of the controls performance in response to small disturbances to the system.

Higher-fidelity models. This thesis used many simplifications. Removing some of the simplifying assumptions is desired to create more generalized models that present more accurate and useful results. Simplifications to remove include the solar flux is constant; atmospheric drag is negligible at orbit insertion; the sun, Earth, and moon are spheres of uniform density; Earth does not rotate; and Earth does not have axial tilt. Of particular interest is how to control the sail so it can still increase altitude when dealing with atmospheric drag. Previously ignored factors to consider include sail operating temperatures, thermal and radiation environments (including the Van Allen belts), and motion in the z-direction. Future work should include how to change the sailcraft's inclination from its parking orbit around Earth to lunar intercept.

Rather than assuming and modeling a rigid ideal sail, higher fidelity modeling of non-flat and nonperfect sails needs to be incorporated in the thrust and attitude controls designs, including structural vibration control to actively dampen the sailcraft's flexible modes. The error state vector will need to be expanded to include not only errors in position and velocity but also errors in orientation and in angular velocity (i.e., have 12 elements instead of 6). Quaternions are recommended to account for the sailcraft's orientation as well as errors in orientation. Quaternions would also be useful to track the E-M system's reference frame rotating and translating in I. In addition, the eclipse factor model will need to be fixed to properly account for when the sailcraft is eclipsed by Earth's umbra. The model should also determine a suitable value of the eclipse factor $0 < \varepsilon < 1$ for when the sailcraft is partially eclipsed in Earth's penumbra.

In the second model, the total elapsed simulation time was 72,000 minutes (50 days), with updates at 0.01-minute intervals, to limit error accumulation without adding too much computing time. One might try making slightly larger time steps and running the simulations for a longer time span to check whether the larger time steps introduce any non-negligible update errors. If any update errors are negligible, continue to use the longer time steps and run the simulations for a longer time span in order to model the trajectory behavior over a longer period without exceeding the capability of the computer.

Control models and goals. The third mathematical model used a CR3BP as the dynamical model. Consider instead a patched conic problem as the dynamical model in cislunar space and an R2BP when sailcraft is near the moon. Also, this model's control goals were stability first and minimum time second. Consider what changes if the minimum time problem is

first and stability second. Likely, the rate of change of an orbital parameter will need to be maximized for the minimum time problem.

If one is inclined to go further, consider how the performance of a linearized controls solution method compares to a nonlinear controls solution method for a sailcraft to traverse from LEO to the vicinity of the moon. Explore the relationship between minimum sail area and maximum payload mass given the constraint that the sailcraft must reach the vicinity of the moon in less than 300 days. Expand the literature review beyond sailcraft to include low-thrust missions that have used a spiral trajectory to transit cislunar space (e.g., ESA's SMART-1). Determine the applicability of these other low-thrust missions' control designs to a sailcraft mission to the moon.

Launch limits. For future work, determine the required mass and area of the solar sail to offset the mass and volume of the CubeSat and the payload. Model whether a payload with a non-uniform density would cause the solar sail to drift off course. Consider whether the CubeSat should be attached to the payload in the launch vehicle or the two are launched separately and meet up in Earth orbit. In either case, consider what limitations that sequence places on the orbit insertion altitude, payload size, and the sailcraft's controls. Determine the allowable ranges of altitudes and inclination or orbit shape for the sailcraft departing Earth orbit and arriving lunar orbit.

Cost and risk. Estimate the overall cost of the design, development, test, and evaluation of the sailcraft and the first unit. Consider how this cost compares to propellant-based orbit transfer to the moon, both in terms of time and cost. Explore sailcraft mission contingency planning, e.g., what is the likelihood and consequence if the payload suffers a MMOD strike en route. Consider if the payload can be protected and if it is worth using this low-cost delivery

method if the risk cannot be fully mitigated. Weigh the cost of the payload contents against the cost of the additional protective packaging.

Hardware. One could select the ADCS hardware, program it with the attitude control designs within, and run the actuator hardware through test conditions. Rukhaiyar et al. are doing related work in Embry-Riddle Aeronautical University's Engineering Physics Propulsion Lab, building a prototype solar sail to capture orbital debris. The 6-unit CubeSat will be a fully autonomous system with a mission lifespan of 10 years and will be deployed utilizing ridesharing from excess payload on primary launches. They have built the 6U frame of the prototype and deployed the four sail booms in lab conditions. They also built a debris capture mechanism, which will soon be integrated with vision and feedback [69].

End of mission. Finally, future work can determine what to do with the sailcraft at the end of its mission. One possibility is to design the sailcraft trajectory and attitude controls from the general vicinity of the moon to a more exact destination such as lowering the orbit to low lunar orbit or changing the inclination and rendezvousing with Gateway in NRHO. If the payload is a communications satellite, consider the controls needed for the sailcraft to station-keep in lunar orbit or at a Lagrange point.

Another possibility is to figure out the trajectory and attitude control designs from the moon back to Earth. That way, the sailcraft could do a continuous loop from Earth to moon to Earth for repeated logistics transfers. For example, a company or agency may want a fleet of sailcraft with staggered departures to continuously transport materials between Earth and the moon and back. Find how the payload limitations from Earth to moon compare to the payload limitations from moon to Earth in this scenario. While sailcraft are not limited by reaction mass, they are limited by the lifetime of the sailcraft in the space environment [19]. I am curious to see

if the transit times and sail lifetime could support this scenario. Then perhaps the sailcraft could

burn up in Earth's atmosphere at the end of its lifetime.

References

[1] "Sun Fact Sheet." https://nssdc.gsfc.nasa.gov/planetary/factsheet/sunfact.html (accessed Sep. 23, 2020).

[2] S. Loff, "Apollo 11 Mission Overview," *NASA*, Apr. 17, 2015. http://www.nasa.gov/mission_pages/apollo/missions/apollo11.html (accessed Dec. 07, 2020).

[3] N. R. Council, *Solar and Space Physics: A Science for a Technological Society*. 2012.

[4] "Near Earth Asteroid Scout (NEAScout)," *NASA Jet Propulsion Laboratory (JPL)*. https://www.jpl.nasa.gov/missions/near-earth-asteroid-scout-neascout (accessed Apr. 26, 2021).

[5] J. A. Dervan *et al.*, "New Moon Explorer (NME) Robotic Precursor Mission Concept," in *2018 AIAA SPACE and Astronautics Forum and Exposition*, 0 vols., American Institute of Aeronautics and Astronautics, 2018.

[6] "NASA's New Solar Sail System to be Tested On-Board NanoAvionics Satellite Bus," *NanoAvionics*, Apr. 29, 2020. https://nanoavionics.com/news/nasas-new-solar-sail-system-to-be-tested-on-board-nanoavionics-satellite-bus/ (accessed Apr. 26, 2021).

[7] S. Potter, "NASA Publishes Artemis Plan to Land First Woman, Next Man on Moon," *NASA*, Sep. 21, 2020. http://www.nasa.gov/press-release/nasa-publishes-artemis-plan-to-land-first-woman-next-man-on-moon-in-2024 (accessed Dec. 07, 2020).

[8] E. Mahoney, "NASA Selects Blue Origin, Dynetics, SpaceX for Artemis Human Landers," *NASA*, Apr. 30, 2020. http://www.nasa.gov/feature/nasa-selects-blue-origin-dynetics-spacex-for-artemis-human-landers (accessed Mar. 08, 2021).

[9] K. Brown, "NASA Picks SpaceX to Land Next Americans on Moon," *NASA*, Apr. 16, 2021. http://www.nasa.gov/press-release/as-artemis-moves-forward-nasa-picks-spacex-to-land-next-americans-on-moon (accessed Apr. 26, 2021).

[10] Y. Zou, Y. Liu, and Y. Jia, "Overview of China's upcoming Chang'E series and the scientific objectives and payloads for Change'E-7 mission," *51st Lunar Planet. Sci. Conf. 2020*, 2020, Accessed: Dec. 07, 2020. [Online]. Available: https://www.hou.usra.edu/meetings/lpsc2020/pdf/1755.pdf.

[11] G. Shih, "China moon mission returns to Earth, vaulting nation into ranks of space powers," *Washington Post*, Washington, D.C, Dec. 17, 2020.

[12] N. Goswami, "The Strategic Implications of the China-Russia Lunar Base Cooperation Agreement," Mar. 19, 2021. https://thediplomat.com/2021/03/the-strategic-implications-of-the-china-russia-lunar-base-cooperation-agreement/ (accessed Apr. 26, 2021).

[13] S. Clark, "Russia looks to China as new space exploration partner," *Spaceflight Now*, Mar. 15, 2021. https://spaceflightnow.com/2021/03/15/russia-looks-to-china-as-new-space-exploration-partner/ (accessed Apr. 26, 2021).

[14] "Apollo 17 Mission Report," LYNDON B. JOHNSON SPACE CENTER, Houston, Texas, JSC-07904, Mar. 1973.

[15] "Presidential Memorandum on Reinvigorating America's Human Space Exploration Program," *The White House*, Nov. 17, 2017. https://www.whitehouse.gov/presidential-actions/presidential-memorandum-reinvigorating-americas-human-space-exploration-program/ (accessed Dec. 07, 2020).

[16]   N. McCarthy, "Infographic: Why SpaceX Is A Game Changer For NASA," *Statista Infographics*, Jun. 08, 2020. https://www.statista.com/chart/21904/estimated-cost-per-seat-on-selected-spacecraft/ (accessed Apr. 26, 2021).

[17]   M. Sheetz, "NASA's deal to fly astronauts with Boeing is turning out to be much more expensive than SpaceX," *CNBC*, Nov. 19, 2019. https://www.cnbc.com/2019/11/19/nasa-cost-to-fly-astronauts-with-spacex-boeing-and-russian-soyuz.html (accessed Apr. 26, 2021).

[18]   J. Simo and C. R. McInnes, "Solar sail orbits at the Earth–Moon libration points," *Commun. Nonlinear Sci. Numer. Simul.*, vol. 14, no. 12, pp. 4191–4196, Dec. 2009, doi: 10.1016/j.cnsns.2009.03.032.

[19]   C. R. McInnes, *Solar sailing: technology, dynamics, and mission applications*. London ; New York : Chichestesr, UK: Springer ; Praxis, 2004.

[20]   B. Wie, *Space vehicle dynamics and control*, 2nd ed. Reston, VA: American Institute of Aeronautics and Astronautics, 2008.

[21]   J. R. Wertz and W. J. Larson, Eds., *Space mission analysis and design*, 3rd ed. El Segundo, Calif. : Dordrecht ; Boston: Microcosm ; Kluwer, 1999.

[22]   "ESA Science & Technology - Earth's plasmasphere and the Van Allen belts." https://sci.esa.int/web/cluster/-/52831-earth-plasmasphere-and-the-van-allen-belts (accessed Feb. 17, 2021).

[23]   C. Katan, "NASA's Next Solar Sail: Lessons from NanoSail – D2," p. 9.

[24]   Y. Tsuda *et al.*, "Achievement of IKAROS — Japanese deep space solar sail demonstration mission," *Acta Astronaut.*, vol. 82, no. 2, pp. 183–188, Feb. 2013, doi: 10.1016/j.actaastro.2012.03.032.

[25]   J. Mansell *et al.*, "Orbit and Attitude Performance of the LightSail 2 Solar Sail Spacecraft," presented at the AIAA Scitech 2020 Forum, Orlando, FL, Jan. 2020, doi: 10.2514/6.2020-2177.

[26]   "JAXA | Small Solar Power Sail Demonstrator 'IKAROS,'" *JAXA | Japan Aerospace Exploration Agency*. http://global.jaxa.jp/projects/sat/ikaros/topics.html (accessed Dec. 08, 2020).

[27]   "NanoSail-D - eoPortal Directory - Satellite Missions," *ESA Earth Observation Portal*. https://directory.eoportal.org/web/eoportal/satellite-missions/n/nanosail-d (accessed Mar. 15, 2021).

[28]   R. W. Ridenoure *et al.*, "Testing The LightSail Program: Advancing Solar Sailing Technology Using a CubeSat Platform," *J. Small Satell.*, vol. 5, no. 2, pp. 531–550, 2016.

[29]   J. Foust, "Solar sail spacecraft begins extended mission," *SpaceNews*, Jul. 02, 2020. https://dev.spacenews.com/solar-sail-spacecraft-begins-extended-mission/ (accessed Dec. 08, 2020).

[30]   B. A. Roston, "LightSail 2 spacecraft successfully deploys solar sail," *SlashGear*, Jul. 23, 2019. https://www.slashgear.com/lightsail-2-spacecraft-successfully-deploys-solar-sail-23585053/ (accessed Apr. 07, 2021).

[31]   J. Heiligers, M. Vergaaij, and M. Ceriotti, "End-to-end trajectory design for a solar-sail-only pole-sitter at Venus, Earth, and Mars," *Adv. Space Res.*, p. S0273117720304130, Jun. 2020, doi: 10.1016/j.asr.2020.06.011.

[32]   J. Heiligers, S. Hiddink, R. Noomen, and C. R. McInnes, "Solar sail Lyapunov and Halo orbits in the Earth–Moon three-body problem," *Acta Astronaut.*, vol. 116, pp. 25–35, Nov. 2015, doi: 10.1016/j.actaastro.2015.05.034.

[33]   G. G. Wawrzyniak and K. C. Howell, "Numerical techniques for generating and refining solar sail trajectories," *Adv. Space Res.*, vol. 48, no. 11, pp. 1848–1857, Dec. 2011, doi: 10.1016/j.asr.2011.04.012.

[34]   X. Duan, G. Gómez, J. J. Masdemont, and X. Yue, "A picture of solar-sail heteroclinic enhanced connections between Lissajous libration point orbits," *Commun. Nonlinear Sci. Numer. Simul.*, vol. 85, p. 105252, Jun. 2020, doi: 10.1016/j.cnsns.2020.105252.

[35]   G. G. Wawrzyniak and K. C. Howell, "Investigating the Design Space for Solar Sail Trajectories in the Earth- Moon System," *Open Aerosp. Eng. J.*, no. 4, pp. 26–44, 2011.

[36]   L. D. Vance, R. T. Nallapu, and J. Thangavelautham, "Solar Sailing Fundamentals with an Exploration of Trajectory Control to Lunar Halo Orbit," presented at the AIAA Scitech 2020 Forum, Orlando, FL, Jan. 2020, doi: 10.2514/6.2020-1207.

[37]   M. Bassetto, L. Niccolai, A. A. Quarta, and G. Mengali, "Logarithmic spiral trajectories generated by Solar sails," *Celest. Mech. Dyn. Astron.*, vol. 130, no. 2, p. 18, Feb. 2018, doi: 10.1007/s10569-017-9812-6.

[38]   A. Caruso, L. Niccolai, A. A. Quarta, and G. Mengali, "Effects of attitude constraints on solar sail optimal interplanetary trajectories," *Acta Astronaut.*, vol. 177, pp. 39–47, Dec. 2020, doi: 10.1016/j.actaastro.2020.07.010.

[39]   G. Mengali and A. A. Quarta, "Rapid Solar Sail Rendezvous Missions to Asteroid 99942 Apophis," *J. Spacecr. Rockets*, vol. 46, no. 1, pp. 134–140, Jan. 2009, doi: 10.2514/1.37141.

[40]   J. Mu, S. Gong, and J. Li, "Reflectivity-controlled solar sail formation flying for magnetosphere mission," *Aerosp. Sci. Technol.*, vol. 30, no. 1, pp. 339–348, Oct. 2013, doi: 10.1016/j.ast.2013.09.002.

[41]   J. Munday, "Propellantless Attitude Control of Solar Sail Technology Utilizing Reflective Control Devices," *NASA Technical Reports Server (NTRS)*, Apr. 06, 2016. https://ntrs.nasa.gov/citations/20160007912 (accessed Jan. 18, 2021).

[42]   H. W. Price, J. Ayon, C. Garner, G. Klose, E. Mettler, and G. Sprague, "Design for a solar sail demonstration mission," presented at the Space Technology and Applications International Forum (STAIF 2000), Feb. 2001, Accessed: Apr. 05, 2021. [Online]. Available: https://trs.jpl.nasa.gov/bitstream/handle/2014/12303/01-0335.pdf?sequence=1&isAllowed=y.

[43]   "Solar Radiation Pressure," *a.i. solutions*. https://ai-solutions.com/_help_Files/solar_radiation_pressure.htm (accessed Oct. 26, 2020).

[44]   S. Soldini, J. J. Masdemont, and G. Gómez, "Dynamics of Solar Radiation Pressure–Assisted Maneuvers Between Lissajous Orbits," *J. Guid. Control Dyn.*, vol. 42, no. 4, pp. 769–793, Apr. 2019, doi: 10.2514/1.G003725.

[45]   *Space Flight: The Application of Orbital Mechanics*. 2011.

[46]   "Graveyard Orbits and the Satellite Afterlife," *NOAA National Environmental Satellite, Data, and Information Service (NESDIS)*, Oct. 31, 2016. https://www.nesdis.noaa.gov/content/graveyard-orbits-and-satellite-afterlife (accessed Mar. 23, 2021).

[47]   N. Bosanac, A. D. Cox, K. C. Howell, and D. C. Folta, "Trajectory design for a cislunar CubeSat leveraging dynamical systems techniques: The Lunar IceCube mission," *Acta Astronaut.*, vol. 144, pp. 283–296, Mar. 2018, doi: 10.1016/j.actaastro.2017.12.025.

[48]   A. Wächter and L. T. Biegler, "On the implementation of an interior-point filter line-search algorithm for large-scale nonlinear programming," *Math. Program.*, vol. 106, no. 1, pp. 25–57, Mar. 2006, doi: 10.1007/s10107-004-0559-y.

[49]   I. M. Ross and F. Fahroo, "User's manual for DIDO 2002: A MATLAB package for dynamic optimization," Department of Aeronautics and Astronautics, Naval Postgraduate School, Monterey, CA, Technical Report Tech. Rep. AA-02-002, 2002.

[50]   A. V. Rao, D. A. Benson, G. T. Huntington, C. Francolin, C. L. Darby, and M. A. Patterson, "User's manual for GPOPS: A MATLAB package for dynamic optimization using the Gauss pseudospectral method," University of Florida, Naval Postgraduate School, Monterey, CA, Technical Report, 2008.

[51]   A. V. Rao *et al.*, "Algorithm 902: GPOPS, A MATLAB software for solving multiple-phase optimal control problems using the gauss pseudospectral method," *ACM Trans. Math. Softw.*, vol. 37, no. 2, p. 22:1-22:39, Apr. 2010, doi: 10.1145/1731022.1731032.

[52]   *MATLAB*. Natick, Massachusetts: The MathWorks, Inc, 2010.

[53]   N. Hale and D. R. Moore, "A sixth-order extension to the MATLAB package bvp4c of J. Kierzenka and L. Shampine," Oxford, Oxford University Computing Laboratory, Numerical Analysis Group, Technical Report 08/04, 2008.

[54]   Y. Kovo, "Space Mission Design Tools," *NASA*, Mar. 03, 2017. http://www.nasa.gov/smallsat-institute/space-mission-design-tools (accessed Jan. 11, 2021).

[55]   C. Acton, N. Bachman, B. Semenov, and E. Wright, "A look towards the future in the handling of space science mission geometry," *Planet. Space Sci.*, vol. 150, pp. 9–12, Jan. 2018, doi: 10.1016/j.pss.2017.02.013.

[56]   S. Cooley, "GMAT," *SourceForge*. https://sourceforge.net/projects/gmat/ (accessed Apr. 13, 2021).

[57]   "STK Astrogator," *Agi*. https://www.agi.com/products/stk-specialized-modules/stk-astrogator (accessed Apr. 13, 2021).

[58]   C. Foster, "NASA Ames Web-based Trajectory Generation Tool," *NASA Ames Research Center Trajectory Browser*, Dec. 22, 2016. https://trajbrowser.arc.nasa.gov/ (accessed Apr. 13, 2021).

[59]   D. Lockney, "Mission Analysis Low-Thrust Optimizer (MALTO)," *NASA's Technology Transfer Program*. https://software.nasa.gov/software/NPO-43625-1 (accessed Apr. 13, 2021).

[60]   D. Lockney, "Copernicus Trajectory Design and Optimization System (Version 5.x)," *NASA Technology Transfer Program*. https://software.nasa.gov/software/MSC-26673-1 (accessed Apr. 13, 2021).

[61]   T. Williams, "Attitude Control Requirements for Various Solar Sail Missions," presented at the Vision-21: Space Travel for the Next Millennium, NASA Lewis Research Center, Apr. 1990, Accessed: Apr. 14, 2021. [Online]. Available: https://ntrs.nasa.gov/api/citations/19910012837/downloads/19910012837.pdf.

[62]   R. Votel and D. Sinclair, "Comparison of Control Moment Gyros and Reaction Wheels for Small Earth-Observing Satellites," p. 7.

[63]   D. Lockney, "NASA Spinoff: Reaction/Momentum Wheel," *NASA's Technology Transfer Program*, 1997. https://spinoff.nasa.gov/spinoff1997/t3.html (accessed Apr. 14, 2021).

[64]   T. Inamori, K. Otsuki, Y. Sugawara, P. Saisutjarit, and S. Nakasuka, "Three-axis attitude control by two-step rotations using only magnetic torquers in a low Earth orbit near the magnetic equator," *Acta Astronaut.*, vol. 128, pp. 696–706, Nov. 2016, doi: 10.1016/j.actaastro.2016.07.006.

[65]   J. Furumo, E. Greer, N. Walsh, and D. Wukelic, "Cold-gas Propulsion for Small Satellite Attitude Control , Station Keeping , and Deorbit," 2013, Accessed: Apr. 14, 2021. [Online]. Available: /paper/Cold-gas-Propulsion-for-Small-Satellite-Attitude-%2C-Furumo/50afaa1e1d4943ddaf6486019cfd657750d9b7cf.

[66]   S. V. Drakunov, "Control System Properties," presented at the EP505 Spacecraft Dynamics & Control, Embry-Riddle Aeronautical University Daytona Beach, FL, Sep. 01, 2020.

[67]   S. V. Drakunov, "System Stability," presented at the EP505 Spacecraft Dynamics & Control, Embry-Riddle Aeronautical University Daytona Beach, FL, Sep. 08, 2020.

[68]   S. V. Drakunov, "Summary of System Stability," presented at the EP505 Spacecraft Dynamics & Control, Embry-Riddle Aeronautical University Daytona Beach, FL, Sep. 24, 2020.

[69]   A. Rukhaiyar, J. Nadeau, A. Duke, and C. Yopp, "Autonomous Solar Sail Debris Capture Prototype," Mar. 25, 2021.

Appendix A

MATLAB Code

```
%Michelle Nadeau EP700 Solar Sail Modeling
%Written on 24SEP2020 by Michelle Nadeau
clear all
format compact


%Simulation parameters
TotalTime=1000; %Total elapsed time, [min] (72000 min = 50 days)
dt=0.01; %Time interval, [min]
t(1)=0; %Initial time


%System parameters
c0=299792.458*60; %Speed of light, [km/min]
L=3.9E20*60^3;%Solar luminosity or flux, [kg km^2/min^3]
mu_sun=132712440040.944000*3600; %Mass parameter of the sun, [km^3/min^2]
mu_Earth=398600.436233*3600; %Mass parameter of the Earth, [km^3/min^2]
mu_moon=4902.80076*3600; %Mass parameter of the moon, [km^3/min^2]
r_sun=695700; %Radius of sun, [km]
r_Earth=6378.1; %Radius of Earth, [km]
r_moon=1738.1; %Radius of moon, [km]
m=5; %Mass of sailcraft, [kg]
Area=%25E-6; %Area of solar sail, [km^2]
eta=1; %Efficiency of solar sail, [dimensionless]
```

```
Error using dbstatus
Error: File: C:\Users\Chelle\Documents\1. ERAU\EP700 Thesis\SolarSailv9.m Line: 23 Column: 41
Invalid expression. Check for missing or extra characters.
```

```
%CH1 Delimitations. Check cislunar regions where mass parameters dominate
d_E(1)=1;
a_E(1)=mu_Earth/(d_E(1)^2);
d_m(1)=384400;
a_m(1)=mu_moon/(d_m(1)^2);
d_s(1)=149.6E6;
a_s(1)=mu_sun/(d_s(1)^2);
for j=2:385
    d_E(j)=d_E(j-1)+1000; %distance of sailcraft from Earth, [km]
    a_E(j)=mu_Earth/(d_E(j)^2); %acceleration of sailcraft due to Earth's gravity, [km/min^2]
    d_m(j)=d_m(j-1)-1000; %distance of sailcraft from moon, [km]
    a_m(j)=mu_moon/(d_m(j)^2); %acceleration of sailcraft due to moon's gravity, [km/min^2]
    d_s(j)=149.6E6; %approximate distance of sailcraft from sun, [km]
    a_s(j)=mu_sun/(d_s(j)^2); %acceleration of sailcraft due to sun's gravity, [km/min^2]
end
figure(1)
plot(log10(a_E(:)),'b')
hold on
plot(log10(a_m(:)),'k')
plot(log10(a_s(:)),'r')
%plot(log10(a_s(:))+log10(1.1),'.') %Check where Earth or moon acceleration
%is within 10% of sun's acceleration
hold off
```

```
xlabel('Distance from Center of Earth [Thousands of km]')
ylabel('Log of Acceleration due to Gravity [km/min^2]')
title('Comparison of Accelerations due to Gravity on Sailcraft in Cislunar Space')


%CH2 Solar Radiation Pressure. Check how SRP differs across cislunar space
%Percentage difference between acceleration due to SRP at closest, furthest from sun
R1=146.6944e6;R2=152.5056e6;
W1=L/(4*pi*R1^2)
W1 = 1.4156e+09 [kg/min^3]
W2=L/(4*pi*R2^2)
W2 = 1.3098e+09 [kg/min^3]
percentagedifference=(W1-W2)/0.5/(W1+W2)*100
pd = 7.7661;
%Takeaway: almost 8% difference between SRP acceleration magnitude at
%closest and furthest points from sun (R1 and R2 are closest and furthest
%distances of moon from sun so I rounded up to 8% since sailcraft can be in
%opposition in orbit around moon)


%CH3 Physical Model. Check validity of assumptions to simplify system
%Acceleration of the center of mass of the sun-Earth system
acc=mu_sun*5.9724E24/(5.9724E24 + 1988500E24)/(149.6E6)^2
acc=6.41e-08 km/min^2 -> takeaway: NEGLIGIBLE
%Reduced mass (two-body problem) of the sun-Earth system
mu=(5.9724E24 * 1988500E24)/(5.9724E24 + 1988500E24)
mu=5.9724E24
%Takeaway: NEGLIGIBLE


%Acceleration of the center of mass of the moon-Earth system
acc2=mu_moon*5.9724E24/(5.9724E24 + 0.07346E24)/(0.3844E6)^2
acc2=1.18e-04 km/s^2 -> takeaway: NEGLIGIBLE
%Reduced mass (two-body problem) of the moon-Earth system
mu2=(5.9724E24 * 0.07346E24)/(5.9724E24 + 0.07346E24)
mu2=7.2567e+22
%Takeaway: NOT NEGLIGIBLE

%Initial conditions for Earth relative to sun
%Assumes Earth has CIRCULAR orbit about sun
R_IE(:,1)=[149.6E6,0,0]'; %Earth position vector in SCI coordinate frame,  [km]
omega_EI=2*pi/(365.2*24*60); %Rate of motion of rotating/translating reference frame E wrt I,
[rad/min]
v_IE(:,1)=[0,sqrt(mu_sun/R_IE(1,1)),0]'; %Earth velocity vector in SCI coordinate frame,
[km/min]
E(:,1)=[R_IE(:,1); v_IE(:,1)]; %Earth position and velocity state vector


%Initial conditions for sailcraft
%Assumes sailcraft has initial CIRCULAR orbit about Earth
altitude_E=1000; %Initial altitude above Earth, [km]
x(1)=r_Earth+altitude_E; %X component of the sailcraft position vector, in ECI coordinate frame,
[km]
y(1)=0; %Y component of the sailcraft position vector, in ECI coordinate frame, [km]
z(1)=0; %Z component of the sailcraft position vector, in ECI coordinate frame, [km]
```

```
vx(1)=0; %X component of sailcraft velocity vector in ECI coordinate frame, [km/min]
vy(1)=sqrt(mu_Earth/(x(1))); %Y component of sailcraft velocity vector in ECI coordinate frame,
[km/min]
vz(1)=0; %Z component of sailcraft velocity vector in ECI coordinate frame, [km/min]
xx(:,1)=[x(1),y(1),z(1),vx(1),vy(1),vz(1)]'; %Sailcraft position and velocity in state space form
xx0(:,1)=xx(:,1); %Sailcraft position and velocity in state space form (without eclipse factor)
xx1(:,1)=xx(:,1); %Sailcraft position and velocity in state space form (for Forward Euler)
r_E(:,1)=xx(1:3,1);
r(:,1)=R_IE(:,1)+r_E(:,1);
r_hat(:,1)=r(:,1)/norm(r(:,1));
```

```
for k=1:TotalTime/dt
    %t(k+1)=t(k)+dt; %to advance time step


    %Desired Earth position and velocity wrt sun
    R_IE(:,k)=E(1:3,k);
    A_IE=[zeros(3), eye(3); -eye(3)*mu_sun/norm(R_IE(:,k))^3, zeros(3)];
    E(:,k+1)=(eye(6)+A_IE*dt+0.5*A_IE^2*dt^2)*E(:,k);


    %Desired position and velocity (sailcraft wrt Earth) Part 1
    r_E(:,k)=xx(1:3,k); %Position vector of the sailcraft from the center of the Earth,  [km]
    A=[zeros(3), eye(3); -eye(3)*mu_Earth/norm(r_E(:,k))^3, zeros(3)]; %State matrix
    B=[zeros(3); eye(3)/m]; %Input matrix


    %Approximate r position vector (Sun to sailcraft) in HEI coordinate frame
    %Assumes no rotation of Earth
    r(:,k)=R_IE(:,k)+r_E(:,k);
    r_hat(:,k)=r(:,k)/norm(r(:,k));


    %Controls
    %1. Determine when sailcraft is eclipsed by Earth's shadow
    ef=1; %eclipse factor
    if norm(r(:,k))>norm(R_IE(:,k)) %sailcraft is on far side of Earth from sun
        %this is the roughest value of r_crit
            a=r_Earth/r_sun*norm(R_IE(:,k))/(1-r_Earth/r_sun);
            b(k)=r_Earth/a*(a-norm(r_E(:,k)));
            c(:,k)=roots([1+b(k)^2/(a-norm(r_E(:,k)))^2 -2*a*b(k)^2/(a-norm(r_E(:,k)))^2
a^2*b(k)^2/(a-norm(r_E(:,k)))^2-norm(r_E(:,k))^2]);
            d(k)=r_Earth/a*(a-norm(c(1,k)));
            %Critical distance: the point at which the orbiting sailcraft enters or exits Earth's
umbra
            r_crit(k)=sqrt((norm(R_IE(:,k))+norm(c(1,k)))^2+d(k)^2); %[km]
            %this is a very close approximation of r_crit, assuming sailcraft
            %does not ascend too quickly, i.e. norm(r_E) at r_crit and at
            %opposition are approximately equal
            %this expression does not account for non-zero z values
            %r_crit=sqrt((norm(R_IE(:,k))+norm(r_E(:,k)))^2+b^2);
            %this is just an approximate value of r_crit. r_crit should be
            %smaller so this is not a conservative estimate
            %also, this expression does not account for non-zero z values
```

```
            if norm(r(:,k))>r_crit(k)  %Earth is between sun and sailcraft
                ef=0; %eclipse factor
            else %Earth does not block sunlight reaching sailcraft
                ef=1; %eclipse factor
            end
    end

    %2. Determine when sailcraft is accelerating due to SRP for on-off switching
    %Assumes instantaneous switching between on and off positions
    %Assumes sailcraft cone angle is 0 when 'on' and 90 degrees when 'off'
    a_r(k)=2*eta*L*Area/(4*pi*norm(r(:,k))^2*c0*m); %Magnitude of acceleration of solar sail at
distance r from sun, [km/min^2]
    T(:,k)=[0,0,0]';
    T1(:,k)=[0,0,0]';
    if k==1
        T(:,k)=[0,0,0]';
    %elseif norm(r(:,k-1)) > norm(r(:,k)) %Sailcraft is approaching sun / "off" position
    %    T(:,k)=[0,0,0]';
    elseif norm(r(:,k-1)) < norm(r(:,k)) %Sailcraft is moving away from sun / "on" position
        T(:,k)=ef*m*a_r(k)*r_hat(:,k); %Overall thrust vector experienced by the sailcraft due to
SRP and on-off steering controls
        %(both transverse and radial), [km/min^2]
        T1(:,k)=m*a_r(k)*r_hat(:,k); %Overall thrust vector, ignoring eclipse factor, [km/min^2]
    end
%    f(k)=dot(R_IE(:,k),r_E(:,k))/norm(R_IE(:,k))/norm(r_E(:,k)); %Cosine of angle between sail-
Earth line and sun-line
%    T1(:,k)=[0,0,0]';
%    if k==1
%        T(:,k)=[0,0,0]';
%    elseif f(k-1) > f(k) %Sailcraft is approaching sun / "off" position
%        T(:,k)=[0,0,0]';
%    elseif f(k-1) < f(k) %Sailcraft is moving away from sun / "on" position
%        T(:,k)=ef*m*a_r(k)*r_hat(:,k); %Overall thrust vector experienced by the sailcraft due
to SRP and on-off steering controls
%        %(both transverse and radial), [km/min^2]
%        T1(:,k)=m*a_r(k)*r_hat(:,k); %Overall thrust vector, ignoring eclipse factor,
[km/min^2]
%    end


    %Desired position and velocity (sailcraft wrt Earth) Part 2
    xx(:,k+1)=(eye(6)+A*dt+0.5*A^2*dt^2)*xx(:,k)+(eye(6)*dt+0.5*A*dt^2)*B*T(:,k); %xdot of System
    xx0(:,k+1)=(eye(6)+A*dt+0.5*A^2*dt^2)*xx0(:,k)+(eye(6)*dt+0.5*A*dt^2)*B*T1(:,k); %xdot
ignoring eclipse factor


%    %Fwd Euler approximation of updated position and velocity vectors (sailcraft wrt Earth)
%    x(k+1)=x(k)+dt*vx(k); %Updated x position
%    y(k+1)=y(k)+dt*vy(k); %Updated y position
%    z(k+1)=z(k)+dt*vz(k); %Updated z position
%    r_E1(:,k)=norm([x(k),y(k),z(k)]); %%%r_E1(:,k+1)=norm([x(k+1),y(k+1),z(k+1)]);
%    vx(k+1)=vx(k)+dt*(-mu_Earth*x(k)/norm(r_E1(:,k)^3))+T(1,k)/m; %Updated x velocity
%    vy(k+1)=vy(k)+dt*(-mu_Earth*y(k)/norm(r_E1(:,k)^3))+T(2,k)/m; %Updated y velocity
%    vz(k+1)=vz(k)+dt*(-mu_Earth*z(k)/norm(r_E1(:,k)^3))+T(3,k)/m; %Updated z velocity
```

```matlab
%      v1(:,k)=norm([vx(k),vy(k),vz(k)]); %%%v1(:,k+1)=norm([vx(k+1),vy(k+1),vz(k+1)]);
%      xx1(:,k+1)=[x(k+1),y(k+1),z(k+1),vx(k+1),vy(k+1),vz(k+1)]';


%To make the For Loop stop if sailcraft exceeds 240000 km from Earth
    if norm(r_E(:,k))>=240000
        k=TotalTime/dt;
    end

end
```

```matlab
%Spacecraft trajectory with Earth shown for reference
figure(2)
[px,py,pz] = sphere(50);                % generate coordinates for a 50 x 50 sphere
cla
sEarth = surface(px, py,flip(pz));
sEarth.FaceColor = 'texturemap';        % set color to texture mapping
sEarth.EdgeColor = 'none';              % remove surface edge color
earth = imread('landOcean.jpg');
sEarth.CData = earth;                   % set color data
hold on
view([90 30])                            % specify viewpoint
daspect([1 1 1])                        % set aspect ratio
axis off tight                          % remove axis and set limits to data range
p=1/r_Earth;
XX(:,:)=xx(:,:)*p;
plot3(XX(1,:),XX(2,:),XX(3,:),'r')
title('Sailcraft Trajectory in ECI Calculated via State Matrix A')
hold off


%Spacecraft Trajectory - with and without eclipse factor
figure(3)
plot3(xx(1,:),xx(2,:),xx(3,:),'r')
hold on
plot3(xx0(1,:),xx0(2,:),xx0(3,:),'b')
hold off
grid on
axis equal
xlabel('X-axis [km]')
ylabel('Y-axis [km]')
zlabel('Z-axis [km]')
title('Sailcraft Trajectory in ECI Calculated via State Matrix A')
legend('With Eclipse Factor','Without Eclipse Factor')


figure(4)
plot(X(1,:))
xlabel('Time Steps')
ylabel('X-Component of Trajectory [km]')
title('X-Component of Sailcraft Trajectory in ECI over Time')


figure(5)
```

```matlab
plot(X(2,:))
xlabel('Time Steps')
ylabel('Y-Component of Trajectory [km]')
title('Y-Component of Sailcraft Trajectory in ECI over Time')


figure(6)
plot(a_r)
%axis([0 1e5 1.66505e-4 1.6654e-4])
xlabel('Time Steps')
ylabel('Magnitude of SRP Acceleration [km/min^2]')
title('Magnitude of SRP Acceleration of Solar Sail Over Time')
%Note the eclipse factor in not included.


figure(7)
plot3(T(1,:),T(2,:),T(3,:))
hold on
plot3(T1(1,:),T1(2,:),T1(3,:))
hold off
axis([3e-4 9e-4 0 2e-5])
xlabel('Thrust X-axis [km/min^2]')
ylabel('Thrust Y-axis [km/min^2]')
zlabel('Thrust Z-axis [km/min^2]')
title('Overall Thrust Vector Experienced by the Sailcraft Due to SRP and On-off Steering
Controls')
legend('With Eclipse Factor','Without Eclipse Factor')


figure(8)
plot(T(1,:))
xlabel('Time Steps')
ylabel('X-Component of Thrust [km]')
title('X-Component of Thrust Vector in ECI over Time')


figure(9)
plot(T(2,:))
xlabel('Time Steps')
ylabel('Y-Component of Thrust [km]')
title('Y-Component of Thrust Vector in ECI over Time')


figure(10)
plot3(r(1,:),r(2,:),r(3,:),'r')
grid on
xlabel('X-axis [km]')
ylabel('Y-axis [km]')
zlabel('Z-axis [km]')
title('Sailcraft Position in SCI Calculated via State Matrices A and A_I_E')


figure(11)
plot(r_crit)
```

```matlab
hold on
plot(vecnorm(r,2,1))
hold off
%axis([0 5e5 1.496e8 1.49615e8])
xlabel('Time Steps')
ylabel('Distance from Sun [km]')
title('Comparison of Critical Distance and Sun-Sailcraft Position Vector Magnitude over Time')
legend('Critical Distance','Sun-Sailcraft Position Vector Magnitude')


figure(12)
plot(vecnorm(r_E,2,1))
%axis([0 inf 0.7e4 0.77e4])
xlabel('Time Steps')
ylabel('Sailcraft Distance from Earth [km]')
title('Sailcraft Trajectory in ECI Calculated via State Matrix A')
```

```matlab
%Removed Items

 %a_transverse(:,k)=(1/norm(r_E(:,k)))*[r_E(2,k) -r_E(1,k) 0]'; %Again, assumes z component is zero
 %T(:,k)=ef*a_r(k)*cos(acos(f(k))-3*pi/2)*a_transverse(:,k); %Transverse acceleration of solar sail
 %T1(:,k)=a_r(k)*cos(acos(f(k))-3*pi/2)*a_transverse(:,k); %Acceleration of solar sail ignoring eclipse factor, [km/min^2]


% figure(12)
% plot3(xx0(1,:),xx0(2,:),xx0(3,:),'b')
% grid on
% xlabel('X-axis [km]')
% ylabel('Y-axis [km]')
% zlabel('Z-axis [km]')
% title('Sailcraft Position in ECI Calculated via Forward Euler Approximation')

% figure(13)
% plot(f)

% figure(14)
% plot(cos(acos(f)-1*pi/2))

% figure(15)
% plot3(n(1,:),n(2,:),n(3,:))

% figure(16)
% plot(c(1,:))

% figure(17)
% plot(b)
```

Published with MATLAB® R2019a